UNCLASSIFIED   12/79

SECURITY CLASSIFICATION OF THIS PAGE (When Data Entered)

REPORT DOCUMENTATION PAGE	READ INSTRUCTIONS BEFORE COMPLETING FORM

1. REPORT NUMBER	2. GOVT ACCESSION NO.	3. RECIPIENT'S CATALOG NUMBER
WHOI-79-92	AD-A083 654	

4. TITLE (and Subtitle)

MOORED ACOUSTIC TRAVEL TIME (ATT) CURRENT METERS: EVOLUTION, PERFORMANCE, AND FUTURE DESIGNS

5. TYPE OF REPORT & PERIOD COVERED

Technical rept.

6. PERFORMING ORG. REPORT NUMBER

7. AUTHOR(s)

James R. McCullough and Wilhelm Graeper

8. CONTRACT OR GRANT NUMBER(s)

N00014-76-C-0197

9. PERFORMING ORGANIZATION NAME AND ADDRESS

Woods Hole Oceanographic Institution
Woods Hole, MA 02543

10. PROGRAM ELEMENT, PROJECT, TASK AREA & WORK UNIT NUMBERS

NR 083-400

11. CONTROLLING OFFICE NAME AND ADDRESS

NORDA
National Space Technology Laboratory
Bay St. Louis, MS 39529

12. REPORT DATE

December 1979

13. NUMBER OF PAGES

117

14. MONITORING AGENCY NAME & ADDRESS(if different from Controlling Office)

15. SECURITY CLASS. (of this report)

Unclassified

15a. DECLASSIFICATION/DOWNGRADING SCHEDULE

16. DISTRIBUTION STATEMENT (of this Report)

Approved for public release; distribution unlimited.

17. DISTRIBUTION STATEMENT (of the abstract entered in Block 20, if different from Report)

18. SUPPLEMENTARY NOTES

19. KEY WORDS (Continue on reverse side if necessary and identify by block number)

1. Flowmeter
2. Acoustic travel time
3. Response

20. ABSTRACT (Continue on reverse side if necessary and identify by block number)

New laboratory measurements and numeric model studies show the present folded-path ATT current meters are stable and sensitive, but are not well suited for mean flow observations in surface gravity waves. Alternate designs which reduce unwanted wake effects are proposed. ATT flowmeter history, principles of acoustic flow sensors, mean flow near cylinders, and the need for linear flow sensors are reviewed.

DD FORM 1473 EDITION OF 1 NOV 65 IS OBSOLETE
S/N 0102-014-6601 |

UNCLASSIFIED   12/79

SECURITY CLASSIFICATION OF THIS PAGE (When Data Entered)

WHOI-79-92

MOORED ACOUSTIC TRAVEL TIME (ATT) CURRENT METERS:
EVOLUTION, PERFORMANCE, AND FUTURE DESIGNS

by

James R. McCullough
Woods Hole Oceanographic Institution
Woods Hole, Massachusetts 02543

and

Wilhelm Graeper
Bundesamt für Wehrtechnik und Beschaffung
5400 Koblenz 1, Federal Republic of Germany

December 1979

TECHNICAL REPORT

Approved for Distribution _Nick P. Fofonoff_____
                          Nick P. Fofonoff, Acting Chairman
                          Department of Physical Oceanography

Table of Contents

List of Figures and Tables

Tables	Page No.

Abstract

New laboratory measurements and numeric model studies show the present folded-path ATT current meters are stable and sensitive, but are not well suited for mean flow observations in surface gravity waves. Alternate designs which reduce unwanted wake effects are proposed. ATT flowmeter history, principles of acoustic flow sensors, mean flow near cylinders, and the need for linear flow sensors are reviewed.

I.   Introduction

Considerable interest has developed in the past several years in upper ocean flow measurements. Engineering designs for off-shore structures, air-sea interaction studies, heat transport (climate) models, pollution dispersion predictions, etc., all need reliable wave-zone estimates of flow.

While both distance and time can be measured with extraordinary accuracy, only relatively crude estimates of flow speed are possible in the ocean. This seeming paradox arises from the broadband nature of ocean flow in which many time and length scales are present simultaneously. Interpretation of the mean speed therefore requires knowledge of both the time and spatial averaging processes used in forming the mean statistical estimates.

Unlike the atmosphere, the ocean density stratification strongly limits mean vertical flow. Below tidal frequencies, horizontal flows, for example, are orders of magnitude more energetic than associated vertical flows. Consequently, it has been adequate in moored studies of low-frequency ocean processes to measure only the more energetic horizontal flow components, a much less demanding instrument requirement. In surface gravity waves or on surface-following moorings, however, large oscillatory vertical velocities are frequently present. To compute correct time averages, unbiased instantaneous horizontal velocity values must be available for the entire averaging period.

Since flow meters now used are at best only quasilinear, their accuracy invariably depends in rather complex ways on the mean, variance, harmonic content, direction and amplitude scales of the flow. The technical challenge of devising flow sensors with predictable instantaneous or even mean response in arbitrary broadband forcing has not been solved. Time and space scales of the averaging process are relatively inflexible and are often variable or unknown.

Traditionally, mechanical propellers, rotors, and floats have been used. In the last decade or so electromagnetic (EM), acoustic travel time (ATT), acoustic Doppler, and laser Doppler sensors have been introduced. Considerable improvement has been achieved particularly in propeller, EM, and ATT methods, but to date no single method has emerged as an in situ (or even laboratory) standard for ocean flow. McCullough (1974, 1976, 1977, 1978, and 1979) reviews moored flowmeter technology. This report discusses acoustic-travel-time (ATT) sensors.

ATT flow sensors offer potentially attractive advantages for moored oceanographic application but as yet are not commercially available in a form suitable for accurate, long-term mean-flow measurements in the wave-zone. In the last decade, size, power consumption, stability, and cost factors have been brought within practical limits. Precision in pipe flow now exceeds 0.5% in commercially available instruments (Lowell, 1977). While further cost and flexibility improvements are desirable in moored instruments, the last major performance limitation is the reduction of flow interference along the acoustic paths.

ATT advantages include:

· Single component, linear response

· High frequency response (>50 Hz)

· High sensitivity and resolution (<1 mm/sec)

· Wide range of spatial averaging (1-10^7 cm)

· Three component averaging within a single volume.

Present disadvantages include:

· Poor wave response (as presently configured)

· Relative complexity (expense)

· Few packaging and sampling options.

This report presents new laboratory and numeric model results for the Neil Brown Instrument Systems (NBIS) mirror-type ATT meter in wave-like flows. As background, the fifty year history of ATT development and present knowledge of flow near cylinders are reviewed. Strategies for improved performance such as larger ratios of sensor separation to diameter, redundant acoustic paths, conditional sampling, and digital linearization are considered. Specific design concepts are presented to stimulate further discussion.

This is largely a progress report on the development of moored ATT sensors. Many topics of central importance to overall moored current meter performance such as mooring motion, compass accuracy, sampling schemes, fouling, endurance, in situ verification, etc., are not treated per se.

II. History

A. Introduction

The history of acoustic technology is reviewed by Hunt (1954 and 1978) and is continued to date by Hersey (1977). Experiments before this century were conducted largely by "gentleman scientists," including such notables as Aristotle, Leonardo da Vinci, Galileo, Newton, and Lord Rayleigh. Galileo (1638) initiated the study of mechanics and concisely described the then known properties of sound. Newton (1686) predicted from theoretical consideration the speed of sound. The unresolved discrepancy between Newton's prediction and the direct measurements of sound speed led the Paris Academy of Sciences to conduct controlled outdoor measurements in 1738. These measurements incorporated the first use of ATT flow techniques. In order to eliminate unwanted bias by the wind, cannon were fired alternately from opposite ends of an 18-mile base line. It is curious to note that earlier experiments sponsored by Leopold de Medici in 1656 had erroneously shown that sound moved at the same speed regardless of the wind direction.

The first travel-time difference measurements in water were made by Fizeau (1851) using light interference techniques. This classic relativity experiment showed that light did not follow the Galilean addition of velocities as it does with sound.

Lord Rayleigh's two volume book (1877) and subsequent 60 publications put the theoretical and practical aspects of acoustics on a firm modern basis. Rayleigh (1877) states regarding sound speed measurements:

> The principal precaution necessary is to reverse
> alternately the direction along which the sound
> travels, in order to eliminate the influence
> of the motion of the air in mass. Down the wind,
> for instance, sound travels relatively to the
> earth faster than its proper rate, for the
> velocity of the wind is added to that proper to
> the propagation of sound in still air.

Thus the principle and theoretical background needed for ATT flow-meters is prominently presented in the major acoustic text of the 19th century.

The necessary ATT transducers and electronic timing circuits were developed over the next 50 years. Practical underwater acoustics started in this century with efforts to use underwater sound for navigation and signaling. For such purposes, R. A. Fessenden in 1912 developed the first moving coil underwater transducer, much like a specialized loudspeaker. The sinking of the TITANIC in 1912 was followed in the same year by the first patents in Britain for echo ranging in air and water. Two years later in March of 1914, Professor Fessenden aboard the revenue cutter MIAMI demonstrated his echo locator and during the cruise discovered its effectiveness as a fathometer. The first piezoelectric quartz acoustic transducer (the "singing condenser") was developed by Langevin in 1917.

Unrestricted German submarine warfare starting in 1914 led to urgent cooperative acoustic development programs in France, Italy, Great Britain, and the United States. By the end of the war ten British warships had been fitted with experimental "Asdic" sounding equipment capable of detecting submarines at distances of more than 8 kilometers. Following the war, Chilowsky and Langevin filed patent for their mutual invention of a device "enabling the location of submarine obstacles as well as the sounding of the sea bottom by observing the reflected waves (of ultra-audible sound)," i.e., the echo sounder and fathometer.

Chilowsky's remarkable acoustic patent filed in December 1924 goes on to describe the ship-mounted Doppler speed log (now called the dual-axis Janis configuration) used as the modern method of measuring ship speed over the ground.

During the same quarter century the development of practical vacuum tubes and associated circuits led to very rapid advances in telephone and radio technology. With the introduction of the "Radiola" loudspeaker in 1926, the Pierce (1925) acoustic interferometer, and the rapid advances in echo sounding publicized in The Hydrographic Review, conditions were ripe for the invention of ATT flowmeters.

The history of practical ATT flowmeters opens abruptly with the independent patent claims filed by Rutten in Berlin (September 1928) and by Hartig and Wilcox in Minneapolis (February 1929). Figure 1 (top) shows the Hartig/Wilcox invention. The pipe-flow principle shown was also intended for open flow such as "wind." The telephone-style transducers probably stem from Professor Hartig's earlier employment with

the telephone company. Measurements were made over the single acoustic path (a), thus avoiding the basic difficulty of unwanted signals from small differential mechanical variations of the instrument. No attempt was made at this stage to reduce difficulties arising from acoustic multipaths and transducer flow disturbance. These problems were treated directly in the next two Hartig/Wilcox patents filed in 1932 and 1935 respectively (see Table 1).

The basically different Rutten invention of 1928 used a central transmitter with separate up- and downstream receivers. Arrival of a sound pulse at the downstream receiver started an electrical timer; arrival of the same pulse upstream stopped it. The acoustic sensors were mounted along the pipe center-line, much as in the Hartig/Wilcox device shown.

Thus between 1912 and 1929 we see the invention of:

· Underwater electro-mechanical and piezoelectric
    transducers

· The echo sounder and fathometer

· The Doppler speed log

· The ATT flowmeter.

B.   The first ship and airship ATT meters

The first ocean tests of an ATT meter were made on a "largely unplanned" trial by R. E. Payne of the Harvard Underwater Sound Laboratory (HUSL) aboard the launch FLYING CLOUD in January 1943. The tests were part of a larger World War II program to develop military applications of acoustics. In an April 1943 memo, M. H. Hebb of the same HUSL team identified the cause of the noisy results of the January tests and correctly described for the first time the theory and design of the modern two transducer ATT flowmeter. Unfortunately, the HUSL ship log program was discontinued that fall (1943) and the results were classified. Except for a few patents and relatively obscure references, the work received little attention.

The airship speed-log program of the same HUSL group was continued and produced the detailed theoretical and experimental results described by Eisenstein et al. (1945). Wolff and RCA had filed a patent claim in May 1939 for a similar device and helped with the US Navy wartime

-5-

Table 1

Early ATT Patents

Inventors	Filed	Recd.	Number	Remarks
Chilowsky/Langevin	1916	1920	502,913	French, echo sounder
Chilowsky	1924	1932	1,864,638	Janis Doppler Log
Rutten	1928	1931	520,484	German, first ATT
Hartig/Wilcox	1929	1932	1,881,543	First single-path ATT
Hartig/Wilcox	1932	1935	2,015,933	Multipath solution
Hartig/Wilcox	1935	1939	2,151,203	Flush transducers
Wolff/RCA	1939	1942	2,274,262	3-station, air, phase
Sproule	1943	1949	623,022	English, 3-station
Gray/US Navy	1945	1950	2,534,712	3-station, air, pulse
Ono	1948	1956	182,549	Japanese, single-path cross-flow
Kritz	1948	1958	2,826,912	2-station, sing-around
Swingel	1950	1956	2,746,291	2-station, air, pipe

.

.

.

Now more than 200 ATT patents issued.

development. As shown in Figure 1 (bottom, insert) the air
speed sensor had a central transmitter with separate up- and
downstream receivers reminiscent of the patent claims of Rutten
(1928), Hartig/Wilcox (1935), and Wolff/RCA (1939). Figure 1
(bottom) also shows the test blimp and similar Navy K-airships
in their hangar. Successful performance of the ATT speed log
was demonstrated in repeated runs over a measured course in New
Jersey, July 1945. The system used a 4 KHz, continuous wave
(CW) carrier with multiplexed single-channel phase detection.

In 1943 Sproule filed a patent claim in England for an ATT
pipe flowmeter in which one transmitter-receiver pair operated
upstream and a second pair operated downstream. Like the first
HUSL ship log (January 1943), Sproule's invention relied on
mechanical stability and probably would not have been suitable
for ocean use. At this stage of the war England and the United
States shared secret acoustic intelligence but it is not clear
what relation, if any, the Sproule invention had to the Harvard
program.

In November of 1945 Gray applied for a US patent for an air
speed indicator much like the Harvard/Wolff device but using
pulse instead of phase detection. The parallel evolution of
CW, pulse, and "sing-around" ATT techniques (discussed later)
appears in historical hindsight to have been beneficial to the
overall effort; when one tehnique became unsuitable, alternate
methods were available.

Two important conceptual advances, now used routinely in
pipe flowmeters, were made by Toshio Ono in a patent filed in
Japan in 1948. First, his device used only two transducers
functioning alternately as transmitters and receivers; and
second, the acoustic path was fixed not directly along the flow
as in earlier meters, but at an angle to it. Simultaneous
pulses were transmitted and arrival time differences measured
directly with an oscilloscope. While the Ono timing technique
now appears rather awkward, Ono correctly recognized the
importance of nulling electromechanical variations by
simultaneous acoustic transmissions. In addition, he
recognized the importance of reducing transducer flow
interference. Later in the same year (1948), Kritz in this
country filed patent for a more fully developed
sing-around-type meter. One of Kritz's several devices also
included the interchangeable transmitter/receiver and
cross-flow concepts.

C.   The first moored ATT meter

The first moored ATT meter shown in Figure 2 was developed for tidal studies by Middleton (1955) as part of his Ph.D. thesis. Thirteen second long phase measurements of 1 MHz sound bursts were made alternately in up- and downstream directions. Single half-hour samples ($\sim$400 in all) could be taken for a week with the vacuum tube circuits shown. Film recorder and battery were housed separately in the anchor and connected to the "fish" with an electric cable. The meter had a single acoustic axis and relied on a fin and compass for direction. The fin shown was later replaced by one with about three times the surface area.

The instrument demonstrated that ATT sensors could be used on moorings, but it also demonstrated the relative simplicity of mechanical sensors, an advantage they still offer. Kalmus (1954) and Suomi (1957) describe pipe and air flowmeters of the same era. Two decades passed before the next serious attempts were made to build moored ATT current meters.

D.   Anemometer development

Suomi (1957), and Barrett and Suomi (1949) appear to be the first to use ATT techniques for micrometeorological experiments. Suomi used a pulse technique but had difficulty reliably measuring the small time differences. Bovsheverov and Voronov (1960) and Kaimal and Businger (1963) used continuous wave (CW) anemometer techniques to by-pass resolution problems of the pulse method. Mitsuta (1966) in Japan and Beaubien et al. (1966) in the US then independently improved the pulse technique. Mitsuta et al. (1967) and Kaijo Denki Co. in Japan developed a 3-axis hybrid pulse/CW anemometer incorporating the stability of the pulse technique with the signal-to-noise advantages of CW.

E.   Modern oceanographic ATT current meters

While air, blood, and pipe-flow ATT meter techniques advanced steadily in the 1950s and 1960s, little progress was made with ocean designs. Moorings were generally unreliable, vacuum tubes and high speed transistors required excessive power, and long-path ATT systems such as that developed by Nowak (1969) required large, stable platforms.

By 1968 sample quantities of the new low power integrated circuit electronics (COS/MOS) became available and Trygre Gytre in Bergen, Norway started work on his ingenious, highly simplified ATT flowmeter. Taking the unconventional approach

of using the rising edge of flip-flops as fast voltage-ramps, he was able to reduce the required electronics to one 15 by 20 cm card with a similar card for the 300-volt battery converter needed to drive the transducers. Prototype Gytre meters (shown later) opened new interest in practical ATT sensors for oceanography. These instruments offered high resolution (mm/sec) and potentially stable, fast, linear response. Approximately 25 devices of varying design were constucted between 1970 and 1976. Ocean applications included: Richardson number and salt-finger free-fall probes, turbulence sensors, and moored current meters.

In comparing the energy consumption and performance of various flow sensors, McCullough (1974) concluded that while overall ATT power requirements were still high, most of the energy was used in the signal processing, not in the sensors. Thus extended operation at sea would eventually become practical. Low power, stable operation was achieved in the laboratory in the mid-1970s by both Gytre (1976) and Lawson et al. (1976), leaving the problem of flow interference by the meter as the last major technical obstacle. Today a number of firms offer commercial ATT meters for air, water, medical, and industrial fluid flow applications. Oceanographic meters are available from France, Japan, Norway, and the USA.

Figures 3, 4, and 5 show a few of the large variety of anemometers and ocean flowmeters developed in the last two decades.

In the 1980s it is anticipated that electronic large-scale integration (LSI) will lead to miniaturized ATT instruments with in situ processing for:

1. Sensor wake avoidance

2. Vector averaging

3. Variance and higher statistical moment processing

4. Three component (u,v,w) sensors

5. Multiplexed processors servicing numerous acoustic paths

6. Shear and vorticity meters

7. Long path meters (systems)

8. Large 3-dimensional arrays with redundant acoustic paths for error analysis and "fail-safe" operation

9. Flexible sampling options.

As might be expected, steps in ATT flowmeter development have been closely linked to advances in other technologies. Key items include:

1. Development of basic sound theory (19th century)

2. Development of the underwater acoustic transducer (1912 on)

3. Development of the vacuum tube and its circuits ($\sim$1910 to 1960)

4. Development of low power integrated circuits (1968 to present)

5. Development of large-scale integration (LSI) and the microprocessor ($\sim$1972 to present)

6. Low volume (custom) LSI (now).

While far from complete, we hope this historical sketch will provide some general perspective from which to view present accomplishments and future possibilities of ATT flowmeters.

III. Principles of Sonic Flow Measurement

A. Introduction

Table 2 divides acoustic flowmeter principles into three broad categories: acoustic travel time difference (ATT), backscatter, and feature advection. Examples of scale sizes, uses, and users are shown. ATT flowmeters measure the difference in time required for sound to propagate with and against the flow. They differ from backscatter (volume reverberation) flowmeters in which remote sound scatterers are insonified and the observed frequency-shift (Doppler) or motion of the acoustic interference pattern (correlation sonar) of the echo is measured. Feature advection schemes measure the time for an acoustic feature to move from one location to another.

B. Methods

1. Acoustic travel time (ATT)

Sound compressional waves in a fluid travel at constant speed with respect to the fluid mass regardless of the relative motion of the sound source or receiver. Thus, sound pressure fronts appear to move faster downstream than upstream to an observer moving with respect to the fluid. ATT flowmeters measure by various techniques the time difference Δt over some path such that

$$\Delta t = t_{upstream} - t_{downstream}.$$

Three measurement strategies for determining Δt are in general use: pulse, phase, and sing-around. Numerous other combinations and techniques are described in the extensive literature ($\sim 10^3$ published papers); all methods measure the same basic quantity, Δt. Satisfactory corrections for _in situ_ changes in sound speed due to temperature, salinity, and pressure effects can usually be applied from measurements of depth and temperature, and knowledge of mean salinity characteristics. Alternately, many instruments incorporate some direct mearurement of c. The dominant error term, however, is the uncertain relation between the integrated flow speed along the acoustic path (the measured value) and the desired free stream velocity. Next, we describe briefly the three basic Δt measurement techniques.

Table 2

Types of Acoustic Flow Sensors

Scale Size	Use	Reference
1) Travel-Time Difference (ATT)		
1-100 cm	Current meters	Gytre (1979); Lawson et al. (1976)
1-1000 m	Pipe and channel flow	Lowell (1977)
1-1000 km	Tomography	Munk & Wunsch (1979); Worcester (1977)
$0.1-10^6$ m	Relative vorticity	Rossby (1975)
2) Backscatter		
A) Doppler		
1 cm	Bloodflow	Newhouse et al. (1978)
1 m	Current meter sensor	McCullough & Terry (1978)
10 m	Ship log	Ametek (1979); Kritz & Howard (1969)
10-100 m	Ship profiler	Regier (1979)
100-1000 m	Long range profiler	Pinkel (1979)
B) Correlation sonar		
100-5000 m	Ship log (other ...)	Dickey & Edward (1978); Andermo & Masreliez (1978)
3) Feature Advection		See section III,B,3

a. Pulse

Simultaneous sound pulses are sent in opposite directions along the same acoustic path. The transmitters then act as receivers and the arrival time of some portion of the acoustic wave (such as the first zero crossing following the first major signal) is timed.

The interval Δt between pulse arrivals (neglecting asymmetric electromechanical delays) is shown by McCartney et al. (1979) to be

$$\Delta t = \frac{2\ell v \cos\theta}{c^2 - v^2}$$

which for $v^2 << c^2$ reduces to

$$\Delta t = \frac{2\ell v \cos\theta}{c^2}$$

where ℓ is the transducer separation, θ is the angle between the flow and ℓ, and $v \cos \theta$ is the spatially averaged flow component along ℓ.

The assumption that $v^2 << c^2$ is well justified in ocean current meters since the sound speed is about 1500 m/sec while flow speeds rarely exceed 5 m/sec (10 knots). Thus for this extreme case $c^2/v^2 = 300^2$, or v^2 is $\sim 10^5$ times smaller than c^2.

The large difference between v and c also makes Δt very small in ocean applications. The sensitivity, $\Delta t/v$, is only 1.3×10^{-9} sec per cm/sec for $\ell = 15$ cm, but as will be shown later, present circuits allow noise levels in Δt as low as an equivalent flow of 0.1 mm/sec, i.e., $\sim 1 \times 10^{-11}$ sec (10 pico sec). Additional discussion is given in Appendix C.

b. Phase

Phase changes of long pulses or continuous wave (CW) transmission are measured. The phase change $\Delta\phi$ at frequency f (again for $v^2 << c^2$) is

$$\Delta\phi = \frac{4\pi f \ell v \cos\theta}{c^2}$$

Without some kind of "speed-range" logic this method has a maximum speed v_{max} at $\phi = \pi$ radians such that

$$v_{max} = \frac{c^2}{4f\ell}$$

(For ℓ = 10 cm, f = 1.5 MHz and c = 1500 m/sec, $v_{max,min}$ = $\pm$ 375 cm/sec).

c. Sing-around

The sing-around method is basically a pulse technique in which each new pulse in one direction is initiated by the arrival of the previous pulse. After n repetitions the sound direction along ℓ is reversed. The difference ΔF in pulse repetition rates then gives Δt in much the same way as in the pulse method. For $v^2 << c^2$,

$$\Delta F = \frac{2v \cos\theta}{n\ell}$$

The small individual Δt intervals are thus accumulated to make a larger and more easily detected difference signal. In addition, c is measured more-or-less directly by the approach, leading some authors and inventors to incorrectly suggest that the speed of sound is not involved in the measurement.

Gytre (1976 and 1979) discusses ATT design issues. Lawson et al. (1976) describe a hybrid pulse/phase technique used in the NBIS meter. Kaimal (1979) and Larsen et al. (1979) review AT™ anemometer design. Lowell (1977) and Newhouse et al. (1978) discuss pipe and bloodflow ATT techniques respectively.

d. Novel ATT methods

A large variety of additional ATT methods have been suggested. A series of 1965 US patents (Class 73/194A) describe "beam bending" sensors in which a narrow acoustic beam is bent by the flow and sensed as a difference signal in two receivers placed parallel to the flow opposite the transmitter. A second method uses variations in sound intensity caused by flow-induced changes on multiple internal acoustic reflections in a tube. M-sequence encoding and AM/FM have been proposed for ATT timing. Larsen et al. (1979) discuss a modern version of the Hartig/Wilcox 1929 concept.

-14-

2. Backscatter

a. Doppler

The radial speed (range-rate) of remote sound scatterers is determined from the frequency-shift (Doppler) of their echo. The Doppler shift Δf is related to the radial velocity v_R, sound speed c, and frequency f_0 to first order in v/c by

$$\Delta f = \frac{2\,v_R}{c}\,f_0 \ .$$

Pinkel (1979), and McCullough and Terry (1978) review oceanographic application of Doppler flowmeters.

b. Correlation sonar

Scatterer motion across the acoustic beam can also be detected. An array of receivers normal to the beam is used to determine the lateral speed of the echo interference pattern by observing its spatial-shift (as opposed to frequency-shift in Doppler) during an interval which is small compared with the scatterer decorrelation time.

One implementation uses a single transmitter, a plane array of receivers, and pairs of acoustic pulses. Two pulses separated by a time τ (short compared with the scatterer decorrelation time) are transmitted. During reception of the first echo, amplitudes at each array element are time-averaged and stored. The second echo is processed in the same way. Next, the recorded echo arrays are computationally "slid" in a computer to find the array displacement vector $\bar{x}$, yielding maximum pulse-to-pulse correlation. The velocity $\bar{v}$, normal to the transmitted beam, is then found from

$$\bar{v} = \frac{\bar{x}}{2\tau} \ .$$

The technique offers the attractive potential of remote sensing of all three velocity components (u, v, and w) in a single remote volume. Dickey and Edward (1978) and Andermo and Masreliez (1978) describe correlation sonar techniques.

3. Feature advection

The time taken for features such as turbulence patches, particles, etc., to pass two observation stations can be measured by correlating up- and downstream signals. In addition, Doppler broadening due to transit-time effects and intensity fluctuations of Doppler spectra (decorrelation time) have been proposed and tested as detectors (see Kennedy and Bilbro 1979). Optic, radar, and acoustic flowmeter versions have been described and patented over the years, but only recently have practical devices begun to evolve in atmospheric and military applications. Further background is found in Morgan and Bowles (1967), Tompkins et al. (1974), Kipphan and Mesch (1978), Barakat and Buder (1979), etc.

IV. Cosine-Response

"Cosine-response" is a recently coined term describing a current sensor's immunity to off-axis flow. If a flow v is at some angle γ to the sensor's axis of greatest sensitivity, then the flow component along the axis is v cos γ. The sensor is said to have "perfect cosine-response" if it measures v cos γ correctly for all γ over the bandwidths of frequency and scale-size accepted by the sensor. "Horizontal" cosine-response refers to γ in the horizontal plane; "vertical" cosine-response refers to γ in the vertical. "Static" and "dynamic" cosine-response refer to response in steady flow and in time/space varying flow respectively.

Somewhat surprisingly, good vertical cosine-response is required even if the vertical flow has no net displacement. This requirement exists for continuously averaging current meters because accurate (or at least unbiased) instantaneous measurements are needed throughout the averaging cycle. Alternately, conditional sampling and/or linearization could be used before averaging.

If a flow sensor has imperfect cosine-response (which they all do to some extent), it is influenced by flow components normal to its axis of greatest sensitivity, i.e., it responds to off-axis flow or has "cross-talk." Low cross-talk levels are desirable for two reasons:

1. Cross-talk complicates the in situ data processing prior to vector averaging. (Estimates of u, v, and w are needed in an iterative process to improve the u estimate, etc.), and

2. Sensors with significant cross-talk cannot be modeled as linear systems.

While often less expensive and easier to build, the response of nonlinear sensors is generally more expensive to calibrate, model, and verify. Since the cross-talk process is inherently nonlinear, off-axis sensitivity for one frequency, wavenumber, and amplitude may differ from that at another, or from response in complex broadband forcing. Testing becomes difficult (expensive) with nonlinear systems since large combinations of test conditions are involved. On the other hand, if the sensor is quasilinear its response and error bounds can be estimated by less elaborate procedures. Thus a basic performance goal for practical component flow-transducers

such as propeller, EM, and acoustic sensors is "good" static
and dynamic cosine-response. How "good" is adequate depends on
the flow complexity and intended final accuracy. Numeric
models such as used below can be used to efficiently predict
the relative importance of various cosine-response
imperfections over a wide range of ocean conditions.

V. Direct-Path Meters

A. Problems

Figure 6 shows an early Gytre-type ATT meter tested at WHOI in 1973-1974. Two diagonal acoustic paths between four transducers measure the horizontal components of flow normal to the long-axis of the meter. The acoustic paths are 10 cm long; transducer cylindrical supports are 1 cm in diameter, i.e., a transducer separation to diameter ratio of 10. The instrument was designed for free-fall shear measurements and has no mooring cage. Shown above the current meter is the WHOI tow carriage and 1 m peak-to-peak horizontal linear oscillator ("slosher"). (The tank is 1.19 m wide, 1.04 m deep, and 20 m long. In 1977 the gravel bottom was replaced with smooth fiberglass, the tow carriage and rails were rebuilt, and a flume capability was added.)

Figure 7 shows the measured dynamic response of the Gytre instrument to simultaneous steady-tow and oscillation parallel to the tow. Speed over the ground, indicated speed, tow carriage position, and meter position are shown for a 2.7 sec oscillation. The top panel shows the response with the acoustic axis aligned with the flow ($\theta = 0^{o}$). The bottom panel is similar except the axis is at 45° to the flow. Speed scales were determined from steady flow calibrations at each angle ($\theta = 0^{o}$ and $\theta = 45^{o}$). The larger distortion in the upper panel ($\theta = 0^{o}$ suggests the importance of dynamic wake effects. The dynamic response, however, is considerably faster than that of rotors and propellers used in the ocean (i.e., see McCullough, 1978, Figure 4; and Weller and Davis, 1979, Figure 14).

The slosher used (Figure 6, top) had a wheel and connecting-rod arrangement generating horizontal linear motion of the form

$$V = -R\omega \sin \omega t - \frac{R\omega \sin 2\omega t}{2[(L/R)^2 - 0.5(1-\cos 2\omega t)]^{0.5}}$$

where R is the wheel radius, ω is its angular velocity, L is the connecting-rod length, and V is the oscillatory speed

transmitted to the current meter. For the tests shown

$R = 39.5$ cm

$L = 77.0$ cm

$\omega = 2\pi/T = 2\pi/2.68$ sec = 2.34 rad/sec .

V is composed of first, second, and higher harmonics which when combined give the asymmetric "calculated speed" shown (Figure 7, dash-line).

The dynamic response (dots) generally follows the calculated kinematic speed over the ground for these conditions and for an additional range of T exceeding that anticipated in ocean surface gravity waves. Further, the dynamic response does not vary appreciably with frequency, i.e., it is accurately predicted by the steady-tow calibration at each angle θ. While harmonic in-line forcing is only a rather special case of broadband three-dimensional forcing, these early ATT slosher experiments strongly motivated further development effort.

Figure 8 shows a major technical problem: non-linear angular response in steady flow, i.e., poor horizontal cosine-response. In the lower panel the single axis-response at various rotation angles θ to the flow is given for a range of speeds. Note that the response does not decrease with θ as desired. The upper part of Figure 8 shows the section along 53 cm/sec. Errors relative to the response at 50° are also shown. The upward trend of the measurements toward higher speeds (lower panel) was later found to be a test artifact; that below ~15 cm appears in other meters and test conditions. The general picture is rather discouraging: <u>the sensor is strongly nonlinear when measuring in its own wake.</u>

B. <u>Solutions</u>

Methods considered for improving the cosine-response were (are):

1. Point a one-axis (or a two-axis) ATT meter into the flow with a large vane.

2. Correct for the wake defect in the calibration.

3. Use streamlined or faired transducer mounts.

4. Mount the transducers on stems extending into the case as in ATT anemometers.

5. Use two parallel rings or bars with inclined acoustic paths.

6. Arrange three horizontal acoustic paths in an equilateral triangle. Use only the two paths with least wake disturbance.

7. Increase the transducer separation to diameter ratio.

8. Fold the acoustic path(s) with a mirror.

9. Use small (fragile) sensors and supports.

10. Use conditional sampling.

11. Use combinations of these.

C. Discussion

As a first step, the mirror method (8) was adapted while work progressed on the more pressing problems of power consumption, stability, and commercial construction. Now that these issues are largely resolved, a new look at alternate transducer configurations seems timely.

1. Add a vane

Large vanes used on many mechanical meters are awkward to handle and may be inadequate in the wave-zone due to length scale and low speed response difficulties (see i.e., McCullough, 1979; and Beardsley et al., 1977).

2. Calibration correction

Since errors do not appear to be strongly frequency dependent (Figure 7) or speed dependent (Figure 8), linearization by digital processing such as described by Horst (1973), Smith (1978), etc., might be applicable. Unlike earlier analog linearization circuits, digital microprocessors now allow complex iterative corrections in situ. Such digitally implemented algorithms are precisely defined, inherently stable, and readily serviced. Cost, space, and power requirements are not prohibitive.

On the other hand, wake-induced errors are also amplitude, wavenumber, and time dependent, i.e., they vary with the scale and previous history of the flow. Dynamic variability of the corrections (factors of 2 or more) and complex cross-axis interference (nonorthogonality) are anticipated from our observations and those of related studies such as Sarpkaya (1976).

At present the laboratory observations and models needed to derive the required correction procedures are not available. Assuming they can be developed, their verification may be slow and expensive. Further, allowing large nonlinearities before bandwidth limiting quasilinear sensors often leads to subtle error conditions such as found in hot-wire and hot-film velocimetry. Simple electronic "linearization" based on steady-flow performance could actually degrade dynamic-flow accuracy in some situations while unnecessarily complicating the electronics and flow testing. Practical examples of how such "over-correction" might originate are illustrated later (Figures 14, 29, and 30). Since it appears accurate electronic linearization may be difficult to develop, we feel direct sensor linearization should be emphasized during the present stage of ATT design evolution.

3. Streamlined or faired transducer mounts

Streamlined supports would have less pressure drag and consequently smaller flow-defects in on-axis steady flow. Additional mechanical cross-section, however, would complicate dynamic off-axis response and cross-talk. Hardies (1975) (see Figure 5, bottom right) has demonstrated modified steady-flow cosine-response using this approach. Associated dynamic response has not been documented.

4. Transducer stems

This method has been routinely used in anemometers (see Figure 3) at similar Reynolds numbers but in quite different turbulence and oscillatory flow conditions. The wake effect at $\theta = 0^{\circ}$ can be substantially reduced with only a small addition of off-axis cage cross-section. Further evaluation of this approach is proposed in Section VIII.

5. Slanted direct paths

This method (see Figure 5, top right) has been used successfully by Williams and Tochko (1977) for benthic boundary layer Reynolds stress studies. While their particular design

is not intended for wave-zone measurements, alternate geometries with good 3-dimensional response may exist. Preliminary measurements with ring mounted sensors (Figure 5c), however, suggest caution.

6. Three horizontal paths

This method looks promising; see Section VIII for discussion.

7. Longer acoustic paths

This is the basic solution. Since flow-defects asymptotically decrease with distance, doubling the transducer separation while keeping the same size cage bars will nearly halve the acoustically integrated wake errors. High strength materials and small transducers could be developed to increase the transducer support separation to size ratio, while maintaining small rugged instruments. Ratios in the range ~ 20 to 50 might represent a reasonable near-term design goal.

8. Mirrors

Horizontal cosine-response is immediately improved but vertical cosine-response suffers (see Section VII).

9. Small sensor supports

    a. The conflicting roles of sensor-support and mooring-support could be separated. Miniature transducers might be delicately mounted near the center of a slender but rugged structural cage.

    b. A slender central mooring rod with spring-out, umbrella-like transducers might be practical in some applications.

10. Conditional sampling

Correct readings are generally not required continuously, so flow conditions might be selectively sampled. Item (6) above is an example.

11. Combination and other methods

Combination of these and other techniques will undoubtedly evolve with time. Perhaps there is a way to avoid the wakes entirely. It is time again for innovative design.

-23-

VI. Flow Near Cylinders

A. Introduction

In moored applications, errors due to meter-generated wakes are roughly an order of magnitude larger than all other ATT errors combined. To better understand the nature of fluid wakes we digress in this section to review the special case of wakes behind cylinders. Off-axis, accelerated flow around the complex structures of practical current meters will naturally be more complex, but the well-studied cylinder case can help illustrate the nature of the problem and may be useful in certain future designs.

B. Wake Regimes

Figure 9 shows the sequence of fully developed wake regimes behind long, smooth circular-cylinders placed normal to steady flow. The stable regimes shown are similar in planes normal to the cylinder axis while the flow in the transition zones tends to be intermittent and more nearly three dimensional in character. Free-stream turbulence causes transitions to occur at lower Reynolds numbers and may cause stable wakes to "wag" from side to side or become irregular. Cylinder roughness has similar effects. Thus the boundaries between wake types are variable and as will be seen below, different stable wake patterns can exist at the same Reynolds number.

The dimensionless Reynolds number R gives the ratio of inertial to viscous forces acting on particles of fluid. The bulk Reynolds number used here is defined in terms of the cylinder diameter D, flow speed V, and fluid kinematic viscosity ν as

$$R = VD/\nu .$$

At small R the viscous forces dominate and wakes are laminar. At large R inertial effects (fluid accelerations) dominate.

From the left for increasing R (or simply increasing speed for a fixed cylinder diameter and fluid kinematic viscosity) the flow regimes are:

1. Laminar. Flow patterns ahead of and behind the cylinder are alike and free of turbulence. Flow

-24-

speeds are accurately predicted by potential flow theory.

2. <u>Twin vortices</u>. Attached vortices, sometimes called Foppl vortices, form behind the cylinder in columns parallel to the cylinder axis. Stability is strongly affected by upstream disturbances.

3. <u>Laminar vortex street</u>. An irregular but periodic street of laminar vortices forms behind the cylinder.

4. <u>Turbulent vortex street</u>. Regular pattern of periodic turbulent vortices appear in what is known as the "Kármán vortex street." This is the familiar wake regime seen in nature. It is also the wake regime of greatest interest in moored ATT flowmeters.

5. <u>Chaotic wake</u>. Large fluid accelerations lead to a totally disorganized wake. Before 1960 this was thought to be the final regime, since increased accelerations at higher R would probably lead to increased flow disorganization.

6. <u>Thin turbulent wake</u>. Surprisingly, organized structure re-emerges above $R \approx 3.5 \times 10^6$.

Also shown in Figure 9 are the dimensionless cylinder drag coefficient C_D and the reciprocal of the dimensionless Strouhal number S. The slanted lines show the speed versus Reynolds number relation for selected values of cylinder diameter and temperature in fresh water. C_D and S are seen to be nearly constant at 1.2 and 0.2 respectively in this range. Selected values of ν are given in Table 3.

The vortex shedding frequency f is

$$f = \frac{SV}{D}$$

An example frequency scale for D = 1.5 cm and S = 0.2 is shown at the right (Figure 9). This frequency is clearly visible in the ATT signals. In some flowmeters it is used directly as the speed signal. The shedding frequency f can also be used effectively in identifying wake sources. Lateral forces on the cylinder appear at frequency f, while forces in-line with the flow are smaller and appear at 2f.

-25-

Table 3

Kinematic Viscosities in cm^2/sec

Temperature, °C	0°	5°	10°	20°	30°
Pure water	0.0179	0.0151	0.0130	0.0100	0.0080
Sea water					
(35°/₀₀, 0 db)	0.0183			0.0105	
(35°/₀₀, 6000 db)	0.0171				
Air (dry, 1 atm)	0.132		0.141	0.151	0.160

Figure 10 shows developing flow patterns around a cylinder at low Reynolds numbers ($\sim$1 to 100). The camera is fixed with respect to the cylinder and the flow is made visible by aluminum powder spread on the water surface. The motion is started suddenly and is held constant during the photo sequence. Greater time elapses between the last two figures than between the others. Similar photos of internal fluid motion are shown in Taneda (1956). Note the growth of the twin attached vortices and their final transition to vortex shedding. In ATT meters the growing wake leads to reduced response in steady flow as will be shown later (Figure 14).

Figure 11 (after Nishioka and Sato, 1978) shows the cross wake velocity structure (top) and wake length (bottom) for low Reynolds numbers similar to those of the previous figure. Coutanceau and Bovard (1977) give further details.

At higher Reynolds numbers the Kármán vortex street develops. Figure 12 shows a typical surface aluminum powder photo at $R = 2 \times 10^3$. The camera is moving at the wake speed causing the cylinder to appear as a white blur near the bottom center. Note the general shape and size of the wake relative to the cylinder diameter. Notice also the irregular pattern of the wake toward the top of the figure. Very steady laboratory conditions are needed to form wakes of even this regularity. More complex flow will exist around meters moored in surface gravity waves.

Contours of mean flow speeds behind cylinders are shown in Figure 13. The three maps at the left give contours of equal speed for three values of R spanning our range of interest. Panel (d) shows the flow speed at 10° intervals along the radial directions indicated in panel (b). Panel (e) shows the maximum flow-defect directly behind the cylinder ($\theta = 0^{\circ}$) for various values of R. Note that large flow-defects (20-40% less than U_∞) occur even at distances of 10 or more diameters downstream. Expressions for mean far-field speeds ($x > \sim 50$ dia) are given in Schlichting (1968), Heinz (1959), etc.

Panel (f) shows the same effect along the $\theta = 20^{\circ}$ radial direction. The free stream velocity beyond the wake is reached within a few cylinder diameters and the variation with Reynolds number is considerably reduced. The largest integrated flow-defect is equal to an equivalent acoustic path loss of about 1.5 diameters. This equals a 15% loss in a 10/1 separation to diameter ratio instrument, somewhat less than

-27-

that at 20° in Figure 8 (which includes the cylinder bow wake
and end effect). The combined wake effect from several
cylinders can be estimated in the Reynolds number range of
interest by linear superposition in a manner detailed by Bragg
and Suk (1971).

C. Measured Low Speed Response

Figure 14 shows the observed voltage response (scaled in
speed units) of the meter in Figure 6 at very low speed (R =
33). A special low-noise tow carriage started at t = 0,
traveled at uniform speed, and stopped 5 to 6 minutes later
having traveled only 70 to 80 cm, or 7 to 8 probe separations.
Before t = 0, the three traces show very low meter/tank system
noise (about 0.1 mm/sec peak-to-peak in a 15 Hz bandwidth).
The larger abrupt changes are caused by an electronic "bug."
Carriage noise (0.2 mm/sec peak-to-peak) exceeds that of the
meter just after start up; total noise grows only slightly with
time indicating the low turbulence level of the wake at R =
33. Anticipated flow pattern (not observed directly) is shown
in Figures 10d and 10e and at the dot above R = 33 in Figure 9.

The top and bottom panels show the response with the
acoustic axis aligned with the flow ($\theta = 0°$). Note large
response reduction as the wake builds with time (distance).
Compare also the general nature of the acoustic response with
the wake evolution of Figure 10. The negative stop transient
at t $\overset{\sim}{\sim}$ 5 min equals the velocity defect just before the stop,
further demonstrating that the speed reduction is caused by the
entrained water of the wake, not by acoustic or electronic
effects. The flow defect at 4 cm/sec is only ∿0.3 of the peak
signal, compared with ∿0.6 here.

In the middle panel the flow is at 20° to the acoustic
axis. The speed reduction is much less, giving a net response
which exceeds that at $\theta = 0°$ except near the carriage start
(t ∿ 0). The "overshoot" at the carriage stop is
correspondingly reduced.

The bottom panel is the same as the top panel except the
water ∿1 m upstream was gently stirred with a pencil-sized
dowel at time A. The disturbance grows with time finally
obliterating the negative stop transient (t ∿ 5.6 m). The
effect illustrates the importance of low tank turbulence in
such demonstrations. It further suggests that laboratory and
open ocean conditions will differ.

-28-

D.   Dynamic Wake Effects

The special case of fully developed wakes behind stationary cylinders in uniform, turbulence-free flow (treated above), may not be very representative of wakes from yawed cylinders in accelerated, turbulent, three dimensional ocean boundary layers. Effects of surface following mooring accelerations will further complicate the flow. While ocean wave dynamics have been studied intensively in recent years, insufficient detail is available to guide ATT flowmeter design. Peculiar effects reported, however, suggest complex behavior with variable mean properties. Zdravkovich and Namork (1977), for example, note vortices shed from only one side of a cylinder, while laboratory tests indicate large changes in C_D.

Sarpkaya (1976) treats variations in drag and mass coefficients of smooth cylinders placed normal to two dimensional oscillatory flow with no mean component. His results show strong dependence (factors of 2) on the ratio of oscillation size to cylinder diameter (Keulegan-Carpenter number). King (1977) provides additional information on oscillating flow with a mean component.

Bell (1979) reviews effects of free-stream turbulence on C_D and notes changes (again factors of 2) with turbulent intensity. His analysis suggests similar variation with turbulent scale. Since the total drag in ATT applications is dominated by the pressure-drag, which in turn is closely related to the wake flow defect, we can anticipate that the ATT integrated flow defects will vary (in some manner) with C_D. (Indeed, the ATT technique might be useful in studying drag since both the shedding frequency and flow defect are sensed directly.) Although dynamic flow observations are still limited, the large observed variations in mass and drag coefficients suggest due caution in predicting three dimensional ocean wakes from mean steady-state two dimensional conditions. Direct acoustic observations of flow defects in waves are needed.

VII. **Mirror-Type Meters**

A. **Section Overview**

Two mirror-type ATT meters (Figures 15-16) were developed. Test results of three versions of the second (NBIS) design are shown in this section and can be summarized as follows.

1. **Flow intensification** of about +0.5 cm/sec is observed at speeds below about 15 cm/sec (Figures 17 and 22).

2. **Zero flow** noise is less than 1 mm/sec peak-to-peak (Figure 18).

3. **Zero flow stability** for 63 days has a standard deviation of 1 mm/sec (Figure 18f).

4. **Gain stability.** No gain changes were noted during the 2 months of tests. Erratic behavior of one axis developed after nine months.

5. **Linearity.** In the special case of steady horizontal flow with one pair of transducers aligned to the flow ($\theta = 0°$) linearity is better than $\pm 2\%$ (a measurement limitation) or 0.5 cm/sec, whichever is larger (Figure 22). Such values, however, do not represent overall accuracy since much larger errors are introduced by meter orientation, vertical flow, and dynamic effects.

6. **Horizontal cosine-response.** Speed and direction rms errors are 4% (0.2 cm/sec at 5.3 cm/sec) and $1.6°$ respectively (Figures 19 and 20).

7. **Vertical cosine-response.** Flow blockage and mirror-type acoustics combine to give poor vertical cosine-response (Figures 23-27). Variations of meter shape change the response but do not correct it (Figures 24-25). Differential blockage of acoustic half-paths contributes to the errors (Figures 26-27).

8. **Model** calculations predict large errors in waves (Figure 28). Provisional tests (Figure 29) suggest errors grow with wave amplitude.

9. **Measured dynamic response** to horizontal oscillation shows significant additional errors (Figure 30).

Tests indicate stable linear response except in mean flows with either vertical flow components or in-line horizontal oscillations. Low mean speed response is both predicted and observed in dynamic flow. Large angle errors are predicted. Detailed discussions of the tests follow. Possible improved designs are proposed in the next section.

B. Instruments Tested

Figure 15 shows the first WHOI moored ATT current meter constructed in 1975 and described by McCullough (1976). Laboratory tests showed long-term zero and gain instabilities later resolved by Gytre (1979). Moored intercomparisons of this ATT meter and a 3-axis Marsh McBirney, Inc. electromagnetic sphere showed large relative velocity differences in waves (see McCullough, 1978). Independent laboratory tests on a similar Gytre meter are given by Collar and Gwilliam (1977). Evans et al. (1979) describe a profiling application.

Figure 16 shows a second mirror-type ATT meter built by NBIS and tested at WHOI in 1978-1979. Test results shown in Figures 17-24, 27-29a and B1-B2 are from this single instrument. How nearly its performance represents the instrument class has not been determined, but is suggested by the results of Figure 25, 29b, 30, and those of Appell (1977). An index of tests is given in Appendix D.

C. Tests of the NBIS Current Meter

1. Flow acceleration

Figure 17 illustrates low-speed flow acceleration in the acoustic sense volume. Flow is from the left at 1.53 cm/sec. Photo sequence made in the WHOI flume at 5 sec intervals shows the bending of a single vertical potassium permanganate dye column as it passes the instrument center-line. As in Figure 15, the acoustic sense volume is located just below the finger-like transducer supports and above the short center post holding the acoustic mirror. One acoustic axis is aligned with the flow ($\theta = 0^\circ$). Measurements of this sequence indicate 16% greater speeds in the sense volume than upstream of the meter. The geometric cross-section of the meter blocking the flow was 6.4% of the free flume cross-section. Similar blockage also causes a 6% increase in apparent sensitivity at higher tow speeds (Figures 21-22).

2. Sampling

Data in Figures 18-24, 29a, and B1-B2 were taken in low-speed, steady flow in the WHOI flume. With the ATT meter in place, the flume speed was allowed to equilibrate (~1 hour) before each day's run. The small drogue seen resting against the meter in Figure 16 (lower right) was used to establish the mean Lagrangian speed upstream of the ATT meter. The drogue size and depth were made approximately equal to that of the acoustic volume. Drogue speeds were measured manually with permanent meter lines marked on opposite walls of the tank and a calibrated stop watch. Dye streaks placed around the drogue were used to estimate drogue slippage corrections. Dye was also used to monitor unwanted shears in the flume. Repeated current meter measurements were made to monitor overall test stability. Air bubbles, the primary source of systematic error in these ATT meter tests, were routinely removed by brushing.

Analog voltages from each ATT axis were independently averaged with an external, single-channel V/F (voltage to frequency) converter and gated electronic counter. The 10-second mean V/F frequencies obtained were manually recorded, averaged, and corrected for zero flow bias. Error bars for data points in the figures represent plus-minus one standard deviation of typically 10 such 10-second means made at each instrument setting. The interval between 10-second observations was usually several seconds (long enough to read, record, and restart the counter), but often minutes or even days elapsed. The 72 vector means of Figure 19, for example, were derived from more than 2000, 10-second averages spaced over 3 days. Rotation and tilt angles were set manually by means of a horizontal index circle, special tilt scales, various guy ropes, fixtures, etc. Repeatability of ~1 mm/sec is suggested by the observational scatter.

3. Zero stability

a. Short period stability

Response to no-flow conditions are shown in Figure 18. The analog voltages from one acoustic axis in very still water are reproduced from strip chart recordings for periods of 10, 20, 200, and 2000 seconds. The water used had been in thermal equilibrium with the room and meter for several days and was allowed to stand overnight prior to the tests shown. Air bubbles were removed. The cause of the dominant 2.1 Hz signal seen best in traces (a) and (b) is unknown.

-32-

Trace (e) shows signal modulations caused by acoustic reflections in the tank. The effect is produced by slowly changing the water level (by siphoning, draining, volume change, or the like). This technique allows simple evaluation of unwanted acoustic reflection in a test tank. Earlier tests at 0.8 MHz were dominated by larger reflections of this nature and lead to the higher acoustic frequency (1.6 MHz) now used. Additional zero flow data for this instrument are shown in Appendix B, Figures B-1 and B-2.

b. Temperature, vibration, and fouling

Provisional temperature tests show no change larger than one cm/sec over the range 5° to 20°C. No systematic vibration tests were made, but handling vibration has not been a problem to date. Preliminary fouling tests suggest no appreciable sensitivity to small barnacles and other growth on the transducers. Additional temperature, vibration, and fouling tests are needed.

c. Long period stability

The bottom trace (Figure 18f) shows the two-axis stability over a 63-day period in the laboratory. Points shown are the means of 20 or more 10-second V/F averages. The standard deviation is 1 mm/sec. (Note, the speed scale in trace (f) is about half that above.) The measurements were made both in still water and by repeated 180° meter rotations in steady low speed (5 cm/sec) flume flow. In the second "dynamic-zero" method the average of the positive and negative readings of each 180° pair gives the response at zero-flow under the assumptions of constant flow speed during the test pair, and linear meter response through zero. In practice, the dynamic method is faster and more repeatable than the no-flow method. Bubbles are less troublesome, waiting periods are greatly reduced, and local shear effects are more easily corrected. The dynamic-zero method also lends itself to use in simple flumes since the absolute speed is not critical, only its consistency during each 180° rotation. The response in near-zero flow was periodically used in (f) as a check of the dynamic-zero assumptions. Dye was used to estimate a residual flow correction, but due to three dimensional flow structure at near-zero speed, such corrections are difficult to make accurately.

d. System test

Tests of zero stability (Figure 18f) make a strong check of ATT electronic and sensor performance. Unlike mechanical

-33-

sensors in which zero-flow requires no sensor response, accurate zero-flow response in ATT meters requires accurate mid-scale electronic response. That is, for ATT meters to operate accurately near electronic mid-scale (the zero-flow condition) many of their components must function properly.

4. Horizontal cosine response

Figures 19-20 show low speed horizontal cosine response in polar coordinates, x-y components, and speed/direction anomalies. Tests were made in the WHOI flume at a nominal speed of 5.3 cm/sec. The measured response (dots) is higher than calculated (solid circle) due to flow acceleration discussed in (2) above. Wake effects of the cage tie-rods (at 45°, 135°, etc.) and transducer supports (at 0°, 90°, etc.) are evident. The tie-rod at 135° was temporarily removed giving the response indicated by the x's between 90° and 180°. The transducer "shadows" at 0°, 90°, etc., were not seen in an earlier meter with a rounded cylinder supporting the four transducer fingers. Error bars (Figure 20) indicate typical ± rms variations for the flume/instrument combination. The somewhat larger error bar with tie-rod removed (bottom panel) is not understood.

Peak-to-peak horizontal cosine-response speed error at 5.3 cm/sec is about ±6% of the mean reading, closely comparable to the 5.5% mean for three earlier design meters tested by Appell (1978) at speeds of 13 and 51 cm/sec (tie-rod Reynolds numbers of ∿500 to 5000).

5. Linearity (steady flow)

Figure 21 shows the conventional calibration function in steady flow. Tank size effects and least squares regression equations in fresh water at 20°C are also shown. (See Figure 22 for tank dimensions.)

Figure 22 combines various linearity estimates for speeds up to 68 cm/sec. The "gain" or ratio of meter response to flow speed should ideally be constant. Thus departures from horizontal in the figure represent nonlinear response, while vertical displacements from the "calculated" dash line represent differences between predicted (see Appendix C) and observed response. Since velocities in the lee of obstructions such as the tie-rods are expected to be smaller than the free-stream velocity, it is surprising that the gain is generally larger than calculated. Clearly flow intensification from the instrument cylinder end-effect more than off-sets the flow defects of the rods.

-34-

The upward slope of the "small tank" data is apparently the result of flow blockage in the WHOI tank since the trend disappears in the larger Scripps tank. The upward trend in both tanks below ∿15 cm/sec is thought to be an instrument hydrodynamic effect seen also in Figure 8 under similar conditions but with a rather different style ATT meter.

Response with the 135° tie-rod removed is shown at (A). The range of all observations in Figures 19 and 20 is shaded at (B). All other measurements in Figure 22 are with one axis aligned with the flow (θ = 0°). The single dye calibration value from Figure 17 (θ = 0°) is shown at (C). The flow speed used to calculate the gain was that of the dye in the sense volume rather than the usual upstream flume speed. Since small systematic bias errors are difficult to evaluate, arbitrary ±0.5 cm/sec dashed lines have been added for reference.

6. Vertical cosine-response

Figures 23 and 24 give the vertical cosine-response of the same instrument. Flume speed was 7.5 cm/sec. The response is seen to be strongly influenced by both meter rotation (θ) and meter tilt (α).

In Figure 24 left, flow is blocked by pressure case and transducer housings as indicated in the sketch below. Response (A) is affected more than (B) due to increased blockage by the transducer housings. At the right, response (A) is again worse than (B) since the scoop-like end-bail presents greater cross-section to the flow (seen best in Figure 27). Errors of opposite sense in the range ±30° tilt may tend to compensate each other in some but not all wave flow (see model discussion, McCullough, 1978).

Reverse flow indication at (C) is surprising and conflicts with simultaneous dye observations showing no reverse fluid motion. Values along line (D) show 5° steps of rotation between orientations (A) and (B).

Figure 25 shows similar vertical cosine-response data for NBIS meters with two slightly different shapes indicated in the insert sketches. Changes are: the meter at the top has a shorter transducer support cylinder and longer mirror stem; the meter at the bottom has a flat end-cap and longer transducer cylinder. All three cages (Figures 24, 25 top and 25 bottom) are the same size.

-35-

Figure 25 top shows two negative response regions. Response of three meters tested at one speed was similar. Figure 25 bottom left shows large scatter in the wake of the flat end-cap. No discernible speed dependence was noted at 10, 31, and 51 cm/sec tow speeds.

Variations in response and lack of speed dependence suggest improved performance in steady tow may be possible at negative tilt angles. The relative importance of end-bail and mirror wakes (right) has not been evaluated but can be readily determined by removing the end-bail and/or changing the mirror size. An open cage such as in Figure 15, but with a longer mirror stem and smaller mirror, presumably would improve the tilt response.

Measurements shown in Figure 25 were made in the David Taylor Naval Ships Research and Development Center (DT-NSRDC) #1 tow basin at Carderock, Maryland. The large indoor basin (shown in Figure A-4) is 15.5 m wide, 3.3 and 6.7 m deep, and 275 m long. The slosher used is described by Kalvaitis (1978). (Upper panel data are by G. Appell, lower panel data are by J. McCullough.) Sampling was made automatically with an HP 9825 data logger at ~20 observations per cycle over an integral number of cycles (typically 10).

For comparison, representative vertical cosine-response functions for EM sensors can be found in Griffiths et al. (1978), Marsh McBirney, Inc. (1975), and Olson (1972); those for propellers in Shonting (1967), Gill and Michelena (1971), Davis and Weller (1979), and Weller and Davis (1979).

7. Acoustic half-path model

a. Flow blockage (large α)

Figure 26 suggests how the negative (reverse flow) portions of the vertical cosine-response curves (Figures 24 and 25) are generated. Each single acoustic axis (A) is composed of 2 "half-paths" separated by the acoustic mirror (see dot and dash segments in large instrument sketch). Each half-path generates a signal with amplitude equal to that of the total axis, but displaced by $\pm60°$ from it. The net response is thus the sum of two large out of phase signals. If either the direction or speed of the flow differs in the two half-paths, large differences including sign changes can occur in the observed sum.

One hypothetical differential gain variation (speed and/or direction) is shown at (B) with resulting response shown at

(C). Instrument sketches (bottom) show orientation of various obstructions to help visualize how differential half-path flow might originate.

Figure 27 shows a dye trace illustrating the proposed mechanism at a worst case tilt angle of +70°. Flow is from the left at 1.5 cm/sec. The dye column was about 3 cm in diameter (the instrument case is 19 cm in diameter) and nearly vertical before reaching the meter center-line. Lower acoustic half-path (dash line in previous figure) is seen to be directly in the wake of the mirror and its support while the upper half-path is relatively unobstructed. The combined effect is suggested as the mechanism causing the observed negative meter response near +70° tilt in Figures 24-25.

b. Flow bending (small α)

If the meter is inclined at angle α to the flow and the integrated mean flow along the first half-path has horizontal component u, and vertical component w, and the downstream half-path has components u + Δu and w + Δw, then the response R for the NBIS geometry is

$$R = [u \cos \alpha - w \sin \alpha] + [\Delta u \sin (\alpha + 30°) + \Delta w \cos (\alpha + 30°)]$$

where the first term in brackets is the desired flow component parallel to the mirror and the second term contains signals due to changes Δu and Δw. In the range α = $\pm$30° tilt (Figure 24), modeled angular flow changes of a few degrees account for the observed net errors. Dye observations indicate flow distortion of the correct sign and approximate magnitude needed to account for the observed response.

8. Modeled dynamic response

Figure 28 shows the envelope of speed and angle errors predicted from the observed steady flow vertical cosine-response (Figures 23-24) and the large-wave kinematic model of McCullough (1978). Response in small waves will generally be more accurate. The overall prediction, however, is for increasingly lower mean readings and large direction errors as vertical flow components increase relative to the horizontal mean flow.

9. Wave amplitude effect

Figure 29 compares measured response to 23 and 60 cm amplitude straight-line sloshing along the instrument cylinder

-37-

axis. Response to the larger amplitude slosh (bottom) compares
favorably with predicted error estimates. The smaller scale
motion (top) does not. Inserts show instrument size relative
to track of motion at signal-to-noise ratio of 0.5.
(Length-scale effects are discussed further in Appendix A.)

10. Measured horizontal dynamic response

Figure 30 shows the measured mean response to steady tows
combined with linear horizontal oscillations at angle ϕ to the
tow. Data were taken at DT-NSRDC with the equipment described
above in section 6. No vertical motions were generated by the
slosher in these tests. Thus if dynamic effects were
negligible the response would lie along the horizontal line
$V/V_0 = 1$ to within the error bounds indicated by the
horizontal cosine-response (Figures 19-20). When the mean
speed exceeds the maximum oscillator speed ($V_0/a\omega > 1$), new
(undisturbed) water is traversed at all times and the measured
and tow speeds generally show such agreement for all slosher
orientations. When tow speeds are smaller than oscillating
maximum speed ($V_0/a\omega < 1$), indicated speeds also agree with
steady carriage speeds except when the tow and the slosh are
collinear ($\phi = 0^{\circ}$) or nearly collinear ($\phi = 15^{\circ}$). (Note:
the signal-to-noise ratio used in this figure is relative to
$a\omega$, the maximum oscillatory speed, instead of $a\omega/\sqrt{2}$ as used
elsewhere in this report.)

Reducing the peak-to-peak size of the oscillation from 4 ft
to 2 ft (120 to 60 cm) at $\phi = 0^{\circ}$ reduces the collinear error,
further indicating its dynamic origin. The reduced response is
apparently caused by secondary flow induced in the tow tank by
the meter, i.e, the stationary water assumption for the tank is
not valid. The importance of such effects in moored
oceanographic applications has not been determined.

The results suggest that peak wave velocities measured when
the vertical flow component is small may have relatively small
errors except when the wave and mean flows are essentially
coplanar.

VIII. New Cage Designs

A. Introduction

In this section three new ATT designs are proposed:

1. A simple alternate cage design compatible with present electronics.

2. A higher performance cage requiring new electronic and transducer design.

3. An in situ calibration standard used to evaluate moored current meters.

Proposals for such designs go back more than a decade, but the concepts are still "new" in the sense that they are as yet untested.

B. New meters

1. Figure 31 shows a four-bar sensor-cage compatible with existing circuitry. Two direct acoustic paths (no mirror) are used in the open cage. Short tubes supporting the transducers protrude diagonally inward several rod diameters to avoid much of the unwanted wake flow-defect shown in Figure 13. Longer diagonal rods, tapered near the ends, might reduce total mean errors further. A similar design is shown in Figure 3a.

2. An electronically more elaborate but potentially more accurate 3-bar design is shown in Figure 32. Three direct paths are measured. The current directions relative to the cage are estimated, and the acoustic path in the largest wake is determined by table look up and is discarded. The other two paths and compass are then used to determine the east-north flow components prior to vector averaging. A correction for cage rotation rate (derived from compass readings) is needed since the acoustic paths do not intersect the vertical rotation axis of the cage. While the processing is more complex, the associated hardware using microprocessor or other LSI circuits may be no greater than with other cage designs. In either design, inclined acoustic paths can be used to measure the vertical flow components. The general design problem is similar in some ways to that of anemometers operating near towers (Gill et al., 1967, etc.).

3. An in situ standard meter

The need for an *in situ* standard meter for calibration and performance evaluation is well recognized (i.e., McCullough, 1978 and 1979). The standard meter must be exposed to the same mooring motion and ocean flow without disturbing the flow past the meter being evaluated. All sensors should have similar length and time scales. As with other calibration devices the standard meter may be more elaborate, harder to handle, more expensive, etc., than meters used for routine observations.

For this purpose we propose mounting cages such as shown in Figure 32 both above and below the candidate meter. Small cables connect the two standard cages and candidate meter to a remote data logger below. All sensors are tortionally coupled and share a common compass. Each cage (of either the 4 or 3 bar type) uses one horizontal and two inclined acoustic paths in each 2-bar plane. Thus in the dual 3-bar configuration there are

(3 acoustic paths per plane)(3 planes per cage)(2 cages)
= 18 acoustic paths in all.

Redundant paths in each cage are used to find u, v, and *their* error bounds. Vertical shear and mean flows at the central meter being tested are estimated from the upper and lower cage observations. Extra acoustic paths allow detection of partial hardware failures and provide back-up redundancy. *In situ* checks of system performance are included in the basic design.

The data logger should allow multiplexed inputs from the meter being tested and low data rate telemetry to monitor performance following launch. Standard meter and tested meter data are logged simultaneously on the same recorder along with temperature measurements at the three sensor levels. Moored tests up to about 3 months duration are needed to allow representative wave and mean flow combinations in one deployment. Laboratory, model, and ocean tests of this and the other designs proposed will be needed. Comparative merits of this concept with alternate backscatter techniques should be evaluated.

IX. Conclusion

Considerable progress has been made in ATT technology in the last half century and particularly in the last decade. Problems of cost, size, power consumption, and stability have become manageable for moored applications. The remaining problem of flow interference along the acoustic path, however, must be solved if the linear-system advantages inherent in ATT sensors are to be realized. Analysis of the general problem and possible solutions suggests that dynamic performance exceeding that of present techniques is feasible. Continued development including an in situ moored standard is encouraged.

Acknowledgments

References

Ametek. Doppler Sonar Navigator. Ametek Straza Division, 790 Greenfield Drive, El Cajon, CA 92022.

Andermo, N. I. and K. G. Masreliez, 1978. Acoustic Log, U. S. Patent 4,068,207 (assignee: Jungner Instr., Solna, Stockholm, Sweden).

Appell, G. F., 1978. A review of the performance of an acoustic current meter. Proc. of a Working Conf. on Current Measurement. W. Woodward, C. N. K. Mooers, and K. Jensen (editors). Tech. Rep. DEL-SG-3-78 University of Delaware, Newark, DE 19711, 35-58.

Barakat, R. and T. E. Buder, 1979. Remote sensing of crosswind profiles using the correlation slope method. J. Opt. Soc. Am. 69(11), 1604-1608.

Barrett, E. W. and V. E. Suomi, 1949. Preliminary report on temperature measurements by sonic means. J. Meteorol. and Atmos. Sci., p. 273.

Batchelor, G. K., 1979. Private communication.

Beardsley, R. C., W. Boicourt, L. C. Huff, and J. Scott, 1977. CMICE 76: A current meter intercomparison experiment conducted off Long Island in February-March 1976. WHOI ref. 77-62, 123 p.

Beaubien, D. J., A. Bisberg, and A. Pappus, 1966. Cambridge Systems, Inc., Final Report No. AFCRL-66-650.

Bell, W. H., 1979. The influence of turbulence on drag. Ocean Eng., 6, 329-340.

Bovsheverov, V. M. and V. P. Voronov, 1960. Acoustic anemometer. Izv. Geophys. Series, 6, 882-885.

Bovsheverov, V. M., B. M. Koprov, and M. I. Mordukhovich, 1973. A three-component acoustic anemometer. Izv. Acad. Sci. USSR Atmos. Oceanic Phys, 9(4), 434-437.

Bragg, G. M. and J. K. Suk, 1971. Arbitrary mean flow in adverse pressure gradients. J. Basic Eng., Trans. Am. Soc. Mech. Eng., 12, 495-500.

-43-

Clutter, D. W., A. M. O. Smith, and J. G. Brazier, 1959.
Techniques of flow visualization using water as the working
medium. Douglas Aircraft Co. Report No. ES 29075.

Collar, P. G., 1978. Near-surface current measurements from a
surface following data buoy (DB1). Parts I and II. Ocean
Eng., 5(3), 181-196.

Collar, P. G. and T. J. P. Gwilliam, 1977. Some laboratory
measurements of an acoustic current meter developed at
Christian Michelsen Institute, Norway. Inst. Oceanogr. Sci.
Rep. No. 47, 37 pp.

Coutanceau, M. and R. Bovard, 1977. Experimental determination
of the main features of the viscous flow in the wake of a
circular cylinder in uniform translation, Part 1 steady flow,
Part 2 unsteady flow. J. Fluid Mech. ,79(2), 231-272.

Davis, R. and R. Weller, 1979. Propeller current sensors.
NATO text, Instr. and Methods in Air-Sea Interactions,
Ustaoset, Norway.

Dickey, F. R. and J. A. Edward, 1978. Velocity measurement
using correlation sonar. IEEE, Plans-78, Position, location
and navigation symposium, 255-264.

Eisenstein, J., K. C. Clark, and F. D. Carlson, 1945. Sonic
true airspeed indicator, Vols. I and II. Harvard Electro-
acoustic Lab. OSRD Report No. 5369 and 5370, 64 and 80 pp.

Evans, D. L., H. T. Rossby, M. Mork and T. Gytre, 1979.
YVETTE-a free-fall shear profiler. Deep-Sea Res., 26,6A,
703-718.

Fizeau, M. H., 1851. Sur les hypothèses relatives a l'éther
lumineux. Ann. Chim. et Phys., (3), 57 (Dec. 1859), 385-404.
(Also Comptes rendus, 33, p. 349 (1851).)

Galileo, G., 1638. Two new sciences. The Macmillan Co., 1914
(also Dover series publ.).

Gill, C. G. and E. Michelena, 1971. An improved biaxial water
meter. Proc. 14th Conf. Great Lakes Res., 681-689.

Griffiths, G., P. G. Collar, and A. C. Braithwaite, 1978. Some
characteristics of electromagnetic current sensors in laminar
flow conditions. Inst. Oceanogr. Sci. Rep. No. 56, 48 pp.

Gytre, T., 1976. The use of a high sensitivity ultrasonic current meter in an oceanographic data acquisition system. Radio Elec. Eng., 46(12), 617-623.

Gytre, T., 1979. The travel time difference current meter. NATO text, Instr. and Methods in Air-Sea Interactions, Ustaoset, Norway.

Hanson, F. B. and P. D. Richardson, 1968. The near-wake of a circular cylinder in crossflow. Trans. AIME 68-FE-5, 1-8.

Hardies, C. E., 1975. An advanced two-axis acoustic current meter. Off-Shore Tech. Conf. Paper No. 2293.

Hersey, J. B., 1977. A chronicle of man's use of ocean acoustics. Oceanus, 20(2), 8-21.

Hinze, J. O., 1959. Turbulence. McGraw Hill, 586 pp.

Horst, T. W., 1973. Corrections for response errors in a three-component propeller anemometer. J. Appl. Met., 12, 716-725.

Hunt, F. V., 1954. Electroacoustics: The analysis of transduction, and its historical background. Harvard Monographs in Applied Science, No. 5. Harvard Univ. Press, Cambridge, U.S.

Hunt, F. V., 1978. Origins in acoustics. Yale Univ. Press, New Haven, CT, 240 pp.

Kaimal, J. C., 1979. The sonic anemometer. NATO text, Instr. and Methods in Air-Sea Interactions, Ustaoset, Norway.

Kaimal, J. C. and J. A. Businger, 1963. A continuous wave sonic anemometer-thermometer. J. Appl. Met., 2(1), 156-165.

Kaimal, J. C., J. T. Newman, A. Bisberg, and K., Cole, 1974. An improved three-component sonic anemometer for investigation of atmospheric turbulence. Flow - Its Measurement and Control in Science and Industry, Vol. 1 (Instrument Soc. Amer.), 349-359.

Kalmus, H. P., 1954. Electronic flowmeter system. Rev. Sci. Instr. 25, 201-206.

Kalvaitis, A. N., 1978. The vertical planar motion mechanism. A dynamic test apparatus for evaluating current meter and other marine instrumentation. U. S. Environ. Prot. Agency, Off. R. and D., Doc. EPA-600/7-78-145. Natl. Tech. Serv., Springfield, VA 22161, 37 pp.

Kennedy, L. Z. and J. W. Bilbro, 1979. Remote measurement of the transverse wind velocity component using a laser Doppler velocimeter. Appl. Optics, 18, 17, 3010-3013.

King, R., 1977. A review of vortex shedding research and its applications. Ocean Engineering, 4(3), 141-171.

Kipphan, H. and F. Mesch, 1978. Flow measurement system using transit time correlation. Flow measurement of fluids. North-Holland Publ. Co., 409-416.

Kovásznay, L. S. G., 1949. Hot-wire investigation of the wake behind cylinders at low Reynolds numbers. Proc. Roy. Soc., A198, 174-190.

Kritz, J. and M. J. Howard, 1969. Channel navigation and docking of supertankers. Navigation, 16, 1, 3-20.

Larsen, S. E., F. W. Weller, and J. A. Businger, 1979. A phase-locked loop continuous wave sonic anemometer-thermometer. J. Appl. Meteor., 18, 562-568.

Lawson, K. D., N. L. Brown, D. H. Johnson, and R. A. Mattey, 1976. A three-axis acoustic current meter for small scale turbulence. Instr. Soc. Am. ASI No. 76269, 501-508.

Lowell, F. C., Jr., 1977. Designing open channel acoustic flowmeters for accuracy, Parts 1 and 2. Water and Sewage Works, 4, 11 pp.

Marsh McBirney, Inc., 1975. Azimuth and tilt response of a spherical electromagnetic water velocity sensor. Tech. Note 2, MMI. 8595 Gov. Circle, Gaithersburg, MD 20760.

Marumo, E., K. Suzuki, and T. Sato, 1978. A turbulent boundary layer disturbed by a cylinder. J. Fluid Mech., 87(1), 121-141.

McCartney, M. L., C. P. Mudd, and R. D. Livengood, 1979. A corrected ray theory for acoustic velocimetry. J. Acoust. Soc. Am., 65(1), 50-55.

McCullough, J. R., 1974. In search of moored current sensors.
Proc. 10th Ann. Conf. Mar. Tech. Soc., Washington, DC, 31-54.

McCullough, J. R., 1976. Moored current meter sensor
development. POLYMODE News No. 12, 6 pp. (unpublished
manuscript).

McCullough, J. R., 1977. Problems in measuring currents near
the ocean surface. MTS-IEEE Oceans '77, 2, 46A1-7.

McCullough, J. R., 1978. Near-surface ocean current sensors:
Problems and performance. Proc. of a Working Conf. on Current
Measurement, W. Woodward, C. N. K. Mooers, and K. Jensen
(editors). Tech. Rept. DEL-SG-3-78, University of Delaware,
Newark, DE 19711, 9-33. (Also WHOI TR-79-92.)

McCullough, J. R., 1979. Techniques of measuring currents near
the ocean surface. NATO text, Instr. and Methods in Air-Sea
Interactions, Ustaoset, Norway.

McCullough, J. R. and W. E. Terry, 1978. Performance of an
oceanographic Doppler flowmeter. WHOI draft manuscript.

Middleton, F. H., 1955. An ultrasonic current meter for
estuarine research. J. Mar. Res., 14(2), 176-186.

Mitsuta, Y., 1966. Sonic anemometer thermometer for general
use. J. Met. Soc. Japan, 44, 12-24.

Mitsuta, Y., M. Miyake, and Y. Koboni, 1967. Kyoto Univer.
Internal Rep.

Miyake, M., R. W. Stewart, R. W. Burling, L. R. Tsvang, B. M.
Koprov, and O. A. Kuznetzov, 1971. Comparison of acoustic
instruments in an atmospheric turbulent flow over water.
Boundary Layer Met., 2, 228-245, D. Reidel Publ., Dordrecht,
Holland.

Morgan, M. G. and K. L. Bowles, 1968. Cross-correlation and
cross-spectral methods for drift velocity measurements.
Science, 161, 1139-1142.

Munk, W. and C. Wunsch, 1979. Ocean acoustic tomography: a
scheme for large scale monitoring. Deep-Sea Res., 26A, 123-161.

Newhouse, V. L., E. S. Furgason, G. F. Johnson, and D. A. Wolf,
1978. The dependence of ultrasound Doppler bandwidth on beam
geometry. Purdue University TR-EE 78-39, 38 pp.

Newton, Sir I., 1686. _Philosophiae naturalis principia mathematica_. Motte's revised translation. Univ. Cal. Press, Berkeley, CA (1960).

Nishioka, M. and H. Sato, 1978. Mechanism of determination of shedding frequency of vortices behind a cylinder at low Reynolds numbers. _J. Fluid Mech._, 89(1), 49-60.

Nowak, R. T., 1969. Measurements of currents in Buzzards Bay with an acoustic current meter. Prepared for Ph.D. Thesis, M.I.T., 164 pp.

Olson, J. R., 1972. Two-component electromagnetic flowmeter. _Mar. Tech. Soc. J._, 6(1), 19-24.

Patent Refs. See Table 1.

Pierce, G. W., 1925. Piezoelectric crystal oscillators applied to the precision measurement of the velocity of sound in air and CO_2. _Proc. Am. Acad. Arts and Sci._ (Boston), 60, ?71-3?2.

Pinkel, R., 1979. The use of acoustic Doppler sonar for upper ocean velocity measurements. NATO text, _Instr. and Methods in Air-Sea Interactions_, Ustaoset, Norway.

Prandtl, L., 1927. _J. Roy. Aero. Soc._, 31, 730.

Rayleigh (J. W. Strutt), 1877. _The theory of sound_. Vols. I and II, Macmillan, New York. (Also Dover, New York, 1945.) 480 and 540 pp.

Regier, L. A., 1979. Near surface currents during the LDE. _POLYMODE News_ No. 66 (unpublished manuscript).

Rossby, T., 1975. An oceanic vorticity meter. _J. Mar. Res._, 33, 213-222.

Rowe, F. D. and J. W. Young, 1979. An ocean current profiler using Doppler sonar. _Oceans 79_.

Sarpkaya, T., 1976. In-line and transverse forces on cylinders in oscillatory flow at high Reynolds numbers. _Offshore Tech. Conf._, Vol. 2, paper OTC 2533.

Schlichting, H., 1968. _Boundary-layer theory_, McGraw-Hill.

Shonting, D. H., 1967. Observations of particle motions in ocean waves. Naval Underwater Weapons Res. and Eng. Station, Newport, RI. Tech. Memo No. 377, Vol. 1.

Smith, J. D., 1978. Measurement of turbulence in ocean boundary layers. Proc. of a Working Conf. on Current Measurement. W. Woodward, C. N. K. Mooers, and K. Jensen (editors). Tech. Rep. DEL SG-3-78, University of Delaware, Newark, DE 19711, 95-128.

Suomi, V. E., 1957. Sonic anemometer. Exploring the Atmosphere's First Mile, Vol. 1, Pergamon Press, New York, 256-266.

Taneda, S., 1956. Experimental investigation of wakes behind cylinders and plates at low Reynolds numbers. J. Phys. Soc. Japan, 11, 302.

Tompkins, W. R., R. Monti and M. Intaglietta, 1974. Velocity measurement by self-tracking correlator. Rev. Sci. Instr., 45, 5, 647-649.

Weller, R. A. and R. E. Davis, 1979. A vector measuring current meter (submitted to Deep-Sea Res.).

Williams, A. J., III and J. S. Tochko, 1977. An acoustic sensor of velocity for benthic boundary layer studies. In Bottom Turbulence, Proc. 8th Int. Liege Colloq. Ocean Hydrodynm., Elsevier Oceanogr. Ser. 19, J.C.J. Nihoul, (editor). Elsevier Sci. Pub. Co., 83-97 (WHOI TR-78-4, WHOI Cont. No. 3843).

Wilson, W. D., 1960. Speed of sound in seawater as a function of temperature, pressure and salinity. J. Acoust. Soc. Am., 32, 1377.

Worcester, P. F., 1977. Reciprocal acoustic transmission in the midocean environment. J. Acoust. Soc. Am. 62, 4, 895-905.

Zdravkorich, M. M. and J. E. Namork, 1977. Formation and reversal of vortices around circular cylinders subject to water waves. J. of Waterway, Port, Coastal and Ocean. Div. Proc. Am. Soc. Civil Eng., 103, WW3, 378-383.

Appendix A

A Large-Wave Kinematic Model of ATT Flowmeter Response

A. Introduction

The numeric model of McCullough (1978) is discussed further
here. The model uses the empirically measured steady-flow
vertical cosine-response function to predict mean response in
large wave-like conditions. The calculation is purely
kinematic, but some dynamic effects are introduced through the
experimentally determined vertical cosine function. The model
does not treat length scales, secondary flows, broadband
forcing, etc. The previous sections, however, show that such
effects are not negligible. The model results then should be
considered as engineering estimates of typical errors
introduced by imperfect vertical cosine-response as wave
amplitudes grow large compared with the instrument. To date,
the model predictions have not been adequately verified in the
laboratory.

B. The Model

1. Assumptions

The model assumes:

        a. Known vertical cosine-response as a single-valued
function of the three dimensional flow direction.

        b. As sketched in Figure 1-A, steady mean flow is
combined with single-frequency, fixed amplitude, planar,
vertical, circular or elliptical orbital flow.

        c. Time and space dependent flow effects are
negligible, i.e., wakes, transients, entrainment, turbulence,
broadband excitation, response length scales, variations with
speed (Reynolds number), etc., are not modeled.

Assumption (a) becomes more realistic as the wave particle
trajectories become large compared with the instrument length
scales. Clearly for oscillations of the size of the sensor and
smaller this assumption is inadequate. As demonstrated in
Figures 14, 29 and 30, response may differ markedly from the
steady-state value.

A-1

The monochromatic forcing assumption (b) closely models conventional laboratory tests, but is not representative of typical broadband ocean surface gravity wave flow. It may better represent some types of mooring motion such as that seen at mid-depths on deep-water surface-following moorings.

The last assumption (c) is not independent. It is listed as a reminder of other important effects not included in this first model.

2. <u>Notation</u> (see Figure A-1)

θ ATT sensor azimuth (horizontal plane)

u, v, w Velocity components, w vertical

V_0 Horizontal mean speed (along +v)

ω Angular orbital velocity (constant)

t Time

$a\omega$ Orbit speed in w direction

$b\omega$ Orbit speed in horizontal plane

V_1 Orbit velocity

$\bar{V}_1$ Mean orbit speed

V_R Resultant velocity (mean plus oscillatory)

α Flow altitude (tilt) angle from horizontal

δ Flow azimuth (horizontal plane)

ϕ Azimuth of orbital plane

Other notation not shown in the figure includes:

β Flow angle relative to meter sensors

V Indicated ATT meter velocity

$\bar{V}$ Indicated mean meter velocity

$\bar{V}/V_0$ "Response Ratio" (ratio of measured to true speed)

A-2

$V_o/\bar{V}_1$ Flow "Signal-to-Noise Ratio" (ratio of mean to mean oscillatory speed)

3. Model

Fluid particles move in fixed planar orbits combined with steady mean flow. The orbital plane is normal to the horizontal plane containing the instrument sensors as indicated in Figure A-1. From the figure, the orbital velocity V_1 is

$$V_1^2 = (a\omega \sin \omega t)^2 + (b\omega \cos \omega t)^2.$$

The mean orbital velocity V_1 over each cycle is

$$\bar{V}_1 = (\frac{a^2 + b^2}{2})^{\frac{1}{2}} \omega .$$

For circular motion, $a = b$ and

$$V_1 = \bar{V}_1 = a\omega .$$

For linear vertical motion, $b = 0$ and

$$V_1 = a\omega \sin \omega t$$
$$\bar{V}_1 = a\omega/\sqrt{2} .$$

The components of mean plus orbital velocity $(V_o + V_1)$ are

$$u = V_1 \cos \omega t \sin \phi$$
$$v = V_o + V_1 \cos \omega t \cos \phi$$
$$w = V_1 \sin \omega t.$$

The desired resultant total velocity V_R is

$$V_R^2 = u^2 + v^2 + w^2 .$$

The flow altitude or tilt angle α is

$$\alpha = \sin^{-1} (\frac{w}{|V_R|}) .$$

A-3

The horizontal flow bearing δ is

$$\delta = \tan^{-1} \left(\frac{u}{v}\right) .$$

Let the axis of the current meter transducers be oriented at some angle θ to V as shown, then the flow azimuthal angle β relative to the meter sensors is

$$\beta = \delta - \theta .$$

4. Empirical vertical cosine-response

From steady flow vertical cosine-response measurements we find the empirical weighting function $H(\alpha,\beta)$ such that

$$u_m = H(\alpha,\beta)u$$

$$v_m = H(\alpha,\beta)v$$

where subscripts m denote measured quantities, and α and β are the flow direction angles relative to the instrument sensors.

5. Integration

For small increments of orbit angle $\Delta\omega t$ the numeric model determines the flow attack angles α. The associated resultant flow V_R is then weighted by $H(\alpha,\beta)$. Linear interpolation was used to find $H(\alpha,\beta)$ between measurements. The weighted response around the orbit was integrated numerically to determine the predicted instrument mean velocity $\overline{V}$ (speed and direction).

Computations were made with HP 9830 and HP 2100 digital computers using 5° steps of $\Delta\omega t$ and trapezoidal integration over quarter and full orbits. Other step sizes and integration methods were used as checks.

6. Nondimensionalized response

The predicted instrument response $\overline{V}$ is nondimensionalized by the true mean speed V_0 and plotted versus the non-dimensionalized flow "signal-to-noise ratio." This flow

A-4

"signal-to-noise ratio" as used here describes the ratio of mean to oscillatory flow. (It is not the same as the usual instrument "signal-to-noise ratio.")

7. Special case

An analytic solution was found showing that $\overline{V}/V_o$ is always single valued for $\phi = 0°$ and circular orbits in the range $0 < V_o/\overline{V}_1 \leq 1$ for arbitrary $H(\alpha,\beta)$. Departures from this condition in laboratory experiments thus represent non-kinematic effects. That is, if the response isn't "flat" below S/N = 1 at $\phi = 0°$, dynamic or other effects are present. Fortuitously the $\phi = 0°$ configuration is the easiest to implement in small tanks and is also the configuration in which wake effects are likely to be the most pronounced.

C. Results

Using the vertical cosine-response measurements of Figure 24, extreme and typical values of V/V_o were calculated. The shaded areas of Figure 28 show the results. Typical values (shown as dot-dash lines) were calculated assuming all θ and ϕ are equally probable. (It is curious to note, however, that this definition occasionally leads to "typical" mean values where no actual value exists.)

Additional model calculations are summarized in Figure A-2 for two meter orientations θ, three orbit polarization angles ϕ, and various "shape" values a/b. The end result is: low speeds and large direction errors are predicted in large waves.

D. Limitations

1. Length scale

In order for wakes (and associated instrument errors) to approach that of steady flow, some minimum horizontal particle displacement is required. The horizontal speed S is

$$S = (u^2 + v^2)^{1/2}$$

$$= [(V_1 \cos \omega t \sin \phi)^2 + (V_o + V_1 \cos \omega t \cos \phi)^2]^{1/2} .$$

For new water to enter the sensor volume of width ℓ, some minimum time τ of order

$$\tau = \frac{\ell}{S}$$

is needed. A longer period (perhaps $\sim 3\tau$) will be required for wake stabilization.

For the special case of linear vertical oscillation ($b = 0$, and $S = V_0$), the displacement L per cycle period T is $L = V_0T$; and the flow signal-to-noise ratio (SNR) is

$$SNR = \frac{V_0}{a\omega/\sqrt{2}} = \frac{\sqrt{2}\,V_0T}{2\pi a} = 0.225\,\frac{L}{a}\,.$$

Suppose as in Figure 29a at SNR = 0.44, the laboratory test has

$$V_0 = 15 \text{ cm/sec}, \quad T = 3.0 \text{ sec}, \text{ and } \ell = 12 \text{ cm}.$$

then $L = V_0T = 45$ cm, the number of sensor lengths per oscillator cycle is $L/\ell = 3.75$, and the water in the sense volume is steadily replaced (horizontally) every $360°/3.75 = 96°$. That is, $96°$ of oscillation pass for each transducer length-scale moved horizontally. Clearly the first model assumption (fully developed wakes at all angles) is questionable.

The laboratory results shown in Figure 29a confirm this suspicion. The predicted large wave errors (dashed line) are much greater than those observed. Time plots of the raw instrument and dye traces show that fully developed response does not occur. The slosher, tow carriage, and tank used in this experiment are shown in Figure A-3.

Larger oscillations in Figure 29b, however, show good agreement between modeled and observed response. Slosh period and tow speeds used here were 8, 35; 5, 72; and 12, 35; sec and cm/sec respectively. Maximum flow attack angles did not exceed $\tan^{-1}(a\omega/V_0) = 53°$ for the three points shown. The instrument housing penetrated the surface in these tests. The tow carriage used is shown in Figure A-4. A complete set of dynamic experiments is not yet available.

A-6

To better understand the instrument and model limitations, a full series of tests for one instrument should include at least:

- Zero and gain checks

- Steady-tow vertical cosine-response at different speeds

- Linear vertical sloshing at different scale-sizes

- Circular vertical sloshing at various angles ϕ and scale-sizes, in both orbital directions

- Full time histories of speed, direction, and position.

(Both orbital directions are needed to test pressure case wake effects.)

2. Broadband forcing

If the sensor response were linear, response to broadband forcing could be estimated from superposition of the monochromatic estimates shown. On the other hand, since errors from instrument nonlinearities are present, models with broad frequency and directional spectra should be evaluated directly to test coupled effects and allow more realistic simulation of ocean conditions.

E. Improvements

The kinematic model used here treats only the "geometry" of the flow. Improved error estimates could be found by including:

a. Instrument response length scales

b. Broadband forcing

c. Dynamic effects (wake evolution, entrained water, etc.).

The need for predictive models for instrument design and data interpretation will not necessarily diminish with improved instrument performance. Instrument nonlinearities always exist and the resulting net effect in time/spatially varying ocean flow is seldom obvious.

Appendix B

Example Tow and Flume Signals

Figure B-1 compares ATT towed current meter response with and without the flume flow. The top trace with the WHOI flume running shows generally noisier response but has more rapid adjustment following the ends of the two tows. The bottom trace of two similar tows made in still water shows lower noise levels with longer, less predictable adjustment periods after the tows. (Traces are for $\theta = 0^{\circ}$ with the NBIS #2 meter.)

The decelerated downstream tow response at (a) takes longer to reach its maximum negative value than in the accelerated situation at (b) where the meter is being towed upstream against the flow. Net response at (c) about equals that at (d) unlike the situation at (a) above.

Typical flume turbulence level is seen just before (a). Increased noise after this first downstream tow does not subside appreciably in the 5 min wait between tows (top trace). Characteristic decrease in response during tows shows the long adjustment period required to reach steady state response (see also Figure 14).

General variability of the signals indicates the difficulty of making precise measurements in still and/or moving water with instruments having large geometric cross-section.

Figure B-2 (from an x-y plotter) gives the combined two-axis response of the same instrument. The top panel shows response to flow from 9 different horizontal directions ($\theta = 0$, 45, etc.). Noise is less with flow along x or y axis since tie-rod wakes are aligned and are farther from the acoustic sense paths. The figure helps visualize speed/direction variability of the observed orthogonal x-y flow components in the flume at 3.4 cm/sec.

The lower panel (b) shows to the same scale, the response in "still" water 15 minutes after a tow and (c) after an overnight wait. Expanded time plots of the single-axis noise of the same instrument are shown in Figure 18. Water noise level, however, can be at least an order of magnitude less (<0.1 mm/sec) as suggested by the $t < 0$ portions of the traces in Figure 14.

All sample traces are 30 seconds long. Data were taken in the WHOI flume February 1979 with the NBIS-1, SN-2, mirror-type ATT meter shown in Figures 16, 17, 27, and A-3. Traces in Figures 18, B1, and B2 were reproduced directly from an HP 7046A x-y recorder.

Appendix C

Predicted Calibration of an NBIS ATT Meter

The calibration of ATT meters can be predicted from knowledge of the sound frequency f, the direct water separation ℓ of the transducers, and the sound speed c in water. Measured departures from the calculated value for the NBIS meter are shown in Figure 22.

For this meter the phase change ϕ is related to the velocity v along ℓ by

$$\phi = \frac{4\pi f \ell v}{c^2}$$

where

$f = 1.605 \times 10^6$ Hz

$\ell = 11.0$ cm (external mechanical separation, Model 1 SN2)

$c = 1483$ m/s (fresh water at 20°C and 1 atm).

The electronic phase to voltage conversion constant k_p is

$$k_p = \frac{1000 \ mv}{\pi \ rad} \ .$$

(Model 2 has $k_p = 2000$ mv/π rad.)

The voltage gain constant then is

$$k_v = k_p \frac{\phi}{v} = 4000 \ \frac{f\ell}{c^2}$$

$$= \frac{(4000)(1.605 \times 10^6)(11.0)}{(1483 \times 100)^2}$$

$$= 3.21 \ \frac{mv}{cm/sec} \ .$$

C-1

The reciprocal constant k_S for converting the measured voltage to a speed is

$$k_S = \frac{1}{k_v} = 312 \; \frac{cm/sec}{volt} \quad .$$

Table C-1 lists sound speeds from Wilson (1960) for typical conditions of temperature, salinity and depth. The values R give the percent change of the squared sound speed from that of C_o at 20^oC in fresh water at one atmosphere (i.e., $C_o = 1483.1$ m/s).

$$R = 100\left[\left(\frac{C}{C_o}\right)^2 - 1\right] \quad .$$

To find a new value of k_S multiply 312 by $(1 + R/100)$. For example, at 0° and 3000 m depth (C = 1500 m/s) R = +2.3% so $k_S = 312 \,(1.023) = 319 \; \frac{cm/sec}{volt}$. Extreme values in the table are seen to be -7.5 and +11.6%; larger variations are possible in other ocean conditions.

Table C-1

Sound Speeds and ATT Corrections

Depth/Salinity	In situ Temperature	Sound Speed	Gain Variation
Z,S	T	C	R
m, °/°°	°C	m/s	%
Surface (fresh)	5	1426	-7.5
	10	1447	-4.8
	15	1467	-2.2
	20	1483	0.0
	25	1497	+1.9
	30	1511	+3.8
Surface (35°/°°)	0	1449	-4.5
	5	1471	-1.6
	10	1490	+1.0
	15	1507	+3.3
	20	1522	+5.3
	25	1535	+7.1
	30	1546	+8.6
200 m (35°/°°)	5	1474	-1.2
	10	1494	+1.4
	15	1511	+3.8
1000 m (35°/°°)	3	1479	-0.5
	8	1500	+2.2
3000 m (35°/°°)	0	1500	+2.3
	3	1513	+4.1
6000 m (35°/°°)	0	1554	+9.8
	3	1567	+11.6

Appendix D

Test Index

Table D-1 Index of New Test Data Given in This Report

Figure	Date	Instr. Type	Figure No. Instr. Photo	Test Facility**	Test Type	Flow Type
7	1974	Gytre-1	6	WHOI	Wave tracking	Horiz. in-line slosh
8 top	1974	Gytre-1	6	WHOI	Horiz. cos-resp.	Steady tow
8 btm	1974	Gytre-1	6	WHOI	Calibration	Steady tow
14	1974	Gytre-1	6	WHOI	Length scale	Steady low speed tow
17	1978	*	*	WHOI	Dye	Steady flume
18a-e	1979	*	*	WHOI	One-axis analog	No-flow
18f	1978-9	*	*	WHOI	Zero stability	Flume and no-flow
19-20	1978	*	*	WHOI	Horiz. cos-resp.	Steady flume
21-22	1978	*	*	WHOI	Calibration	Steady tow and flume
21-22	1979	*	*	Scripps	Calibration	Steady tow
23-24	1978-9	*	*	WHOI	Vert. cos-resp.	Steady flume
25a	1977	NBIS 100,200,300	Insert	DT-NSRDC	Vert. cos-resp.	Steady, 3-instr. tow
25b	1979	NBIS-29	Insert	DT-NSRDC	Vert. cos-resp.	Steady, 3-speeds tow
27	1979	*	*	WHOI	Dye	Steady flume
28	1978-9	*	*	WHOI	Model resp.	Orbital
29a	1979	*	*	Scripps	Mooring heave	Dynamic (small amp.)
29b	1977	NBIS-200	Insert	DT-NSRDC	Mooring heave	Dynamic (larger amp.)
30	1979	NBIS-29	Insert	DT-NSRDC	Entrainment	Horiz.-slosh
A-2	1978-9	*	*	WHOI	Model resp.	Orbital (cont.)
A-3	1979	*	*	Scripps	Mooring heave	Dynamic (small amp.)
B-1	1979	*	*	WHOI	Lab techniques	Steady (flume & tow)
B-2a	1979	*	*	WHOI	Analog x-y	Steady flume
B-2b-c	1979	*	*	WHOI	Tank noise	No flow

*NBIS-SN2 shown in Figures 16, 17, 27, and A-3 (sketched in Figures 19, 23, 24, 26, 29a, and A-1).

**WHOI test facility shown in Figures 6, 16; Scripps in A-3; DT-NSRDC in A-4.

Figure 1.

Early ATT flowmeters. Upper panel shows Hartig/Wilcox 1929
patented invention for pipe and open flow. Frequencies of two
transmitters 4 and 68 were separately adjusted to give an
integral number of wavelengths along path (a) between receivers
41 and 44. Flow speed could then be calculated from the two
frequencies, distance (a), and the sound speed.

Lower panel shows "sonic true airspeed indicator" developed
at Harvard Underwater Sound Laboratory (HUSL) during World
War II. ATT device is shown mounted on a Navy K-airship in
1944. Sensor head (insert) used a central 4 KHz CW
transmitter, separate up- and downstream receivers, and phase
detection of air-speeds in the range 0-70 knots. A fabric
tunnel lead from transducer head to processor electronic rack
mounted in gondola at right. Response showed close agreement
with estimated air speed over calibrated course. (From first
Hartig/Wilcox patent (top) and Eisenstein et al., 1945
(bottom).)

FLUSH MOUNTED HEAD

PROJECTED HEAD
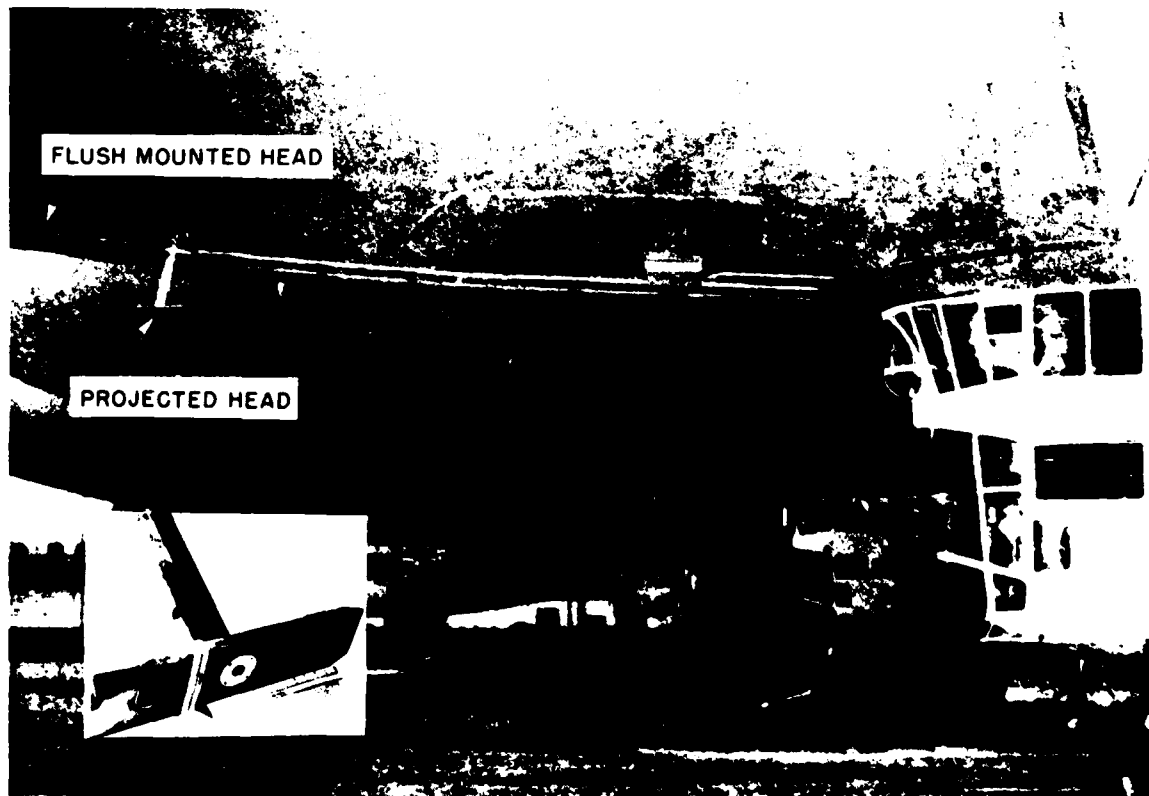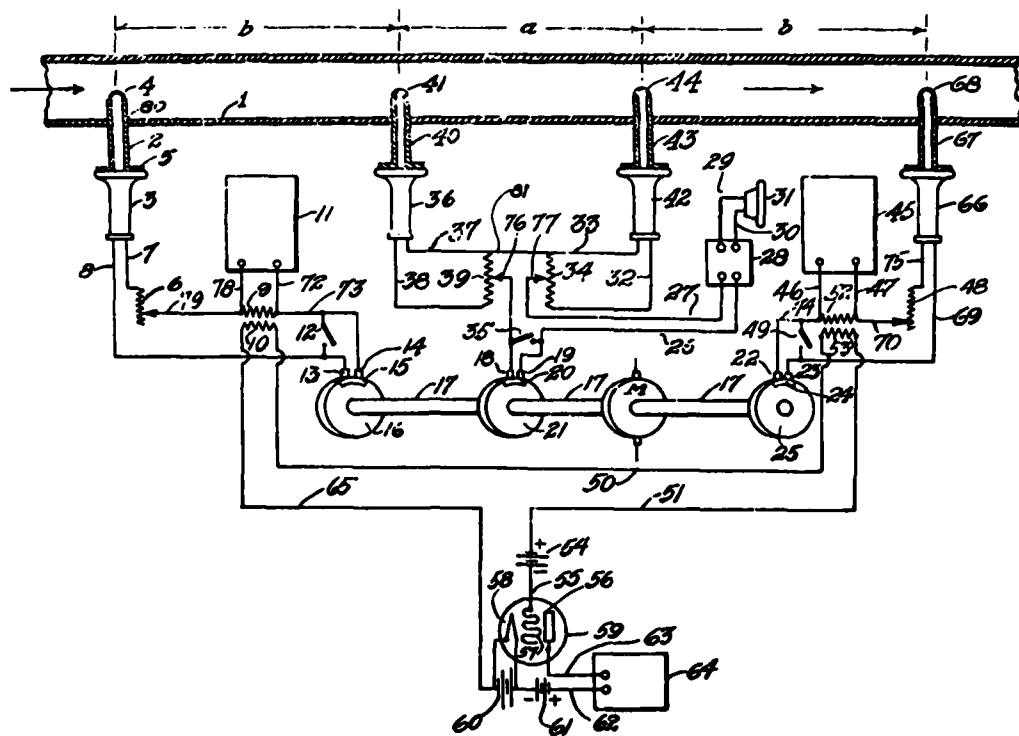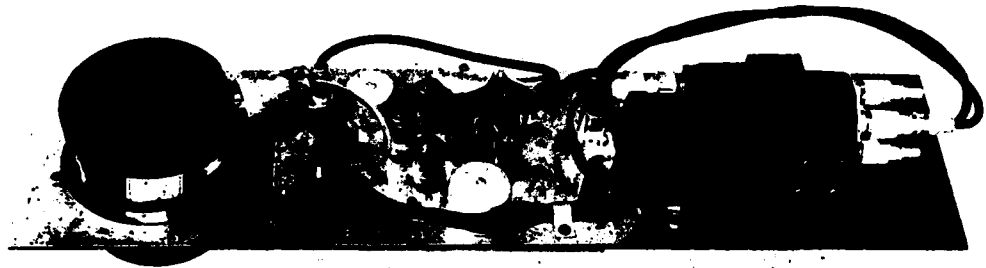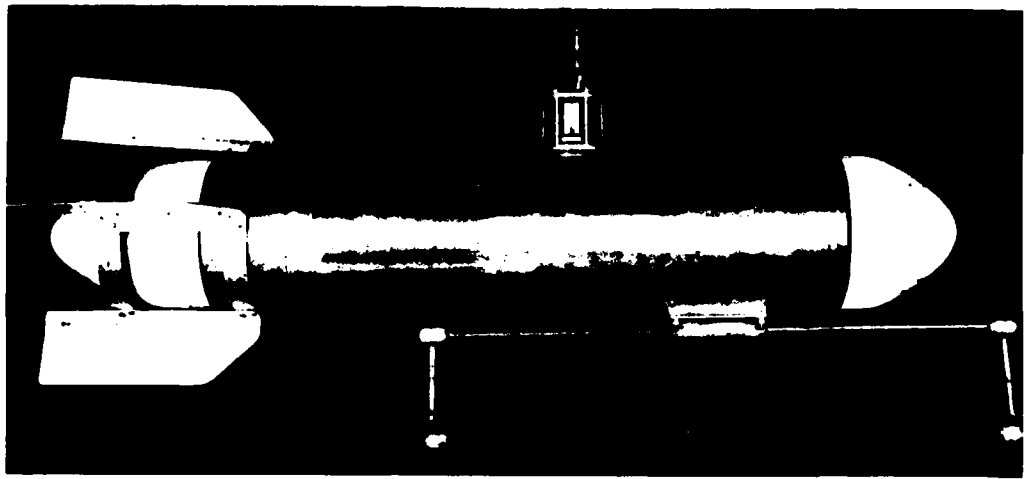
Figure 1

Figure 2.

First moored ATT meter. Fin (top-left) aligned single 55 cm-
long acoustic path into flow. Phase detection of 1 MHz sound
was alternately determined for 13 sec each in the up- and
downstream directions. Chassis (bottom) has from the left:
aircraft magnetic compass-transmitter, vacuum tube phase
circuit, and coaxial switch. Components shown were connected
by an 8-conductor cable to batteries and photographic data
logger in mooring anchor. About 1400 observations could be
autonomously recorded (from Middleton, 1955).

Figure 2

Figure 3.

Sonic anemometers.   a) Open cage, two component meter with four
diagonal transducer stems.   Kaijo Denki Co., circa 1972 (Japan).
b) Two axis nonorthogonal sensor array with central transmitter
(from Bovsheverov et al., 1973).   c) Three axis meter with
separate transmitters and receivers.   EG&G model 198 (from
Kaimal et al., 1974).   d) Intercomparison (from Miyake et al.,
1971).   e) Three component anemometer, circa 1974, Kaijo Denki
Co., model PAT 311.

a

b

10 cm

c

d

e

-54-
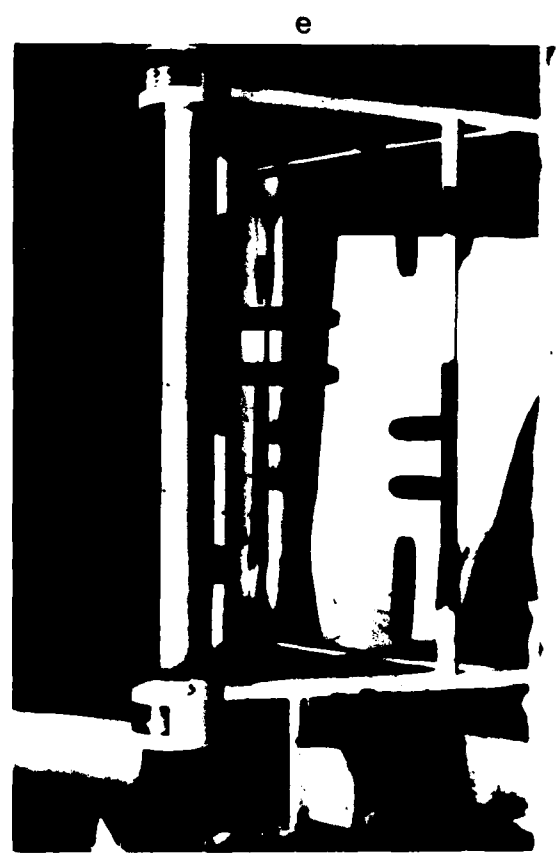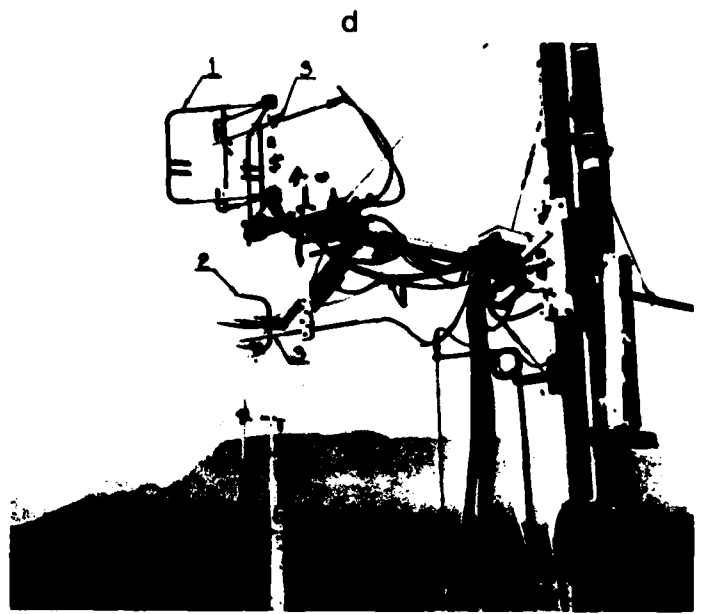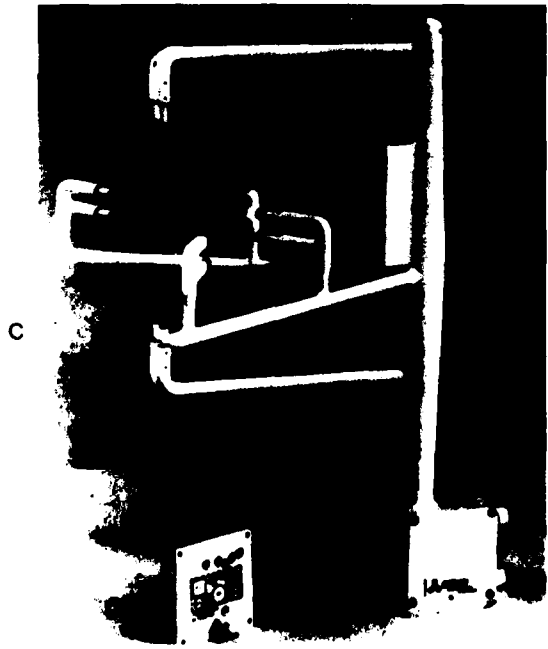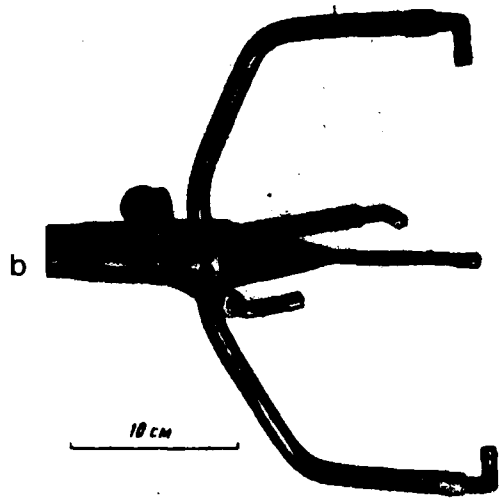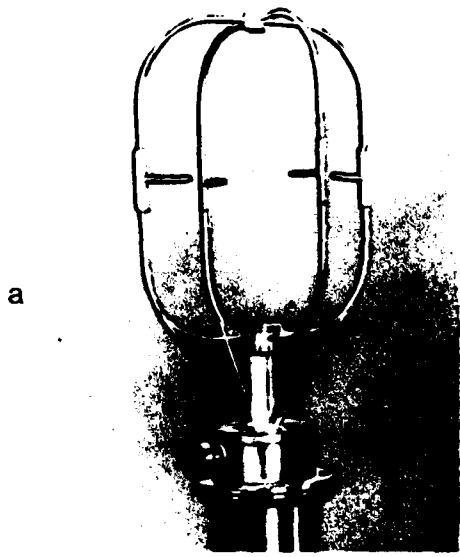
Figure 3

Figure 4.

ATT current meters.   a) Medium length ($\sim$10 m) multiple path ATT volume transport system being installed at an angle to flow in California aqueduct (from Lowell, 1977).   b) Transducer mount for direct path ATT meter, suggested by Gytre, 1979 (Norway). c) Cluttered two-axis, wire-lowered meter tested at Scripps and WHOI, built by OKI, $\sim$1969 (Japan).   d) Two-axis, 50 m and 150 m WHOI tower and bottom mounted system (from Nowak, 1969).   e) Three-axis submarine mounted turbulence probe (from Lawson et al., 1976).

d

25m

6m

20m

ACOUSTIC PATH LENGTHS OF
50 AND 150 m
WHERE TESTED

N

315° T

225° T

OCEANOGRAPHIC
INSTRUMENT ROOM

PLAN AND SOUTH SIDE VIEW
BUZZARDS BAY ENTRANCE LIGHT STATION

a

b

c

e
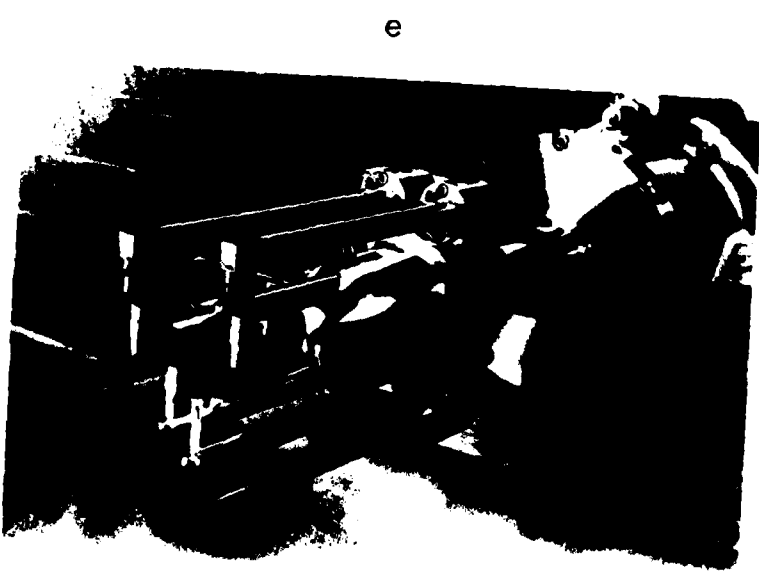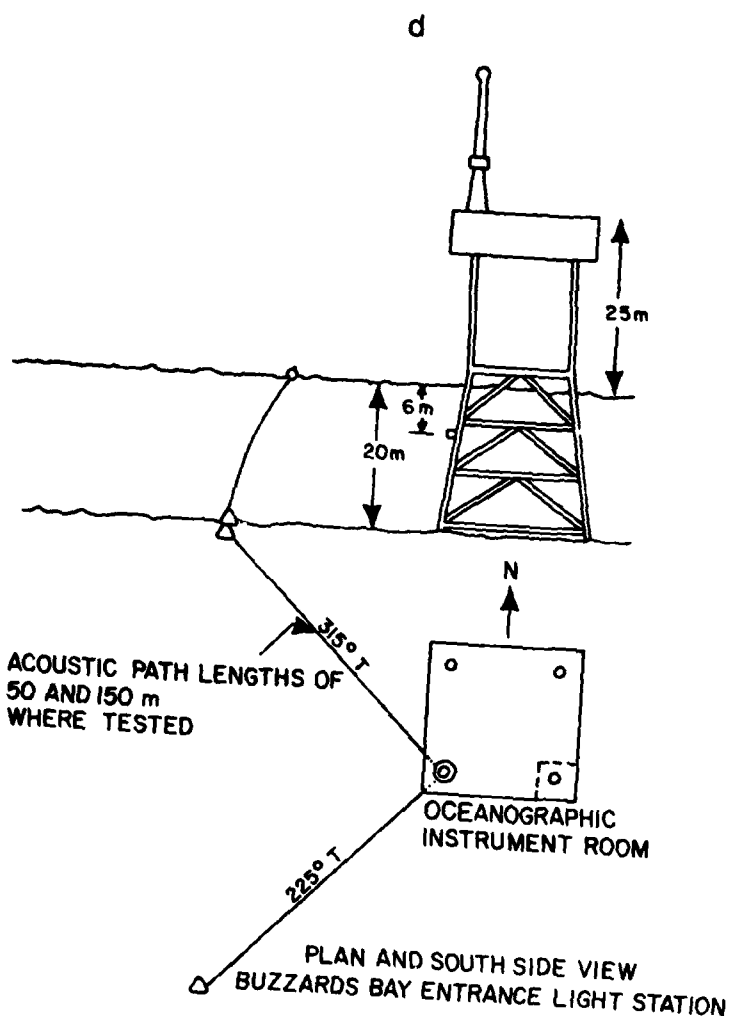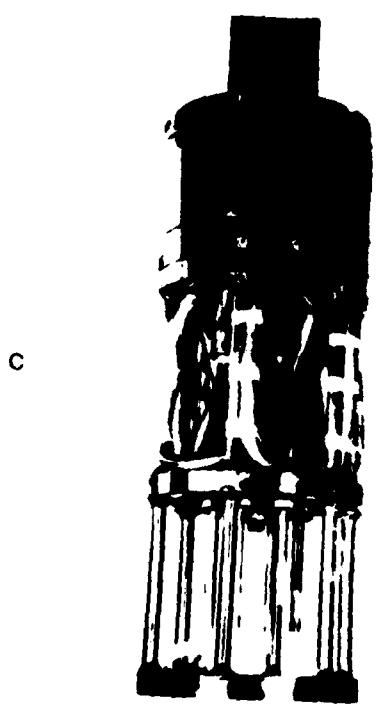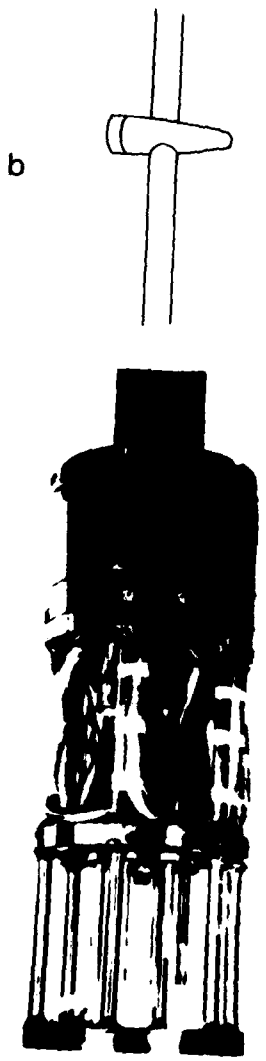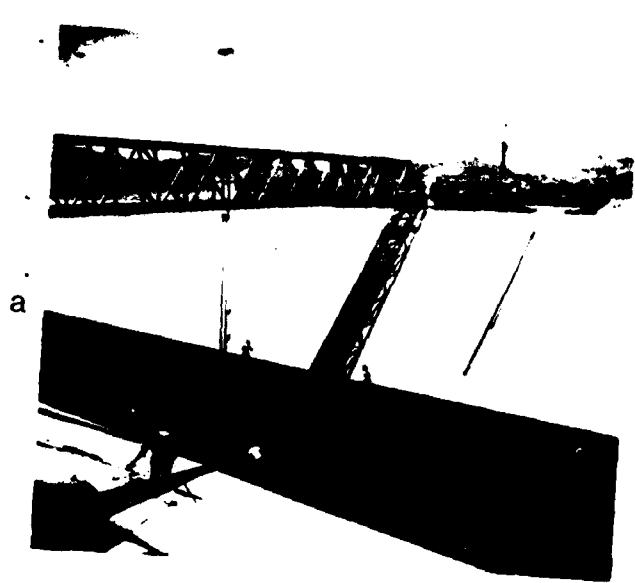
Figure 4

Figure 5.

ATT current meters (continued). a) Autonomous two-axis moored
current meter by Simrad, Inc., 1979 (Norway). b) Wire lowered
two-axis meter by Crouzet, Inc., circa 1974 (France). c)
Three-axis, ring mounted, direct path meter by NBIS, 1978 (USA).
d) Four-axis, three component benthic boundary layer probe
(from Williams and Tochko, 1977). e) Wire lowered Crouzet ATT
meter, circa 1973 (France). f) Two-axis, faired-ring
transducer and electronics (from Hardies, 1975).

a

b

c

d

A_1 A_2

A_4 A_3

B_3 B_4

B_2 B_1

e
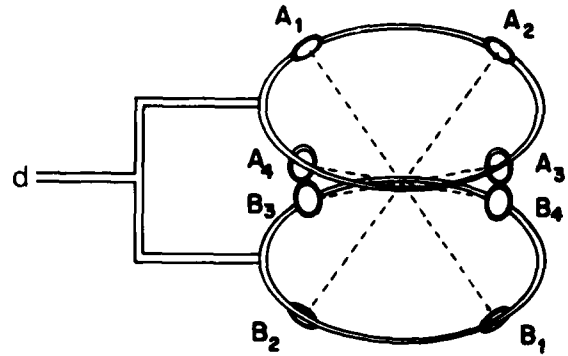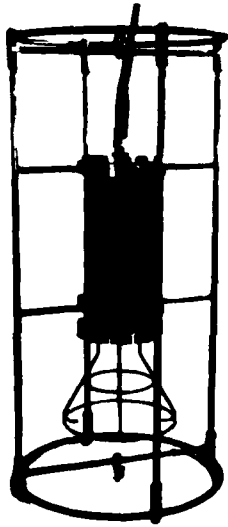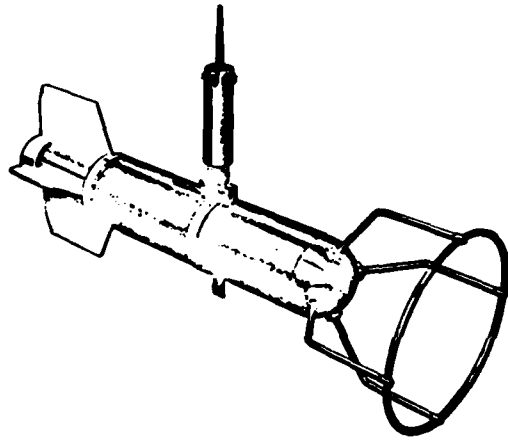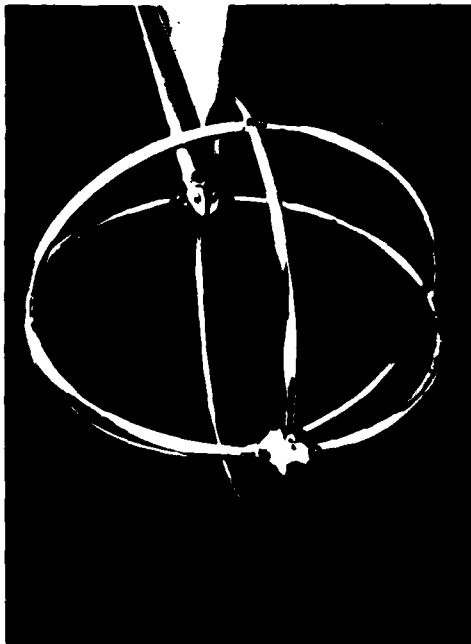
f
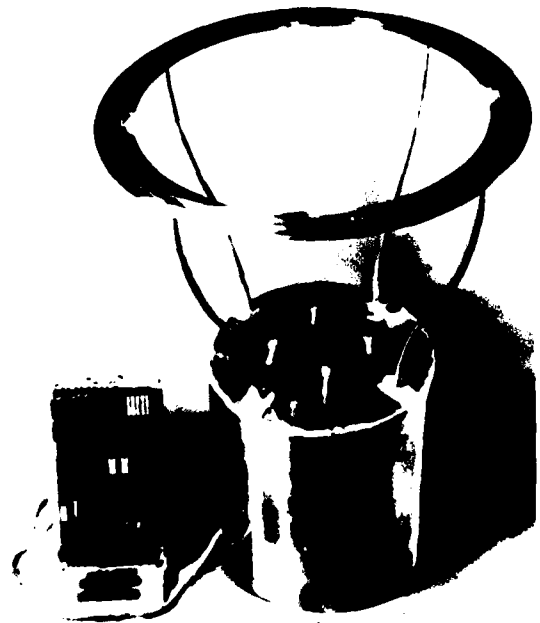
Figure 5

Figure 6.

Early two-axis, direct-path Gytre ATT flowmeter tested at WHOI
in 1974. Transducers (bottom) are encapsulated discs near ends
of four cylindrical rods. Acoustic path length (diagonal
separation) is 10 cm, rod diameters are 1 cm. Framework at top
includes tow carriage and 1 meter peak-to-peak in-line slosher
used in dynamic tests.
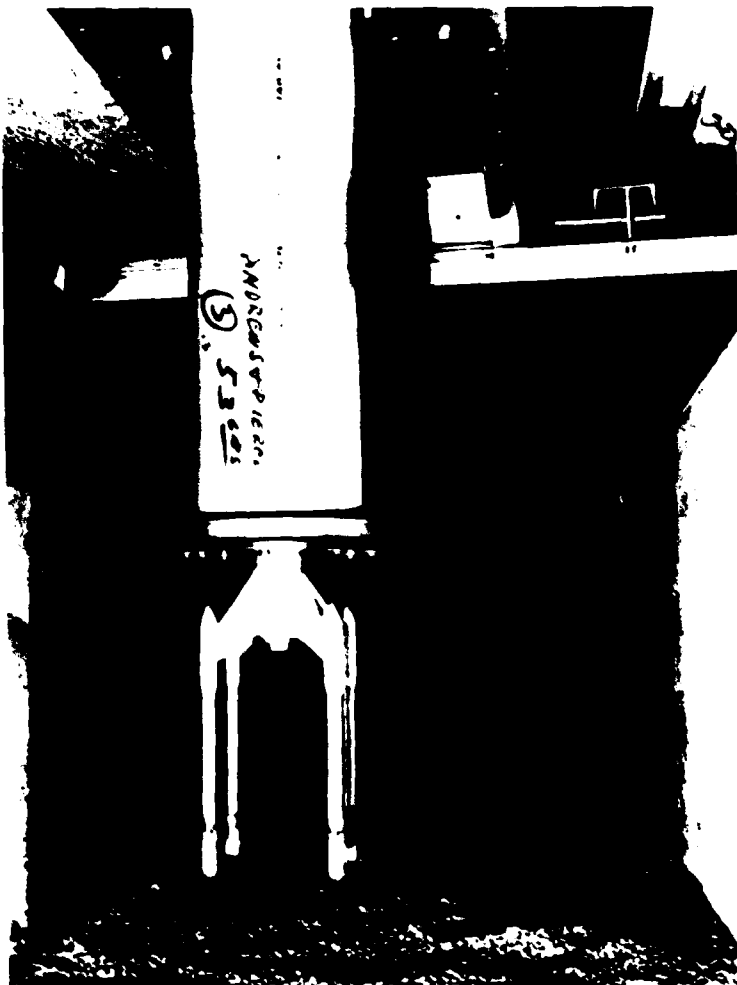
Figure 6

Figure 7.

Dynamic response of meter shown in previous figure. Indicated response (dots) and kinematic speed over the ground (dash line) are in close agreement. Tow and oscillatory motion are collinear at constant depth along tank center-line. Upper frame shows response when acoustic axis is aligned with tow ($\theta = 0^{\circ}$). Bottom frame is same except that the flow is midway between the two axes ($\theta = 45^{\circ}$). Speeds are scaled from steady tow calibrations. Meter position over the ground (solid-curve) retraces previous path for major portion of each cycle.

Figure 7

-62-
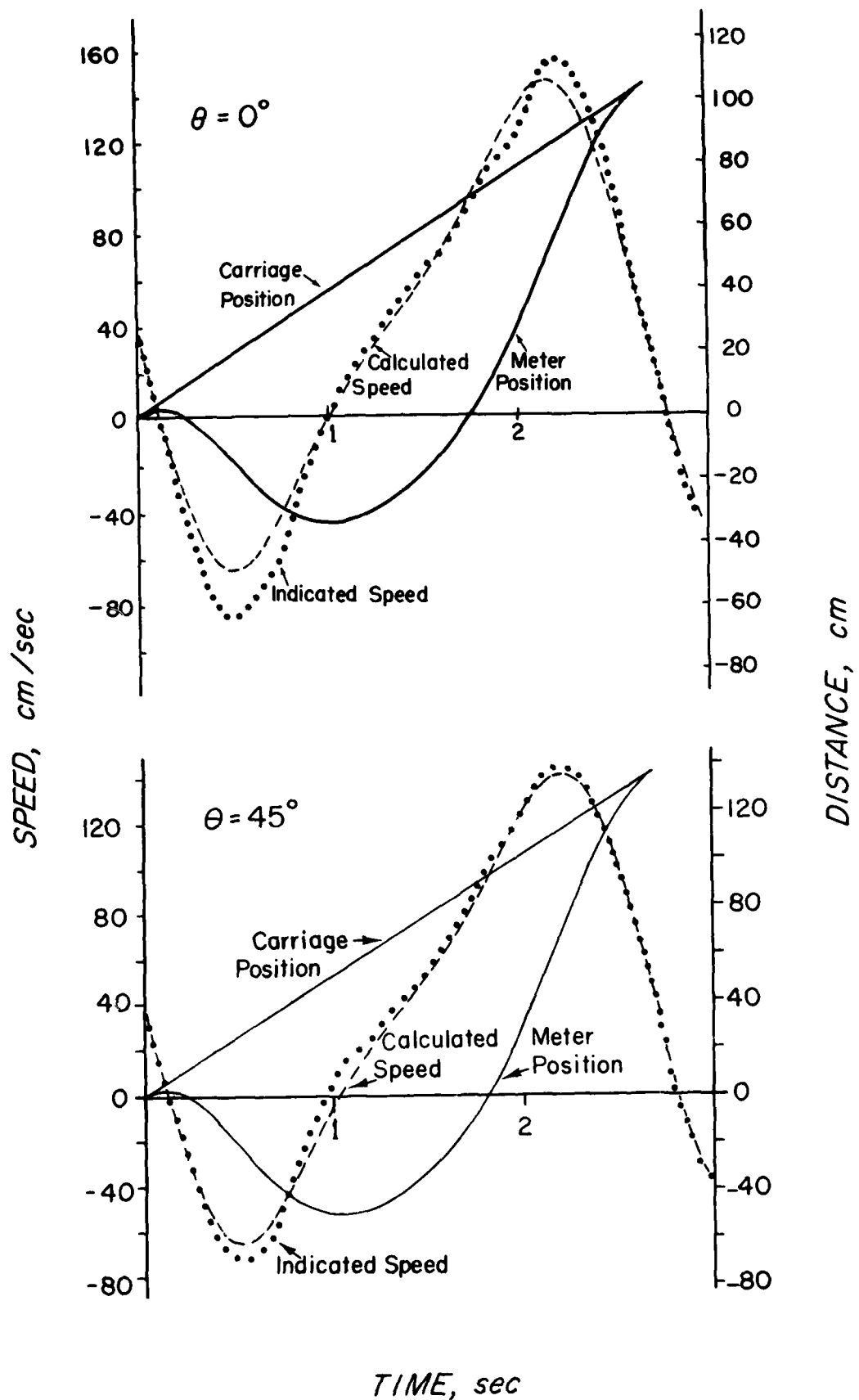
Figure 8.

Horizontal cosine-response. Single axis response (bottom) as function of steady tow speed and meter rotation angle θ. Section along 53 cm/sec tow speed (arrow) is shown versus rotation angle θ above. Percent error (arbitrarily normalized to zero at θ = 50°) is shown with percent error scale at right.

Figure 8

-64-
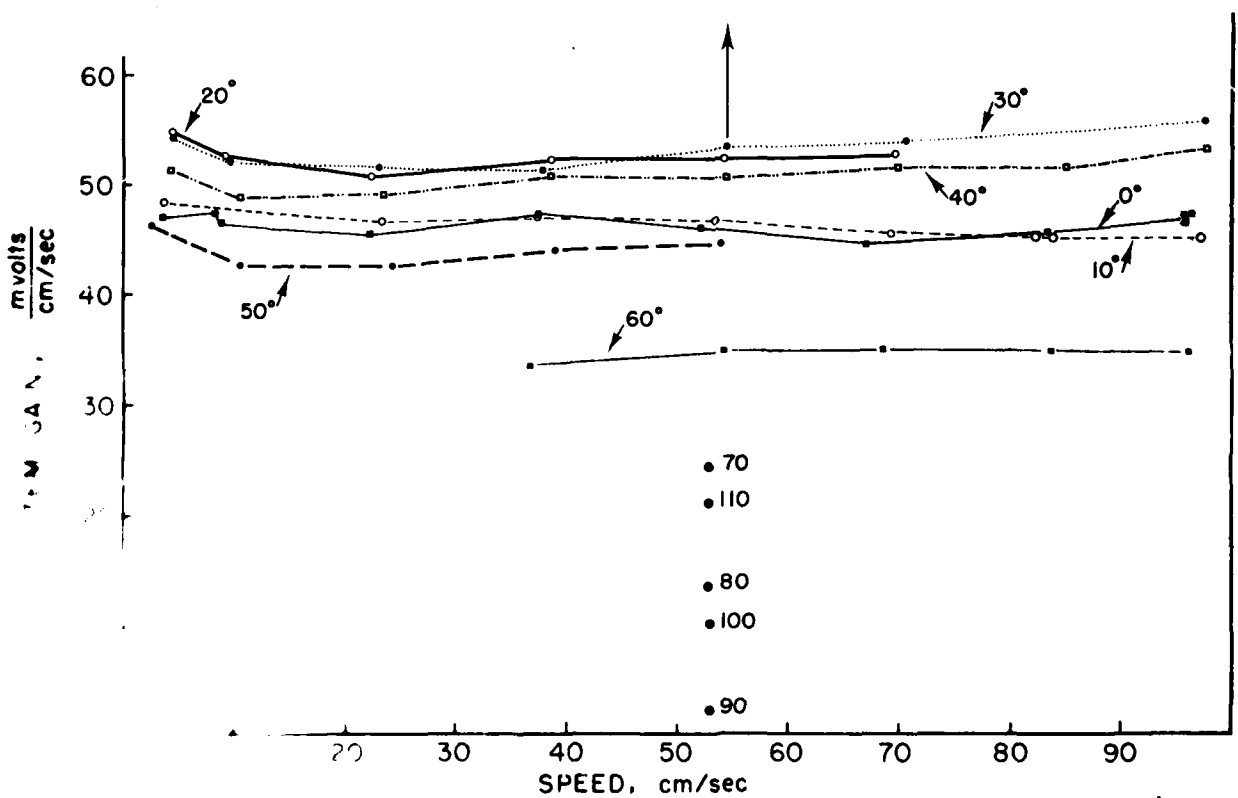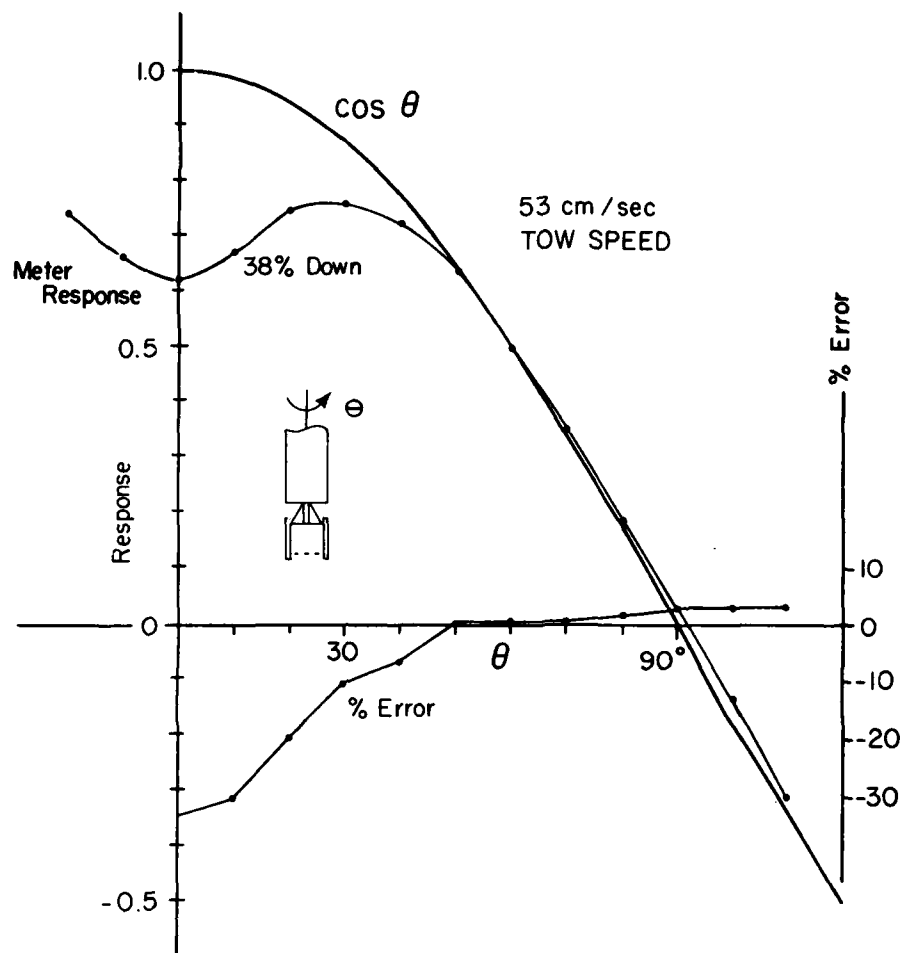
Figure 9.

Flow patterns behind cylinders in steady flow. Flow regimes versus Reynolds number include from the left: laminar, twin attached vortices, laminar wake, transition zone, Kármán vortex "street" with turbulent wake, transition zone, supercritical flow with turbulent wake, and high Reynolds number thin turbulent vortex street.

Values of particular interest in moored ATT design lie along the dashed diagonal lines. Shedding frequency for 1.5 cm diameter cylinder is shown at right edge. Drag coefficient C_D and inverse of Strouhal number S are shown above. The equation (right) relates Reynolds number R to flow speed V, cylinder diameter D, and fluid kinematic viscosity ν.

CYLINDER FLOW REGIMES

15 cm dia STROUHAL FREQUENCY, H3

$R = \dfrac{VD}{\nu}$

REYNOLDS NUMBER

10 10^2 10^3 10^4 10^5 10^6 10^7

SPEED, cm/sec

KNOTS

LAMINAR FLOW

TWIN FIXED VORTICES LAMINAR STABLE

UNSTABLE LAMINAR WAKE

TRANSITION ZONE

TURBULENT VORTEX STREET

TRANSITION ZONE

TURBULENT NO VORTEX STREET

TURBULENT THIN VORTEX STREET

Dia = 0.5 cm, 20°C
5°C
Dia = 15 cm, 20°C
5°C
Dia = 15 cm, 20°C

$\dfrac{1}{S}$

C_D

Figure 9

-66-
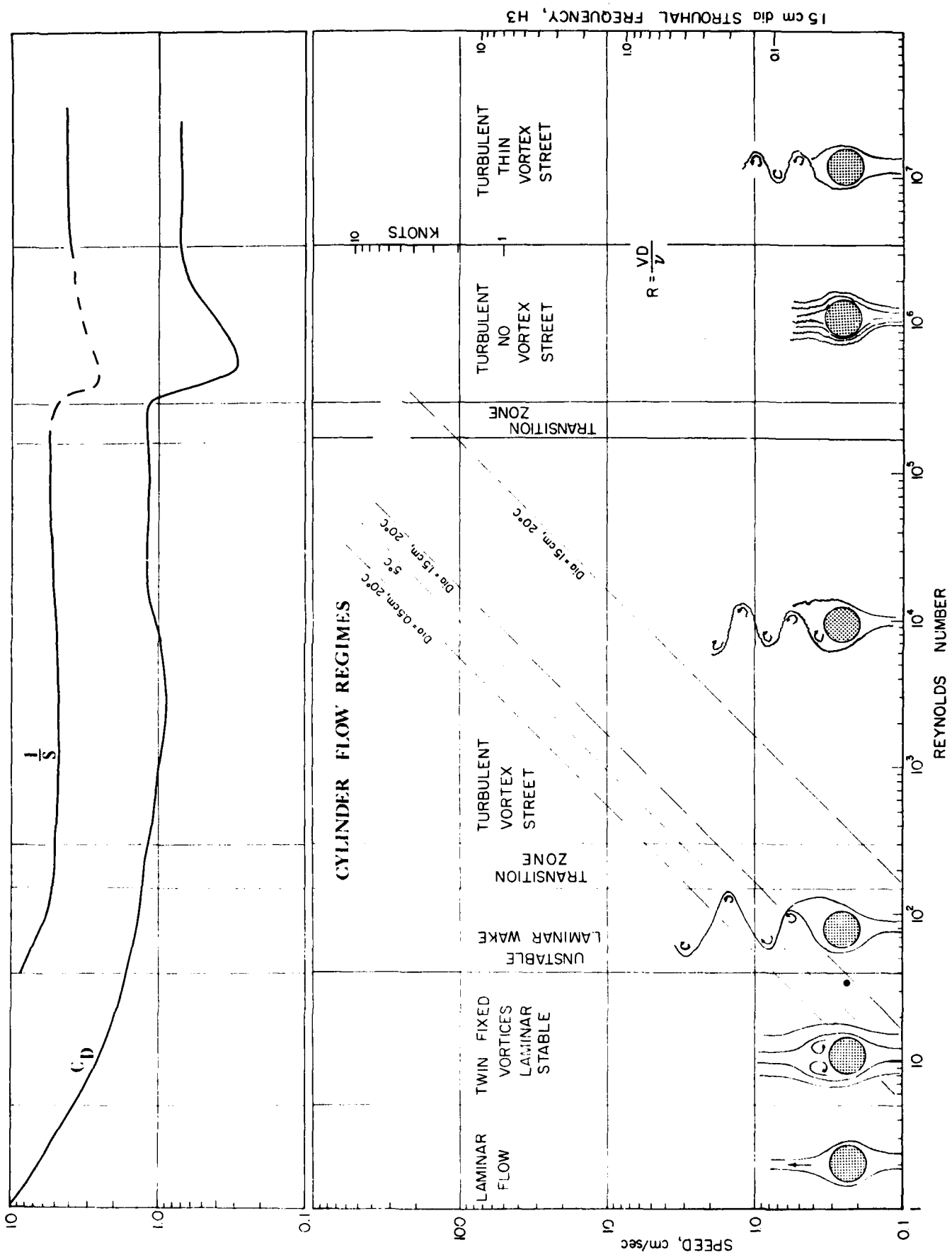
-99-

Figure 10.

Low Reynolds number wakes behind cylinders. a) Laminar flow.
b,c,d, and e) Developing twin vortices. f) Stable vortices
start transition to laminar wake. Flow visualization used
surface aluminum powder (from Prandtl, 1927).

a

b

c

d

e

f

Figure 10

-68-
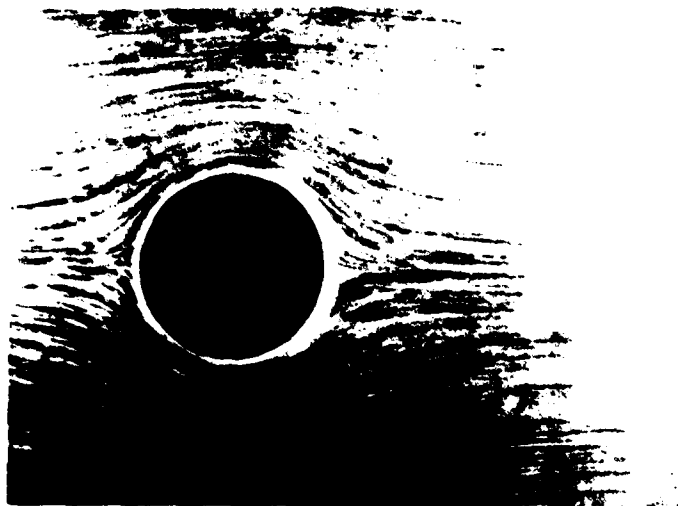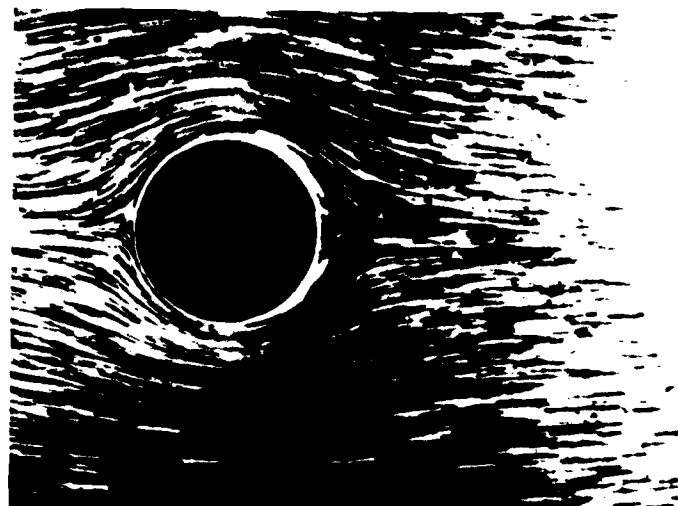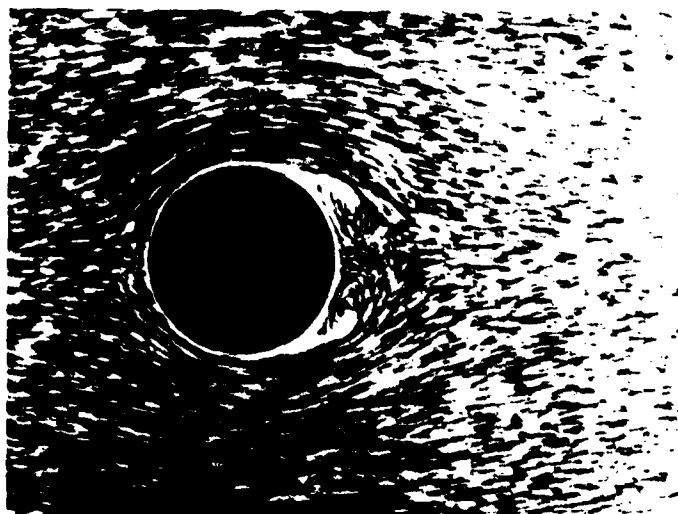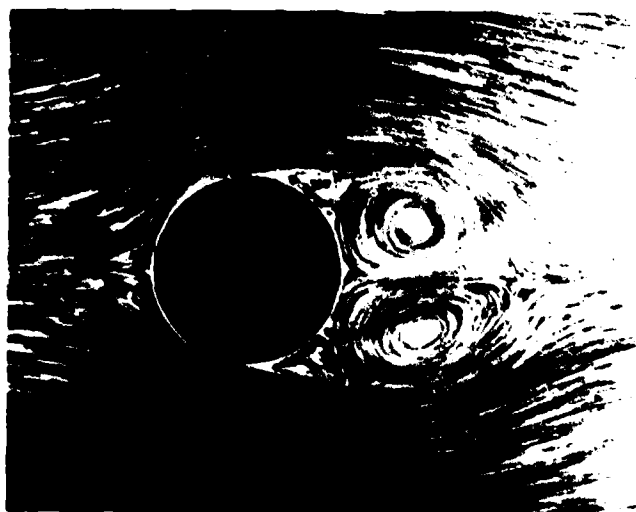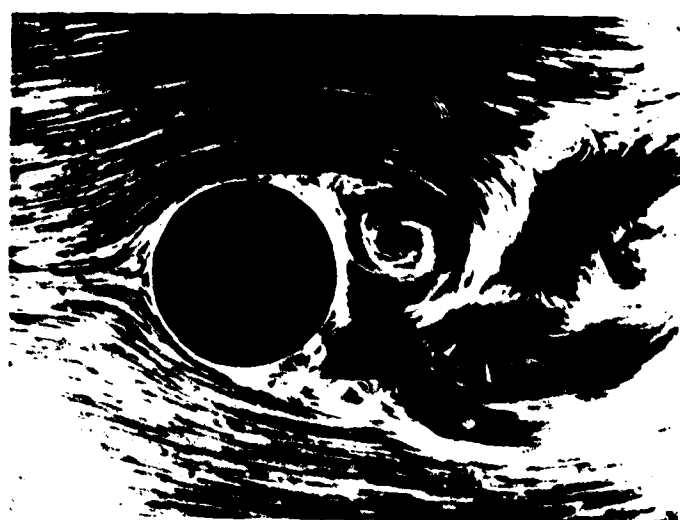
Figure 11.

Observed mean properties of low Reynolds number wakes behind
cylinders. Top: mean-speed distribution across wake at R = 48
and 70 along 3 sections at distances x = 1, 1.8, and 3.2
diameters downstream from the cylinder center. Bottom: wake
length in cylinder diameters for a range of Reynolds numbers
(from Nishioka and Sato, 1978).
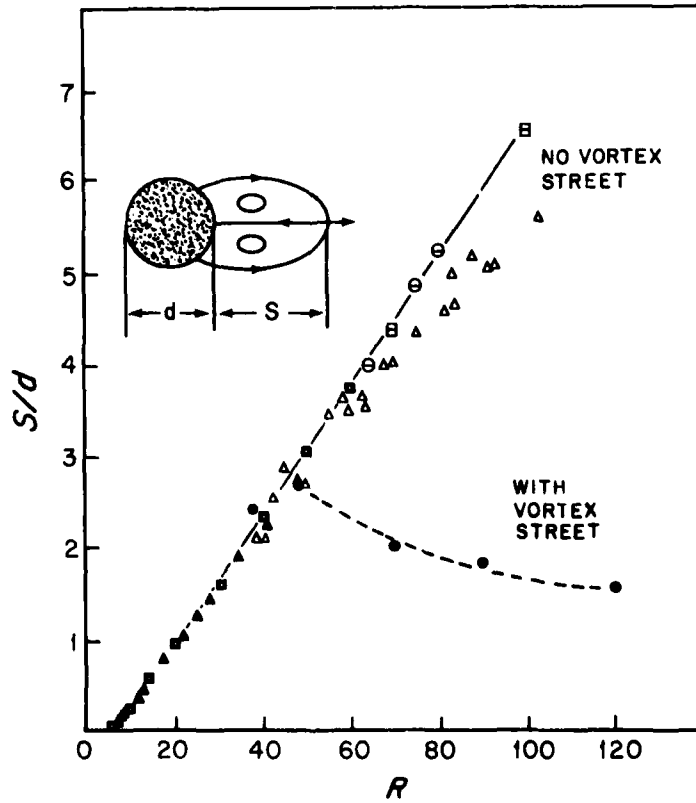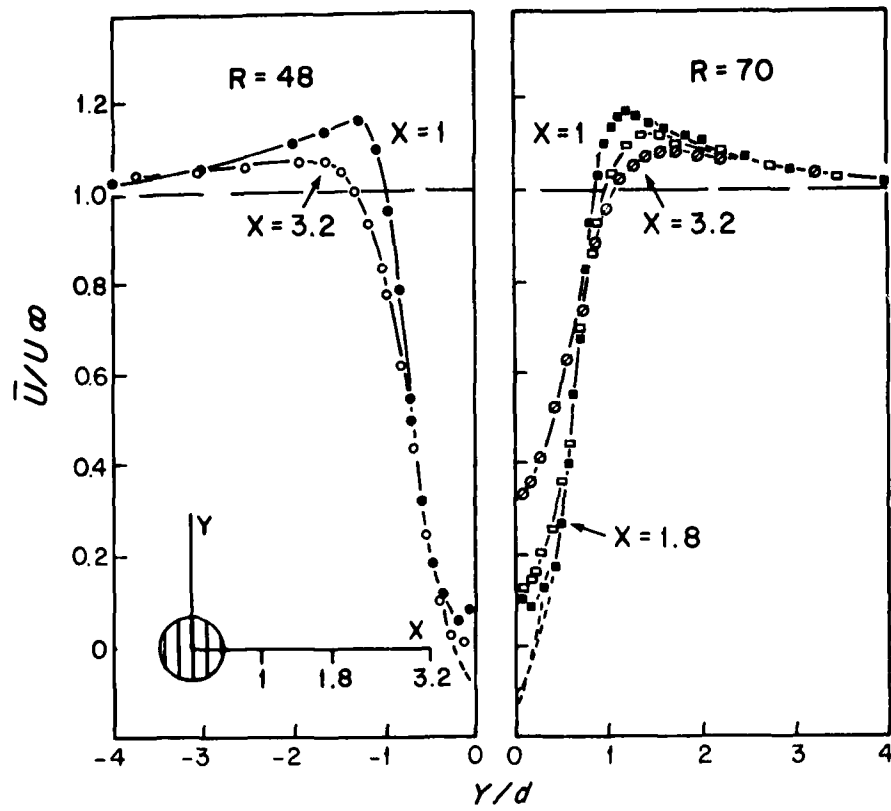
Figure 11

Figure 12.

Kármán vortex street. Fully developed wake behind cylinder shown as white streak at bottom. $R = 2 \times 10^3$, $D = 1.27$ cm, $V = 15$ cm/sec. Note large wake size relative to cylinder diameter, also large irregular eddy about 8 cm from the top. Minimizing adverse effects of such wakes is the central unsolved problem in ATT design (from Clutter et al., 1959; via Batchelor, 1979).

-72-

Figure 12

Figure 13.

Measured mean speed in the wake of long circular-cylinders in cross flow. Panels a, b, and c show half-plane contours of speed at three Reynolds numbers. Flow is from left; upstream (bow) wake is not shown. (d) Speeds along radial directions θ in panel (b) are shown as a function of distance from the cylinder surface. (e) Measured speeds on axis ($\theta = 0°$) behind cylinders at several Reynolds numbers. (f) Same as (e) except $\theta = 20°$. Distances are in units of cylinder diameters. Speeds are mean vector magnitudes $|\vec{U}|$ normalized by the free-stream speed U_∞.

Note in (e) large ($\sim 20\%$) speed defect in wake directly behind cylinders ($\theta = 0°$) even at large distances. By $\theta = 20°$ (f), however, cumulative effect is reduced to that equivalent to having no flow over about 1.5 dia of the acoustic path, i.e., down 15% for a 10/1 separation to diameter ratio. Plots are based on measurements by Hanson and Richardson (1968), Kovasznay (1949), Marumo et al. (1978), and Nishioka and Sato (1978).
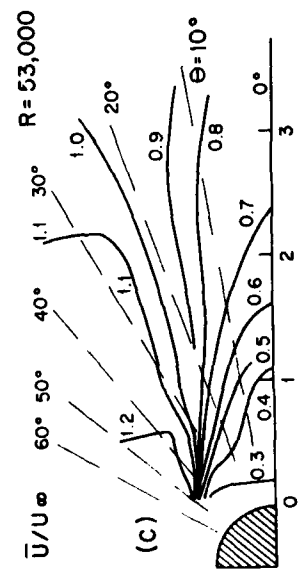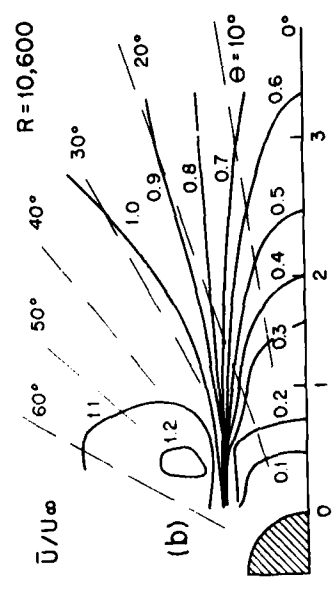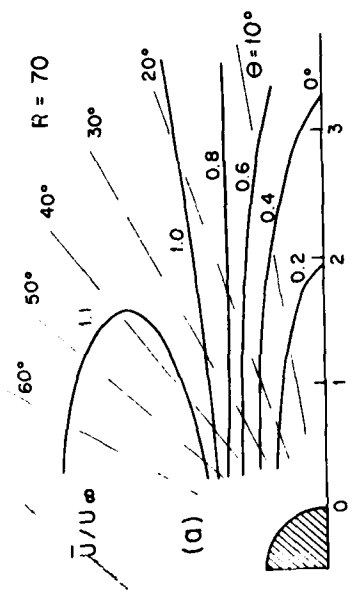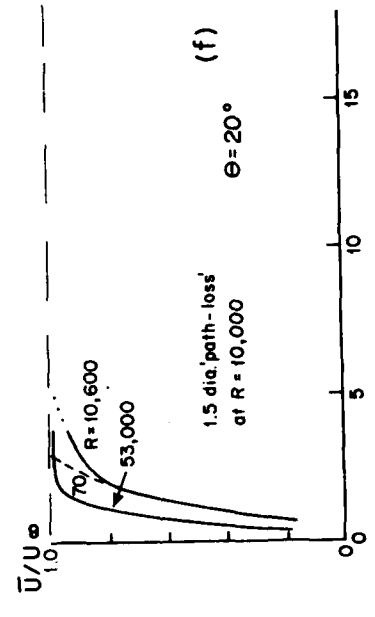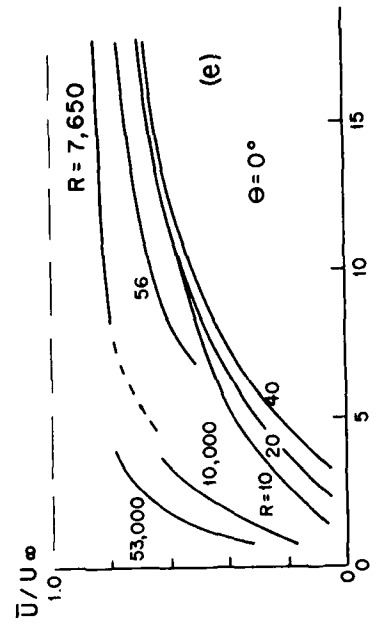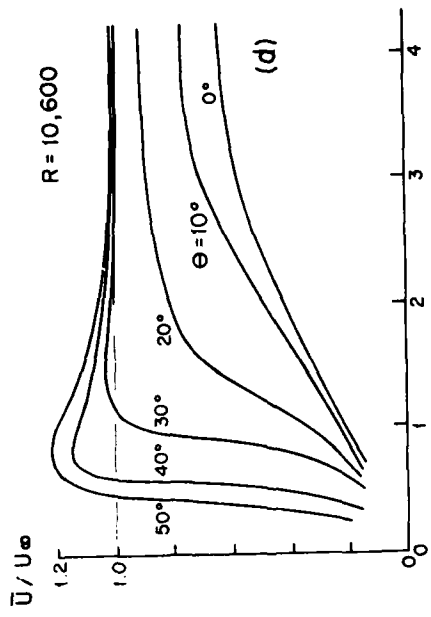
DISTANCE, *dia*

Figure 13

-74-

Figure 14.

Measured low speed ATT response. Meter shown in Figure 6 is
towed at ∿2.2 mm/sec (R = 33) with one acoustic axis aligned to
the flow (θ = 0°) and at θ = 20°. Tow starts at t = 0,
stops 5 to 6 minutes later having covered a distance of only
70 cm. Response at θ = 0° is <u>less</u> than at θ = 20°.
Negative response at end of tow equals flow defect just before
tow stop. Bottom panel has the same condition as at top but
water is gently stirred at time (A) about 1 meter upstream of
the instrument. Short period noise level (grass) before tows
is less than 0.1 mm/sec. Periodic small signal jumps were
caused by an electronic problem. About 2.5 min or 4 probe
separations of travel are required (top panel) for approximate
signal stabilization.

Figure 14

-76-
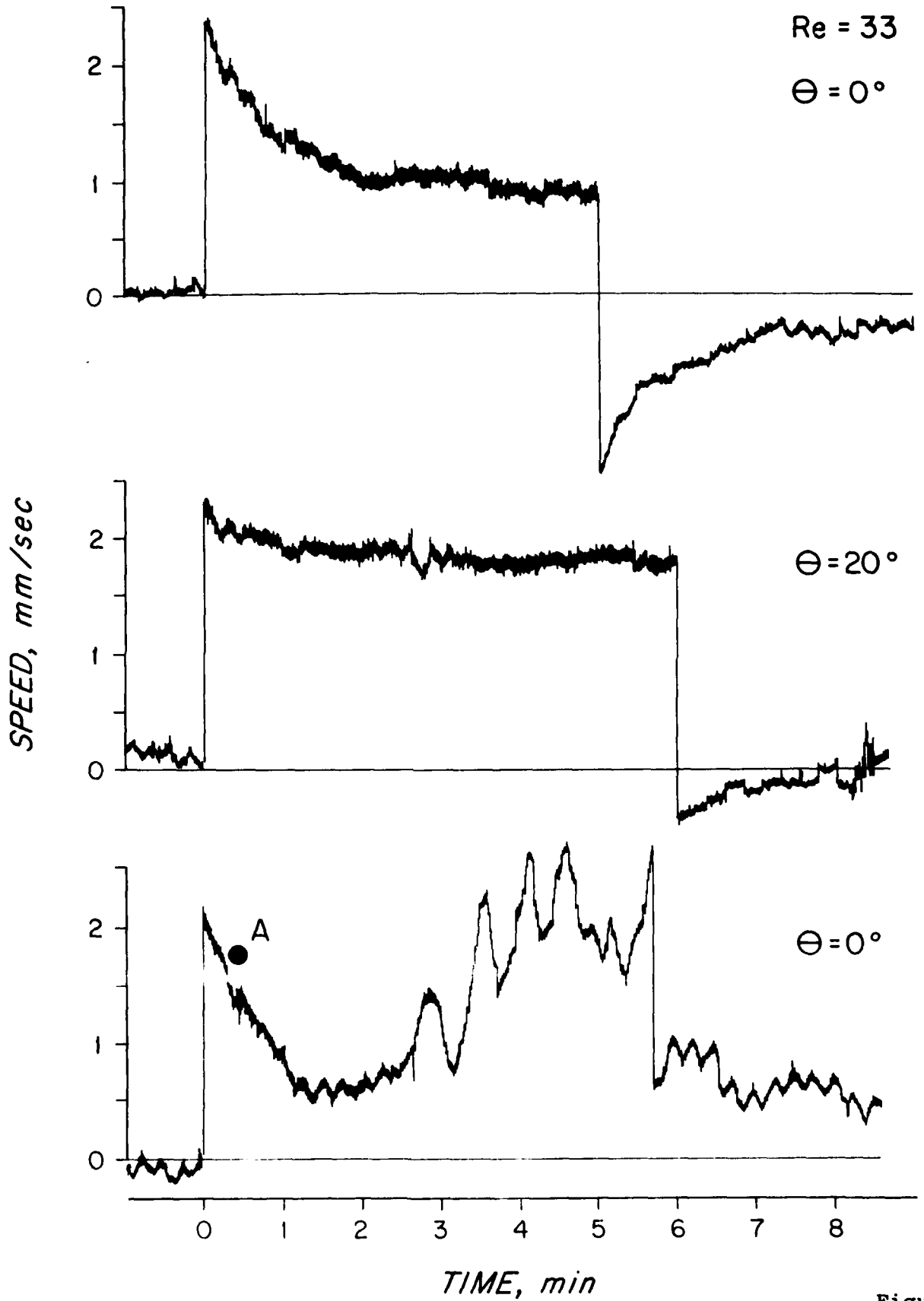
Figure 15.

First sea-going, mirror-type ATT current meter tested at WHOI
(November 1975). Acoustic paths are at 45° angles to
mirror. Sense volume is kept relatively open and separated
from pressure case.

END
DATE
FILMED
6 80
DTIC

Compass

Power

Pressure

Clock

Control

V/F

Counter

A/D

MUX

Recorder

Cassette Tape Recorder

Acoustic CM Electronics

Pressure Transducer

Thermistor

Start Plug

Mirror

Compass

Electronics

Test Connector

Battery

High Voltage Power Converter

End Cap

Acoustic Transducer

Cage

107 cm

64 cm

Figure 15

-78-
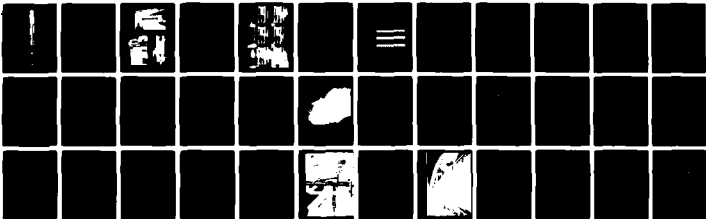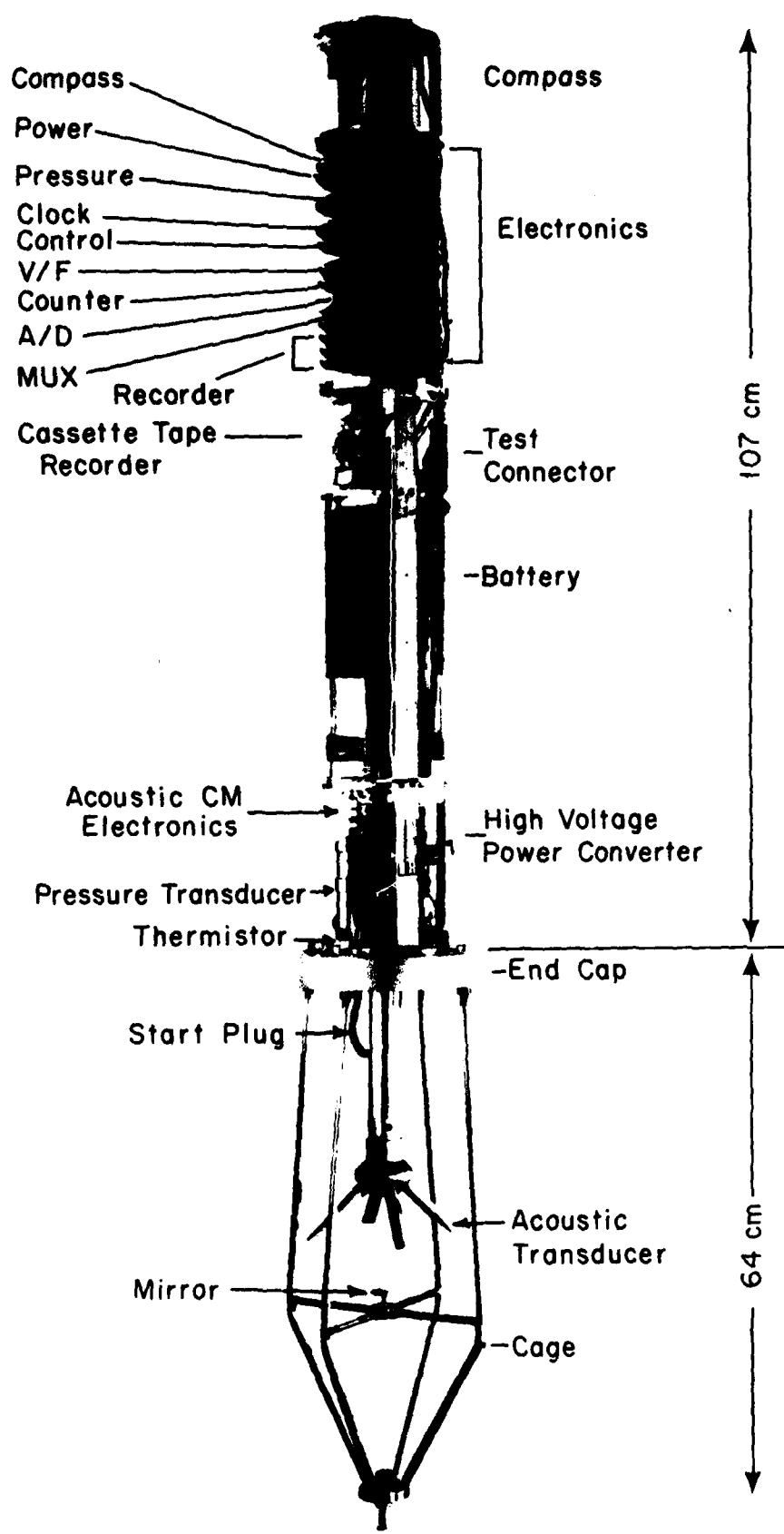
Figure 16.

NBIS acoustic current meter in WHOI tow and flume facility
1978.   Indoor ∿1 x 1 x 20 m tank has tow carriage (top) and
eye-level glass walls (bottom). Water can be pumped (flume) at
speeds up to 8 cm/sec. Drogue (half-rotor, line and bobber)
lower right, and dye are used to determine flume speed at
transducer level. Vertical dye streaks monitor shear and aid
flow visualization around current meter.

-80-
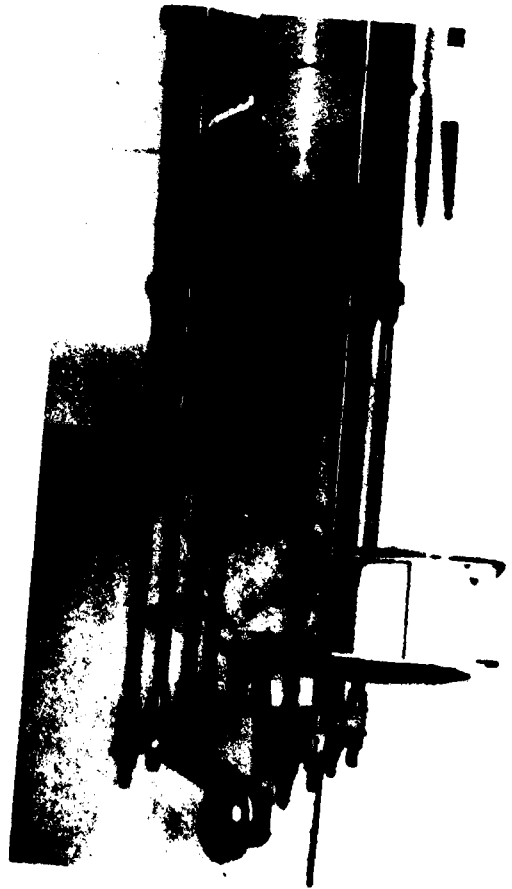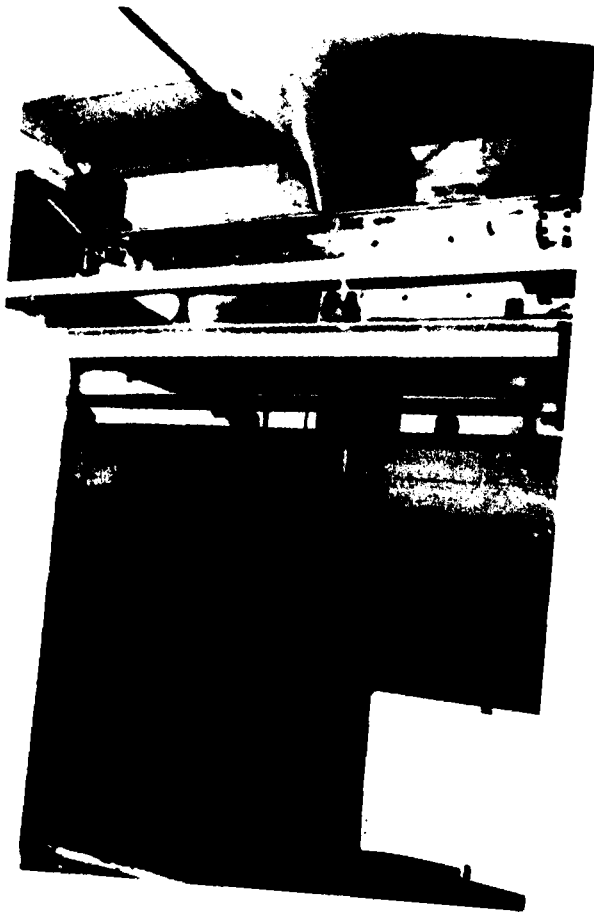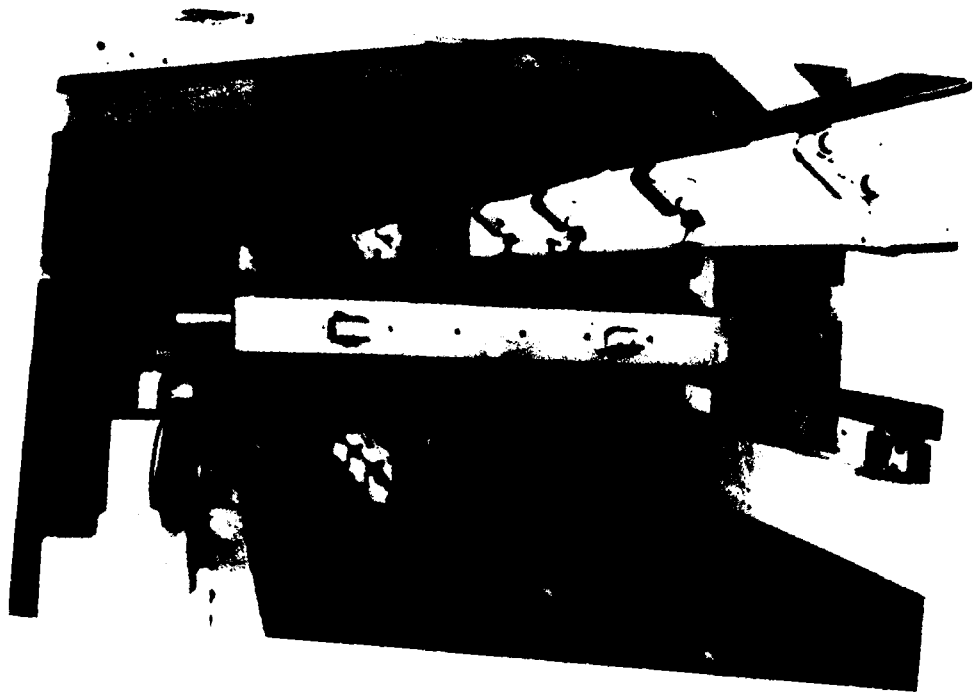
Figure 16

Figure 17.

Dye motion (top to bottom by column) through NBIS mirror-type meter. Time sequence shows flow acceleration in acoustic sense volume below finger-like transducer supports. Photos are taken at 5-second intervals.

Figure 17

Figure 18.

Response in still water. Traces a-d show single-axis analog
voltages from NBIS meter for increasingly longer sample perioas
shown at right. Similar trace (e) shows modulation caused by
slowly lowering the water surface. Modulation is a tank effect
caused by acoustic reflections. Noise level (a-e) is an order
of magnitude larger than shown in Figure 14, but still is small
(<1 mm/sec) compared to typical ocean flow speeds.

Trace (f) shows laboratory zero stability on 10 separate days,
for two axes of one instrument over 63 consecutive days. Each
point is the mean of 20 or more 10-second averages. Standard
deviation of points shown is 0.1 cm/sec for each axis (open and
closed circles). Stability of zero-flow also monitors
mid-scale electronic performance, an important system test.

Figure 18

-84-
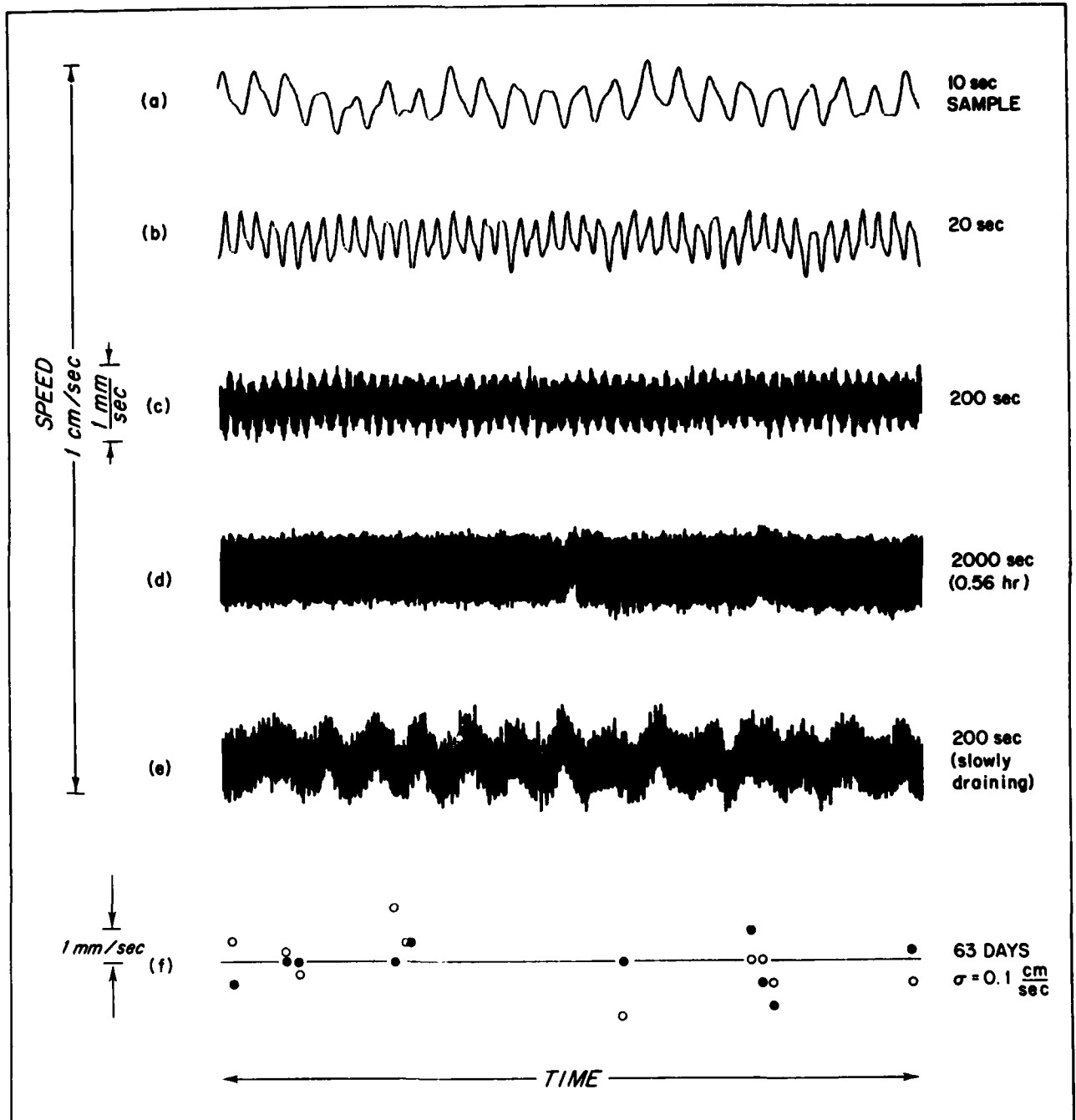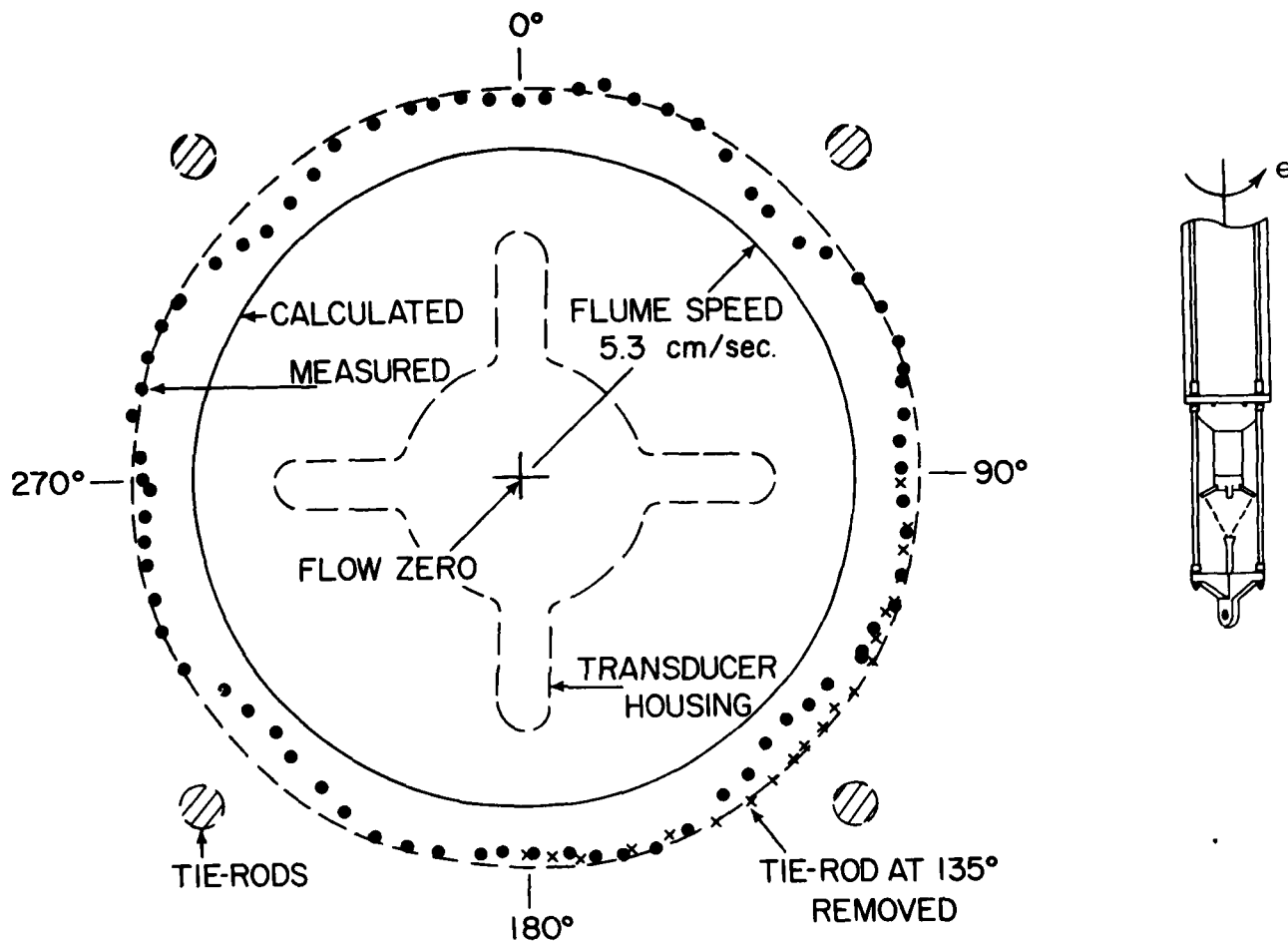
Figure 19.

Horizontal cosine-response. Polar diagram of vector-response
(dots) shows systematic magnitude variations with direction.
Flow defects caused by cage tie-rods and transducer supports
are seen at θ = 0°, 45°, 90°, etc. Removal of tie-rod at
135° increases response to that shown by X's. Response
magnitude is greater than predicted (solid circle). Plan views
of tie-rod and transducer locations are superimposed on voltage
diagram. Meter outline and rotation sense are sketched at
right. Nominal flow speed is 5.3 cm/sec.

Figure 19

Figure 20.

Horizontal cosine-response (continued). Response components
(top) show clipped triangular wave form before removal of
arbitrary electronic bias. Flume (and meter) stability is
indicated by typical error bars shown. Direction and speed
anomalies (below) have 1.6° and 4% rms variations. As
before, X's (bottom panel) show response with one tie-rod
removed. Nominal flow speed is 5.3 cm/sec.

Figure 20

-87-
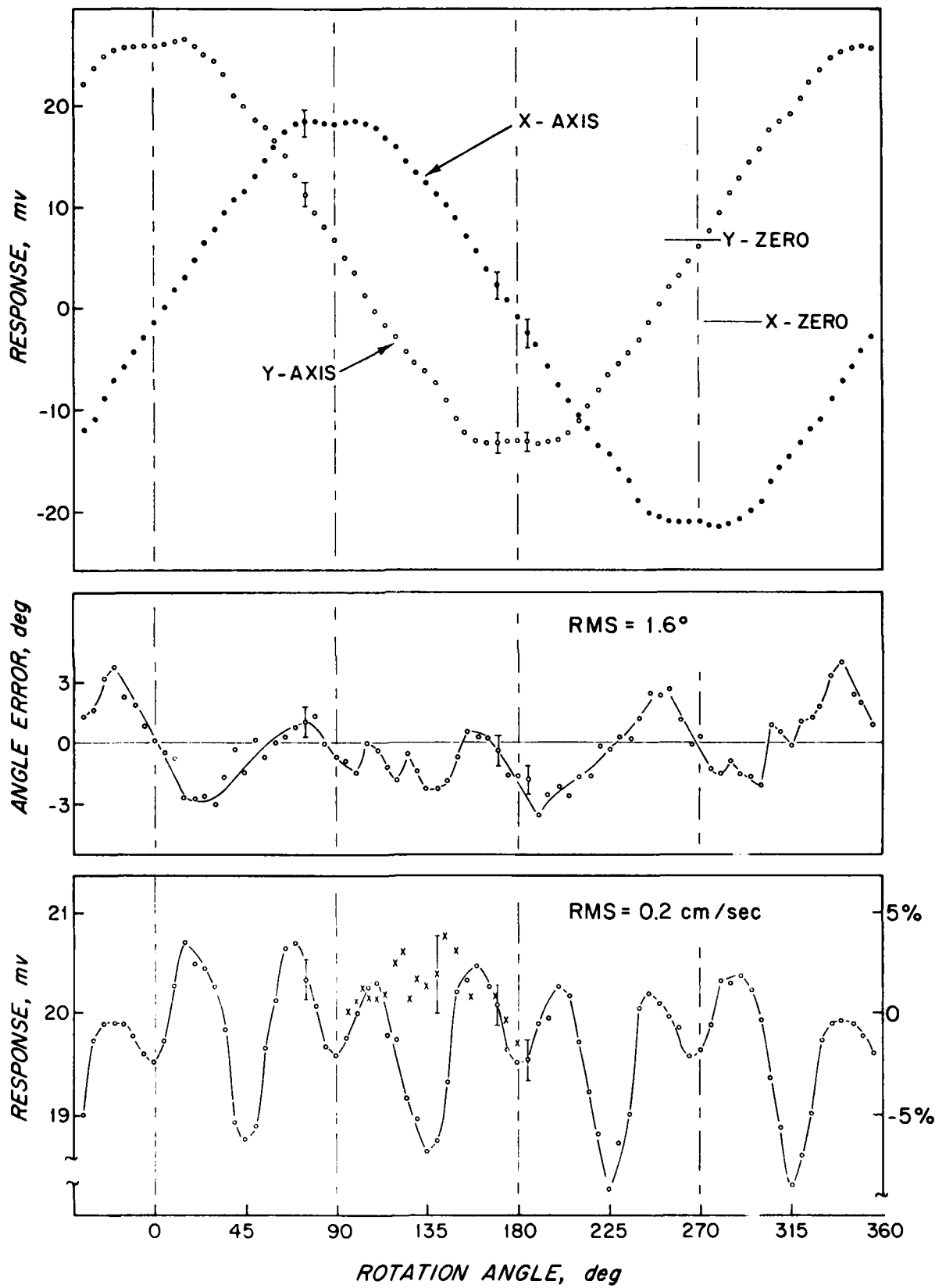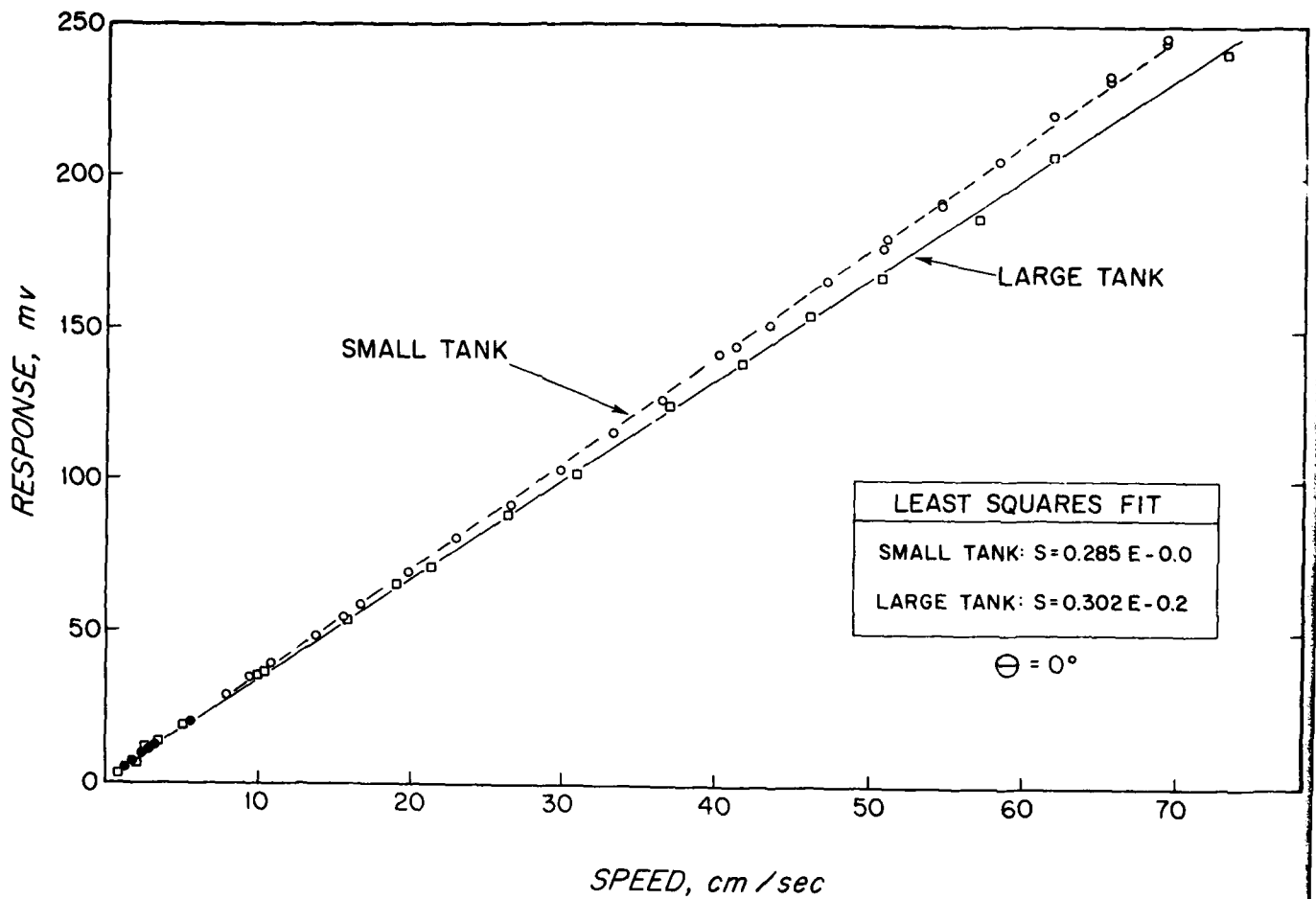
Figure 21.

Steady flow calibration. Uncorrected "small tank" data show 6% increase in response due to flow blockage by the meter. Equations (box) give least squares linear regression functions for observed voltage E and speed S.

Figure 21

Figure 22.

Steady flow calibration (continued). Combined observations from previous 3 figures and other calibration data show dependence of instrument sensitivity or "gain" (mv out per cm/sec in) as a function of steady flume and tow speed. Departures from the horizontal represent gain nonlinearities; vertical separations from calculated response (dash-dash line) represent effects not included in conventional ATT response model (see Appendix C). Curved dash line pair gives ± 0.5 cm/sec range about percent response scale at right.

Shaded block (right) shows range of calculated temperature effect in fresh water. Point (A) is "free flow" gain with tie-rod removed. Shading (B) indicates range of observations with rotation angle θ shown in Figure 19. Single dye observations (C) using flow speed in ATT sense volume (see Figure 17) agrees closely with calculated value at 1.5 cm/sec. Other individual points (circles, squares) are means of several independent 10-second average values with one axis aligned with the flow ($\theta = 0^\circ$).

Small tank gain grows steadily with speed due to flow blockage effects not seen in larger tank. Both small and large tank data show systematic gain increase equivalent to about +0.5 cm/sec at low speeds. Flume (filled-circles) and tow (open-circles) data show no systematic differences.

SMALL TANK

LARGE TANK

10 %

0 %

CALCULATED
TEMPERATURE EFFECT
(15° C .... 20° C)

FREE FLOW
(CALCULATED FOR 20° C)

-10 %

± ½ cm/sec

GAIN, mv / cm/sec

● FLUME

◇ DYE   119 cm x 104 cm TANK

○ TOW CARRIAGE

□ TOW CARRIAGE   240 cm x 190 cm TANK

SPEED, cm /sec

-90-
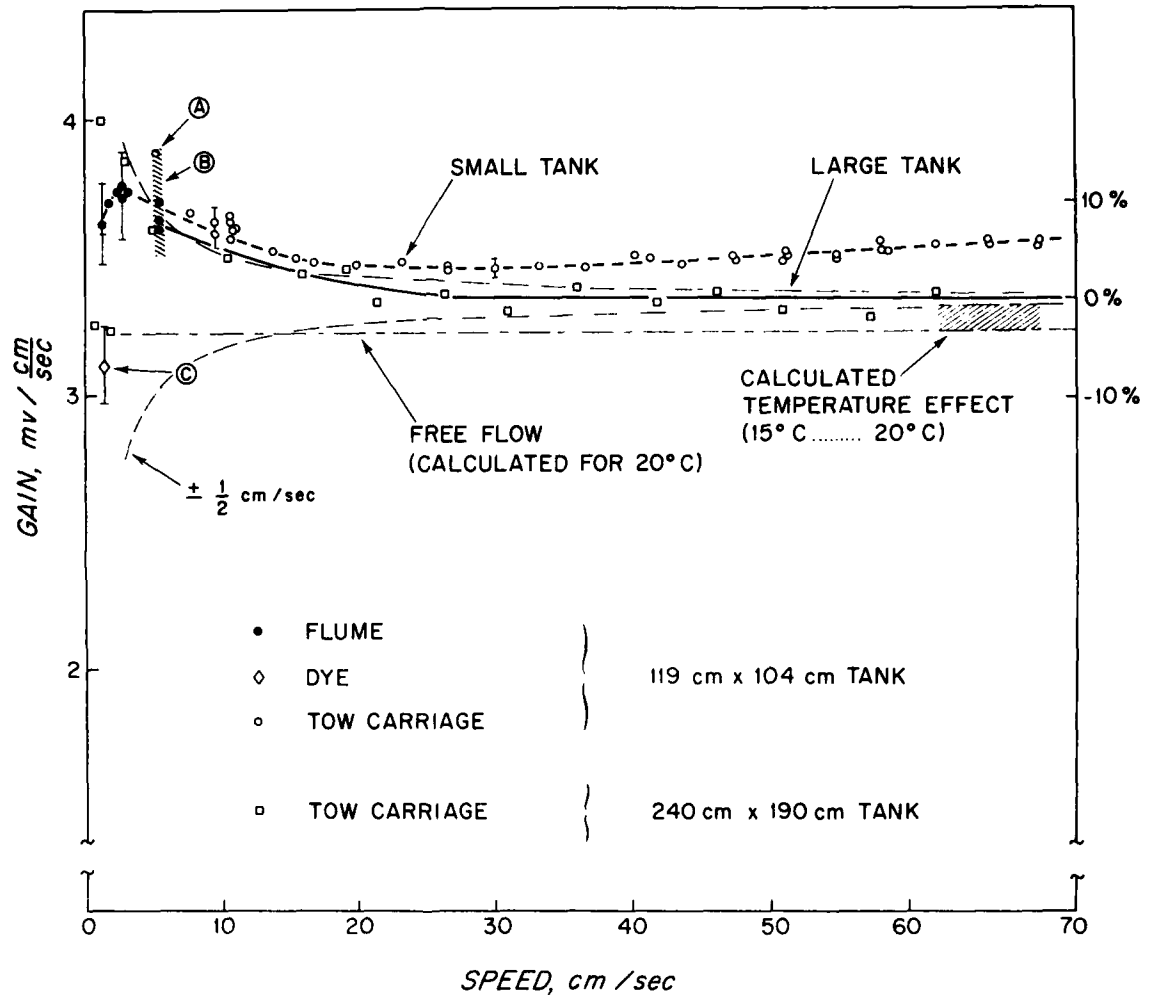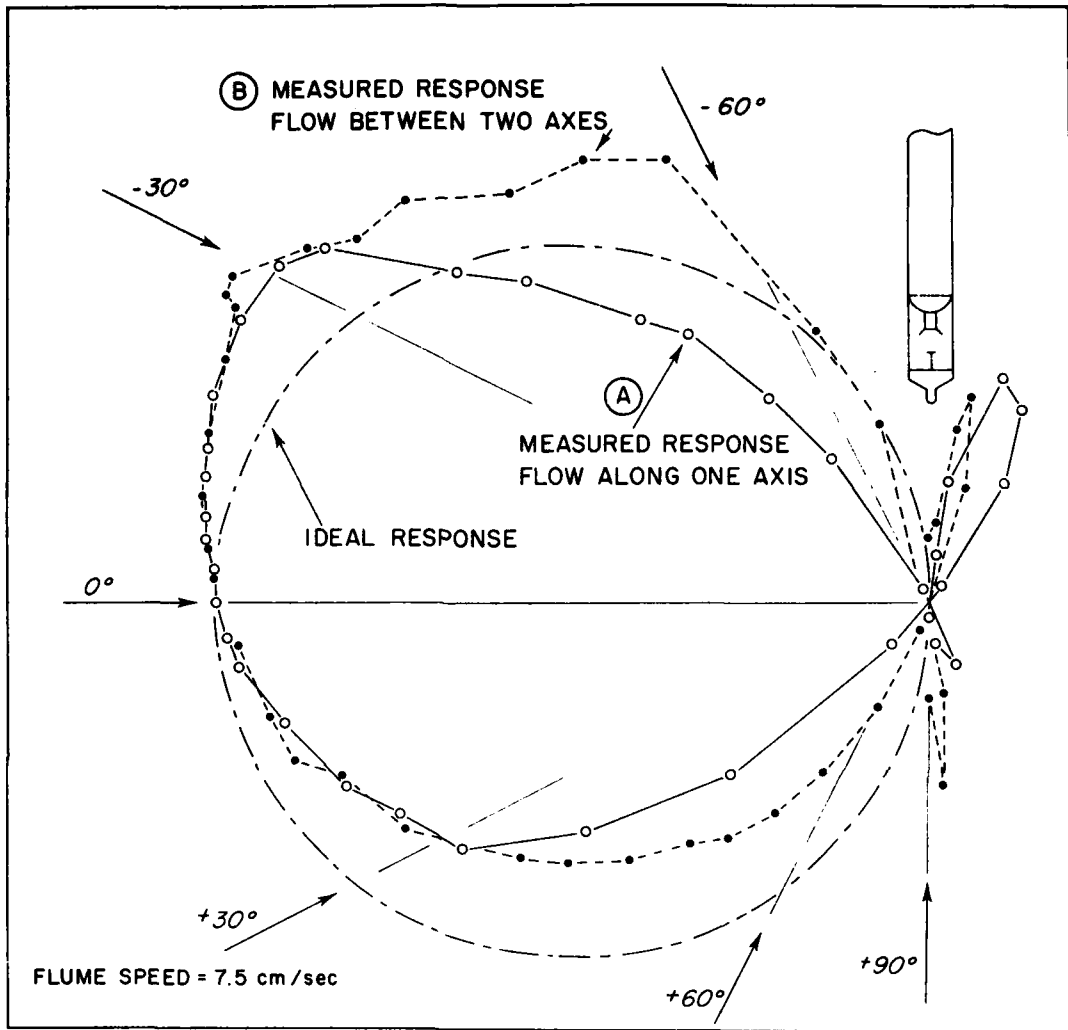
Figure 22

Figure 23.

Vertical cosine-response. Meter is tilted in steady flow to
test immunity to off-axis flow (orthogonality of sensors). (A)
Response with one axis aligned to steady flow, and (B) response
with flow midway between two axes. Significant differences
from desired cosine-response (dash-dash circle) are indicated.
Nominal flume speed is 7.5 cm/sec. Only one 180° segment of
the response is shown; other half will be mirror image about
±90° line.

Figure 23

Figure 24.

Vertical cosine-response (continued). Curves (A) and (B)
correspond to those in previous figure. Wakes of pressure case
and transducer supports cause low readings at left. Curve (B)
is generally higher than (A) since flow is less obstructed
between transducers ($\theta = 45^o$). End-bail and mirror wakes
cause negative (reverse) response at (C), actual flow does not
reverse. Dots (D) show response in 5° steps between curves
(A) and (B) at $\sim 60^o$ tilt. All data are arbitrarily
normalized to unity response at tilt angle $\alpha = 0^o$. Small
error bars and scatter over several days of observation show
highly repeatable response of instrument in $\pm 30^o$ tilt range.
Measured cosine-response departs markedly, however, from
desired cosine function (dot-dash line).

Sketches below depict meter orientation at various angles with
flow toward the right.

FLUME SPEED = 7.5 cm/sec

FLOW BETWEEN TWO ACOUSTIC AXES

FLOW ALONG ONE ACOUSTIC AXIS

COSINE

TILT ANGLE, deg

RESPONSE

WATER FLOW

FLUME

METER ORIENTATION

-93-
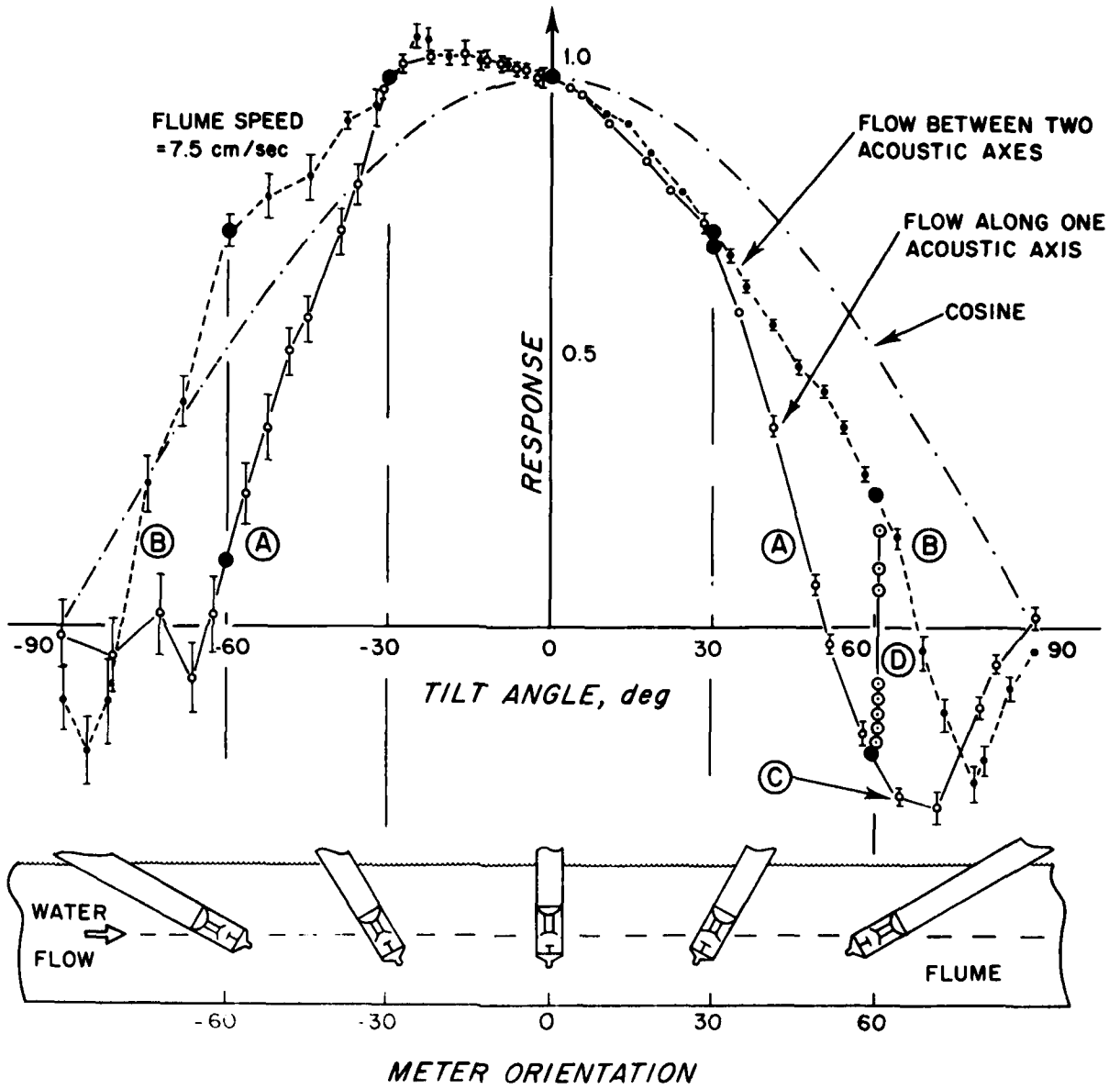
Figure 24

Figure 25.

Vertical cosine-response for meters of two slightly different
shapes sketched. Response differs in end-cap wake left but has
similar negative response in mirror wake at right. Flat
end-cap causes erratic data lower left. Response is not a
strong function of individual instrument of one design (top) or
of speed (bottom). As in previous figure, response departs
significantly from desired cosine function (dash line). Tests
were made in the DT-NSRDC #1 tow basin with meters completely
submerged and towed in horizontal position. (Data (top) from
Appell, 1978.)
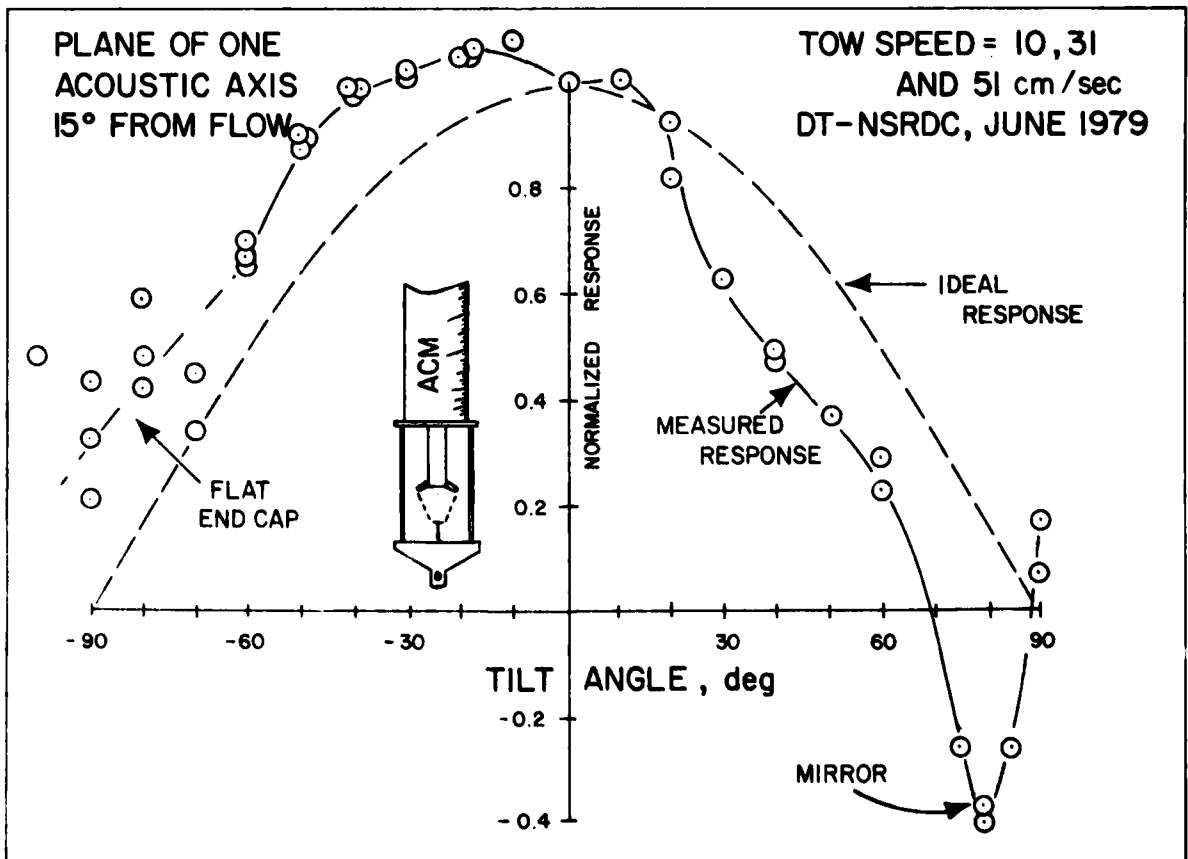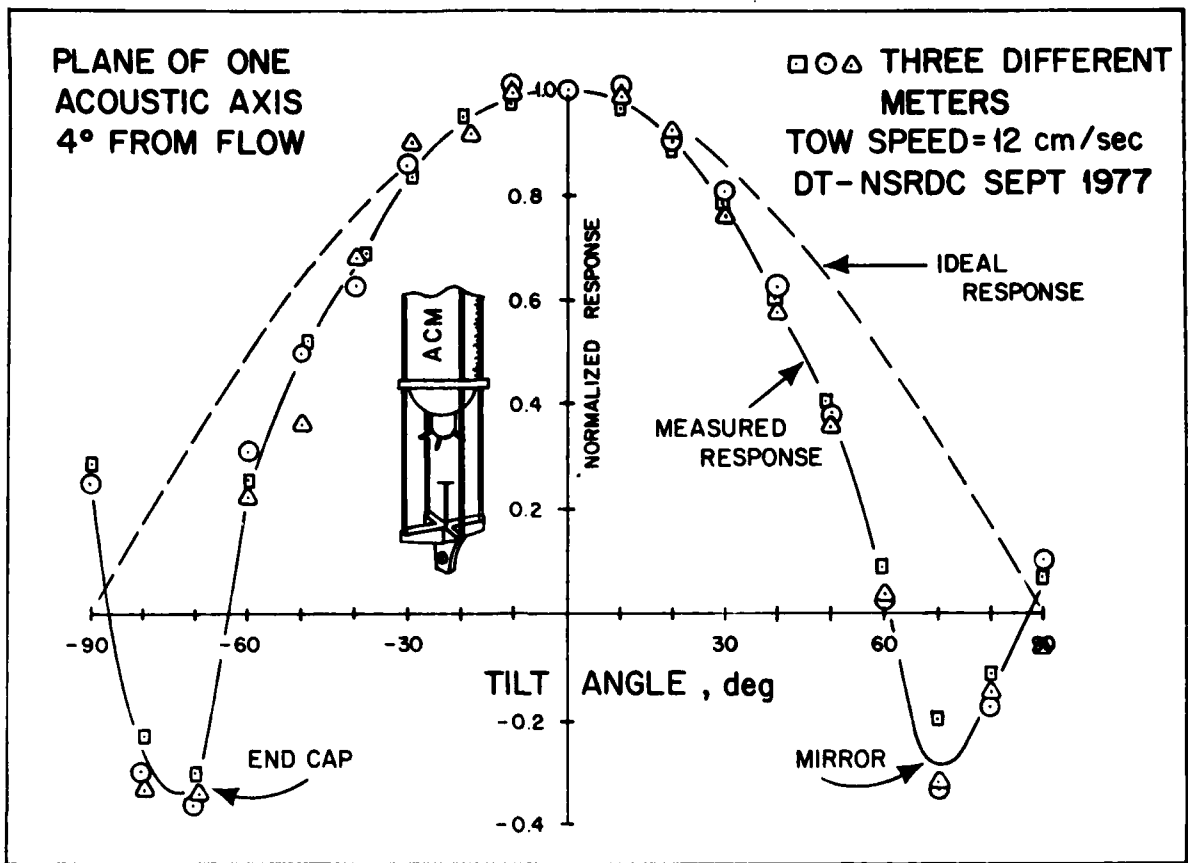
Figure 25

-95-
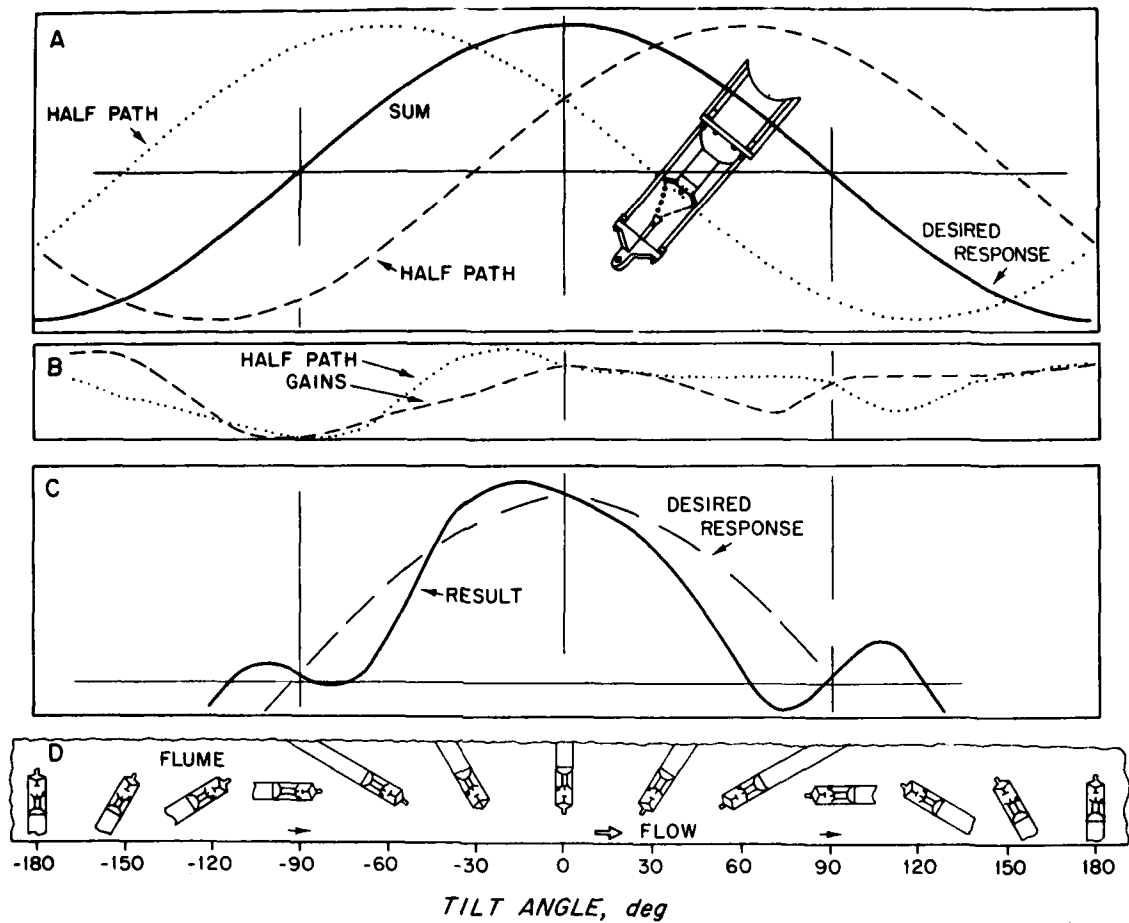
Figure 26.

Qualitative model of unexpected "reverse" response shown in previous two figures. A) Two acoustic half-paths (dot and dash lines of insert) lie on an equilateral triangle and thus have response equal to that of the entire axis but shifted by $+60^\circ$ from it. Their sum (solid line) is the total response of one axis. If response of either half-path is altered in speed and/or direction, the resulting sum is affected. Hypothetical half-path gains (B) combine to give response (C).
Sketches (D) show meter orientation to help visualize how differential flow interference might occur on acoustic half-paths. Small dot on one transducer prong helps follow its position.
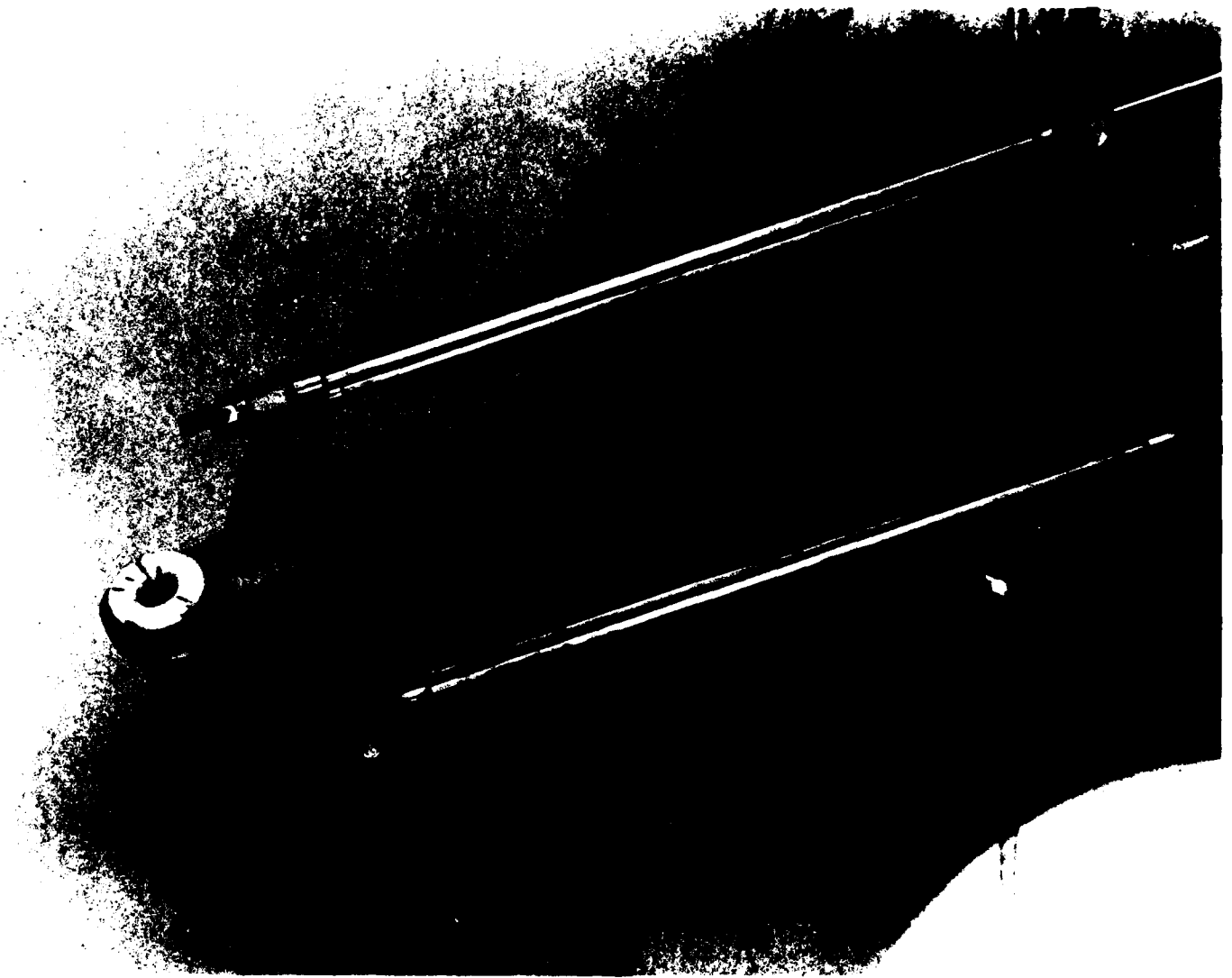
Figure 26

Figure 27.

Dye flow-visualization. Previously vertical dye column is
distorted by meter held at large positive tilt angle (α =
+70.5°). Steady flow is to the right at 1.5 cm/sec. Note
"shadowing" effect of mirror and end-bail on lower acoustic
half-path represented by dash-line in (A) of previous figure.
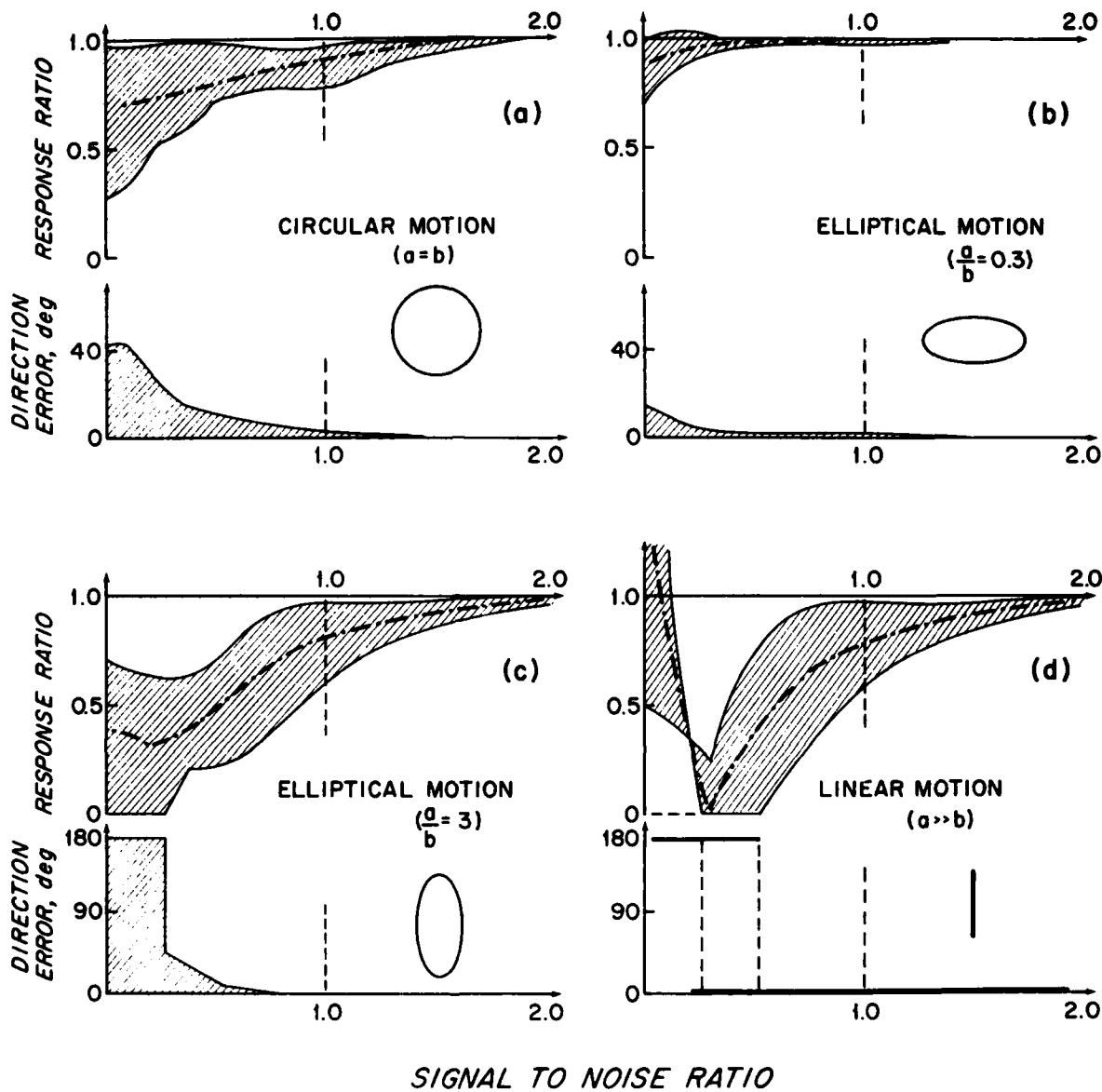
Figure 27

Figure 28.

Model response in large oscillating flow. Modeled response
to: (a) vertical circular orbital waves, (b-c) elliptical
oscillations, and (d) linear vertical oscillations. "Response
ratio" gives the meter mean reading in units of the true mean.
Flow "signal-to-noise ratio" gives the ratio of mean to
oscillatory speed. Estimates are for oscillatory motions large
compared with the meter size. Measured steady flow response of
Figure 24 is used for the numeric model input discussed in
Appendix A.

Figure 28

-98-

Figure 29.

Measured wave amplitude effect. As shown in the inserts,
response to straight-line oscillatory motion normal to a steady
tow was tested for small amplitude oscillations (a = 23 cm)
top, and larger amplitudes (a = 60 cm) bottom panel. Kinematic
model predictions (based on steady flow vertical cosine-
response) agree well for the larger motions but disagree in
smaller ones (above). The difference emphasizes the importance
of flow-scale in the instrument mean response.

   Since the flow-scale is not available internally, in situ
electronic corrections based on response in one wave amplitude
band will not generally be applicable in flow with arbitrary
amplitude distribution. Provisional results shown need further
verification. (Test data upper panel courtesy R. Weller,
Scripps; lower panel after McCullough, 1978).

Figure 29

-100-
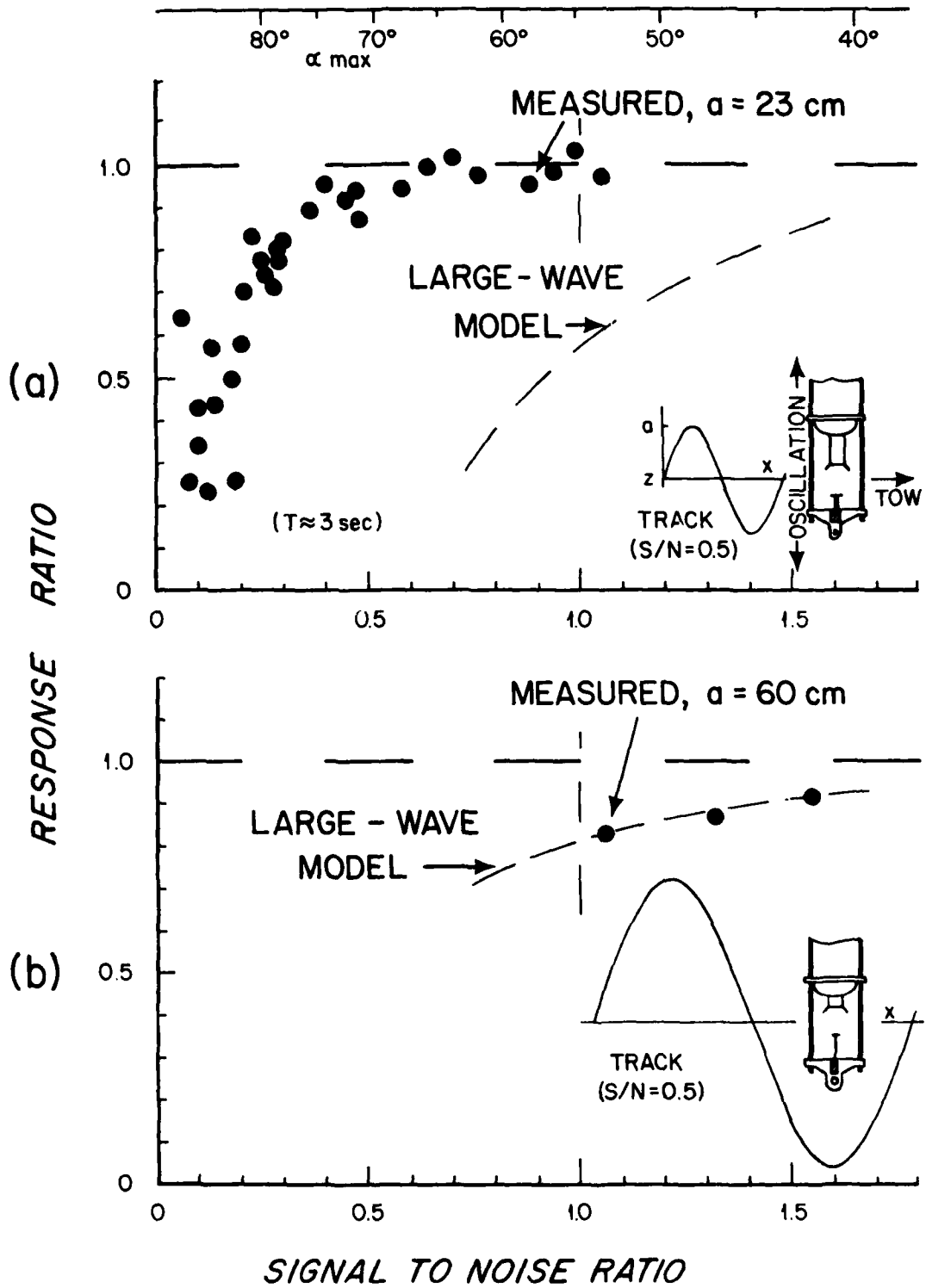
Figure 30.

Measured mean response in linear horizontal dynamic flow. A
flat end-cap, mirror-type, NBIS meter was towed and oscillated
horizontally in a straight line at angles ϕ to the steady tow.
Only horizontal motions were introduced by the test fixture.
Large dynamic errors are indicated when meter passes through
its own wake ($\phi = 0°$ and $\phi = 15°$). The sketch shows meter
and slosh orientation; table lists nominal slosh periods and
tow speeds of data above.

RESPONSE TO LINEAR
HORIZONTAL OSCILLATION
2 AND 4 ft p-p STROKES
DT–NSRDC, NBIS NO. 29, 9 JUNE, 79

Figure 30

-102-
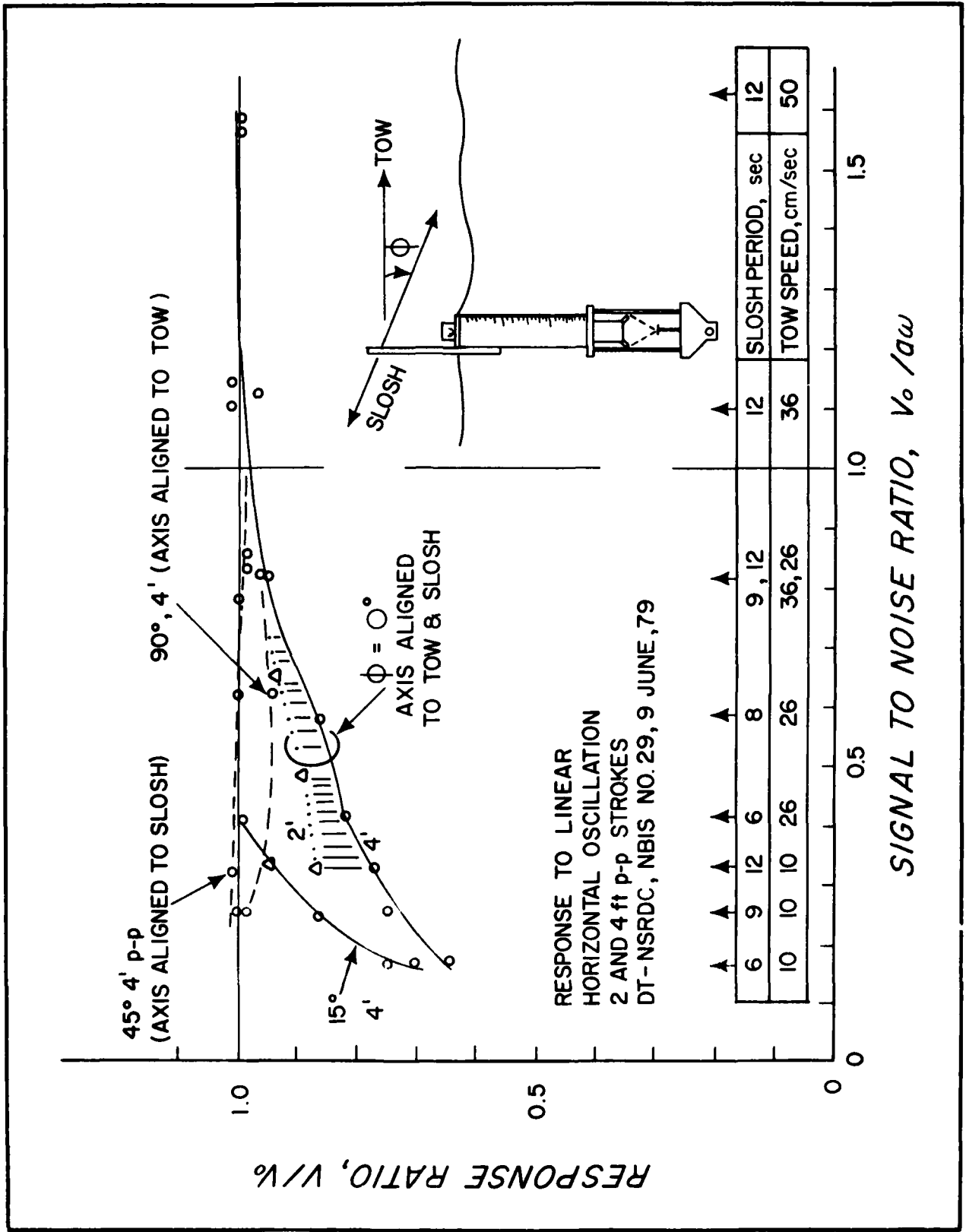
Figure 31.

Proposed 2-axis sensor cage. Two diagonally opposite tie-rods
of a 4-rod open cage similar to that shown in Figures 3a and 15
are attached to the instrument housing. Acoustic transducers
extend diagonally into cage to avoid primary flow defect in
tie-rod wakes (Figure 13). Direct acoustic paths (no mirror)
avoid differential-shadowing effect (Figures 24-27) and
hopefully improve vertical cosine-response. Length and shape
of the transducer supports and proximity to the instrument case
will need to be optimized empirically.

7½" O.D. PRESSURE CASE

END CAP

WIRE GUIDE TO TRANSDUCERS

OPTIONAL HEMISPHERICAL FLOW CAP

TENSION MEMBER AND WIRE GUIDE

TRANSDUCER POD ~3 ROD DIA LONG

ACOUSTIC PATH

CROSS BRACE

BEND

BEND
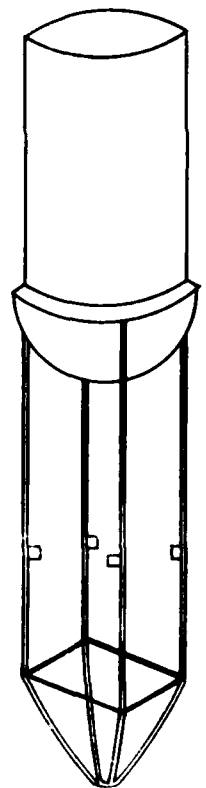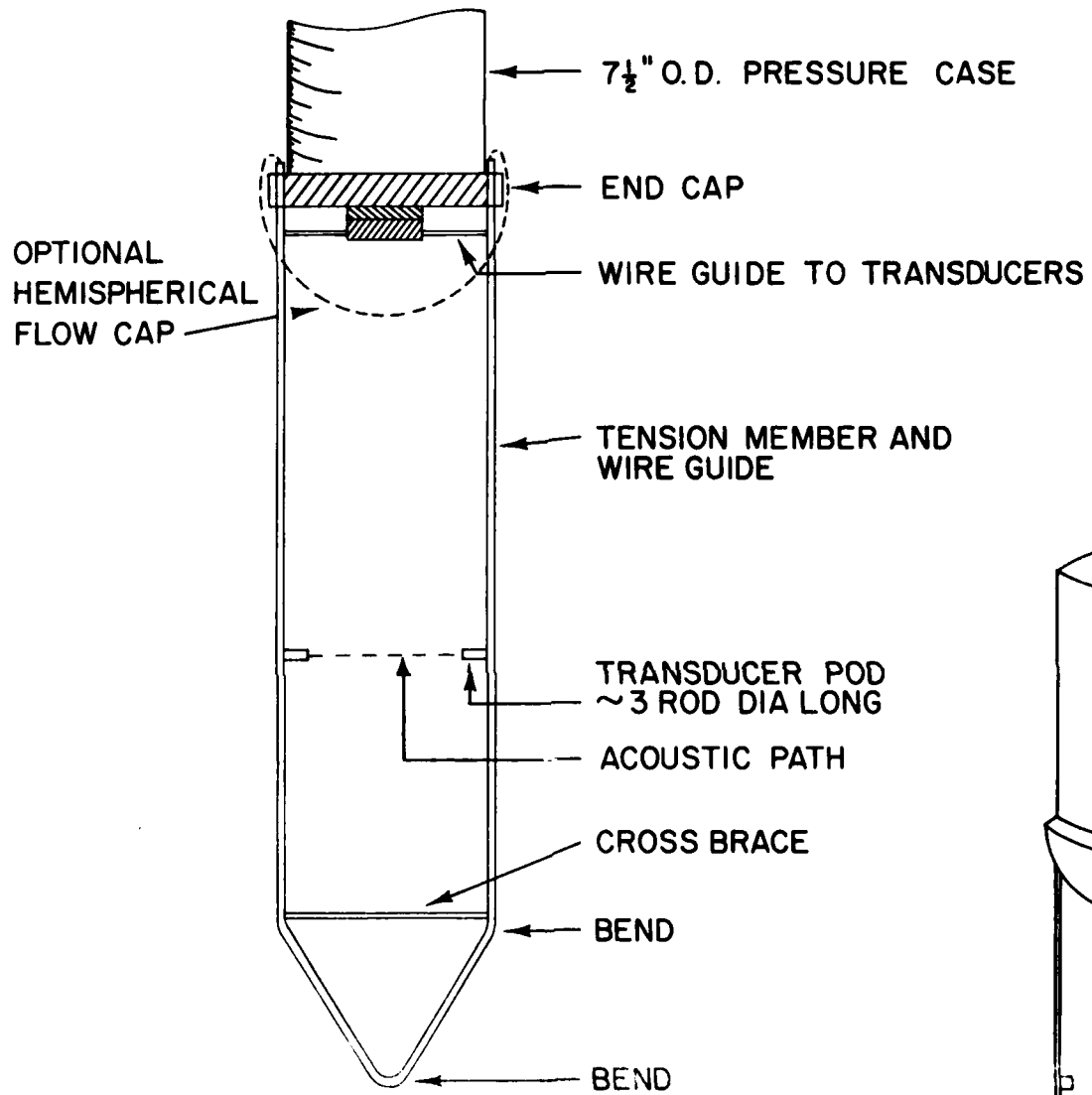
Figure 31

Figure 32.

Proposed <u>3-axis</u> sensor cage. Open symmetrical cage design
using 3 vertical bars (left) has 3 acoustic paths AB, BC, and
CA. Triangles (center) show plan views of successive rotations
of the cage and associated wakes. Dotted acoustic path in
major wake region is measured but is not used in final vector
averaging. Cage rotation angles are indicated at the right.

CAGE	ACOUSTICS	LOGIC	ROTATION
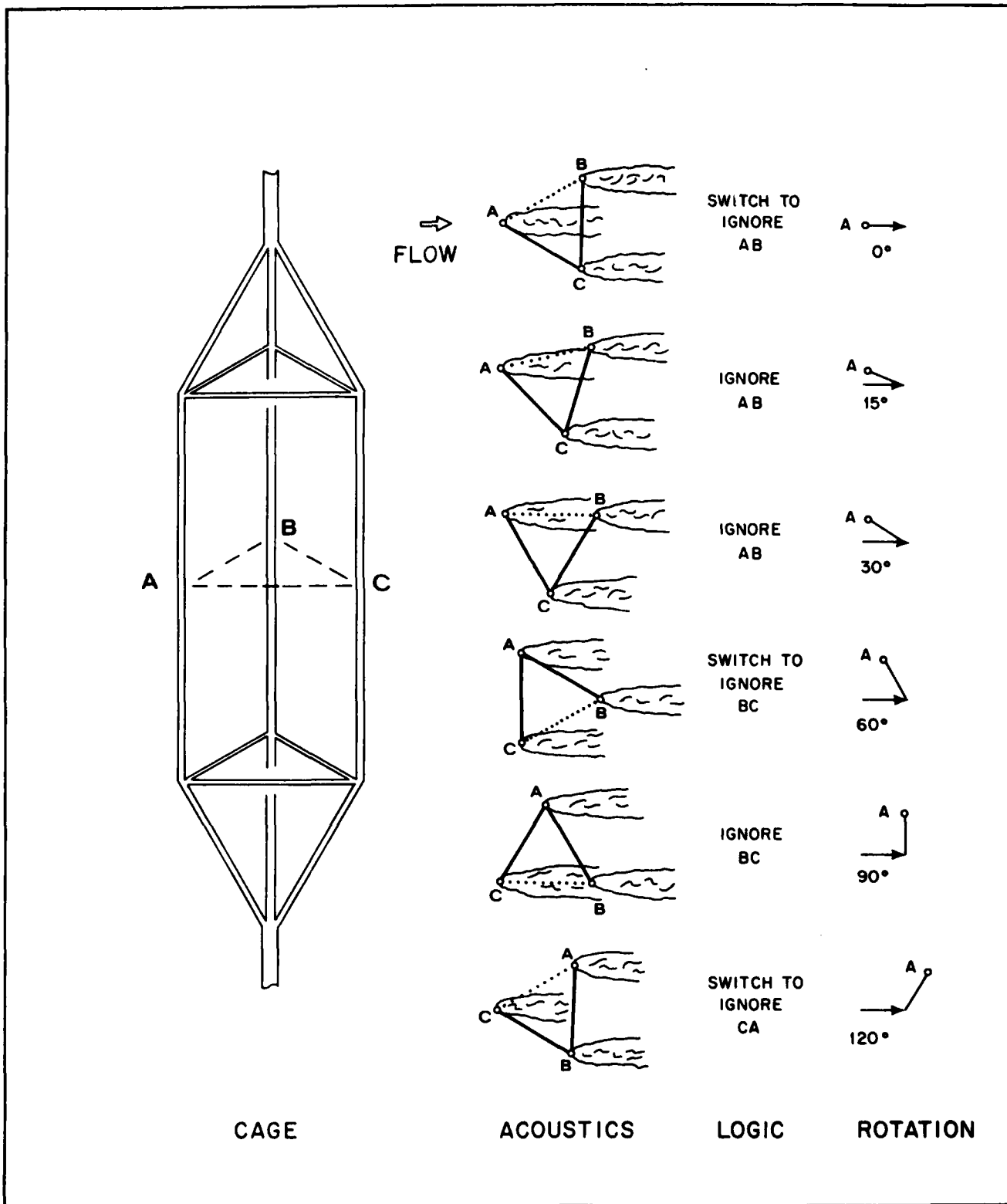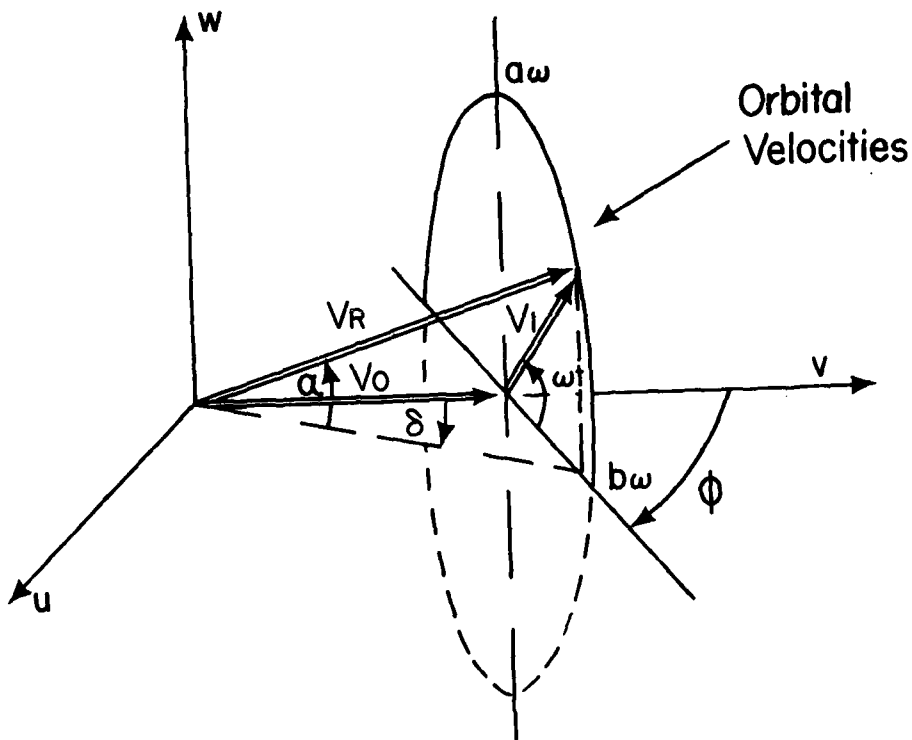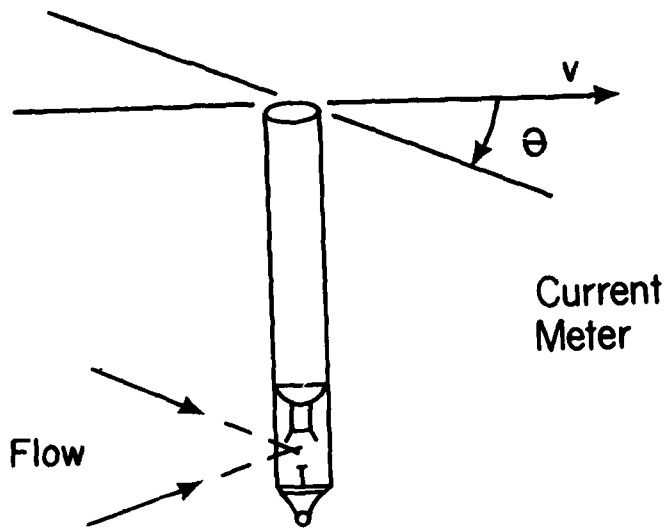
Figure 32

Figure A-1.

Notation for large-wave kinematic response model.

Figure A-2.

Predicted response of meter shown in Figures 16-17 in large waves. Response is indicated at two meter rotations ($\theta = 0°$ and $45°$), three orbit orientations (coplanar $\phi = 0°$, normal to mean flow $\phi = 90°$, and diagonal $\phi = 45°$), and several orbit shape factors a/b. Response is generally low, but is somewhat better at $\theta = 45°$ than at $\theta = 0°$.

Figure A-2

-109-
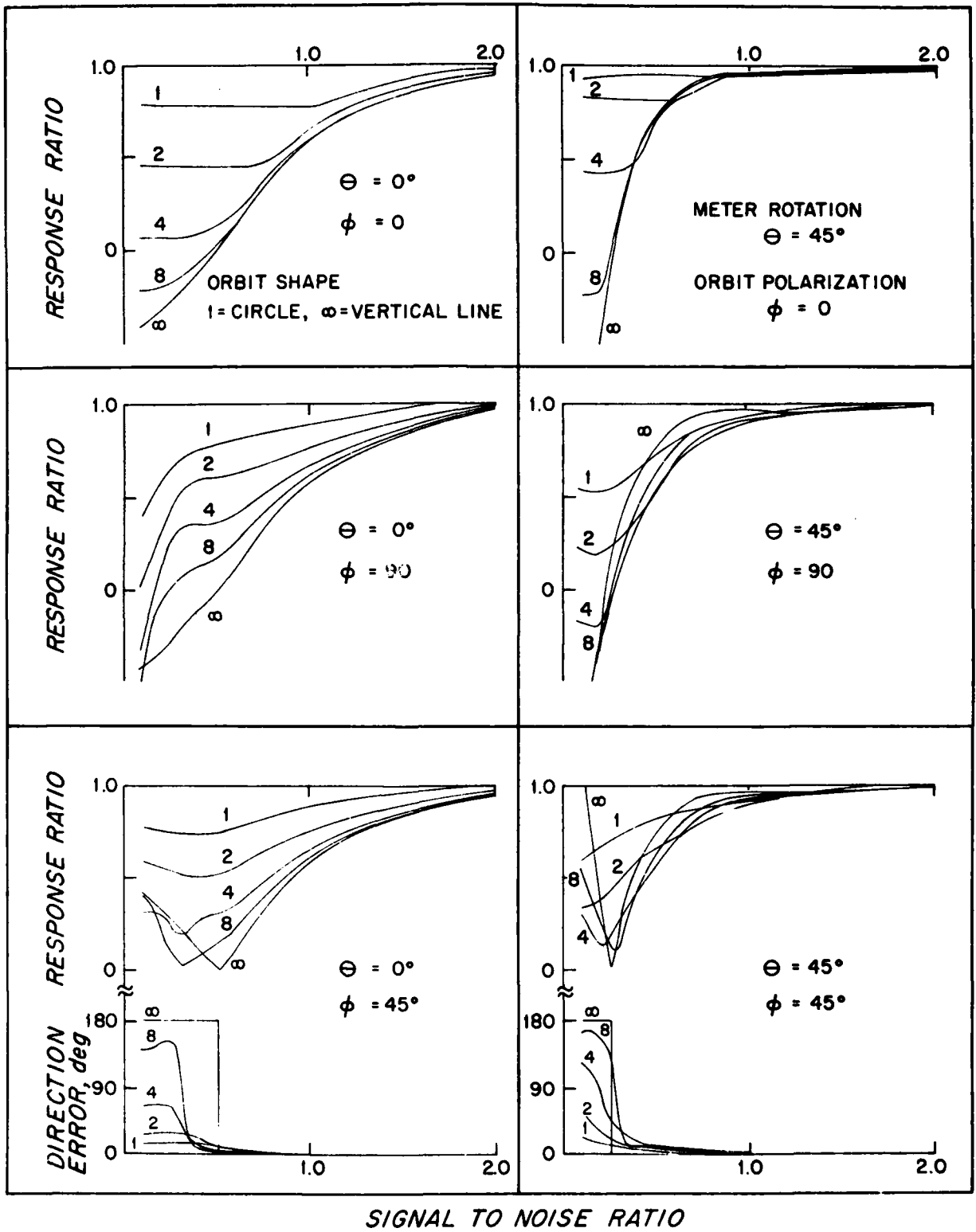
Figure A-3.

Scripps tow tank, carriage, and linear slosher in 1979.
Horizontally mounted ATT meter was oscillated across tow in
pendulum-like motion to simulate linear vertical mooring
motions in steady flow. See results Figure 29 top. (Photo
courtesy of R. Weller, Scripps).
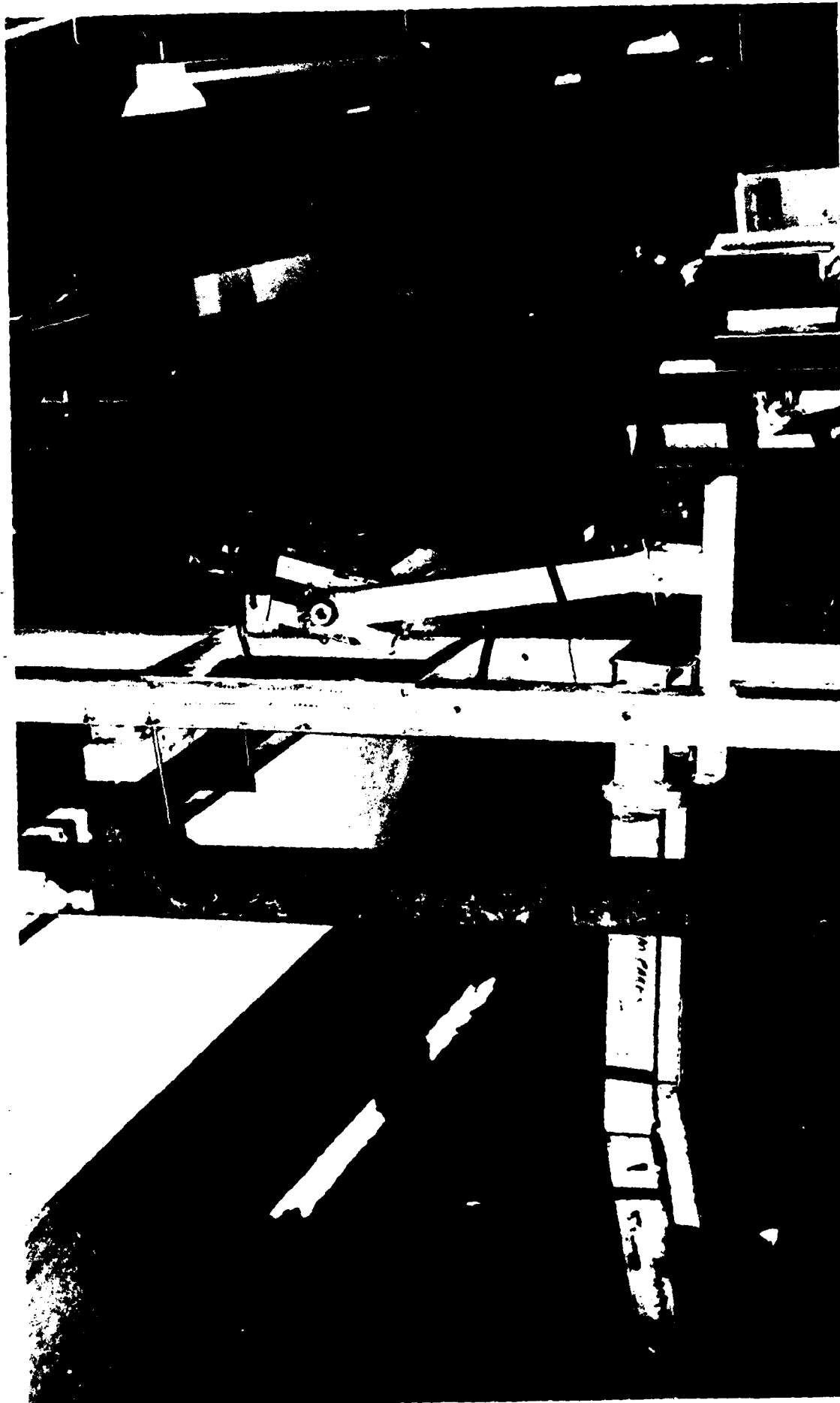
Figure A-4.

DT-NSRDC #1 tow carriage and basin used to obtain results shown in Figures 25, 29b, and 30. (Photo courtesy of A. Kalvaitis, NOAA, NOS.)

-113-
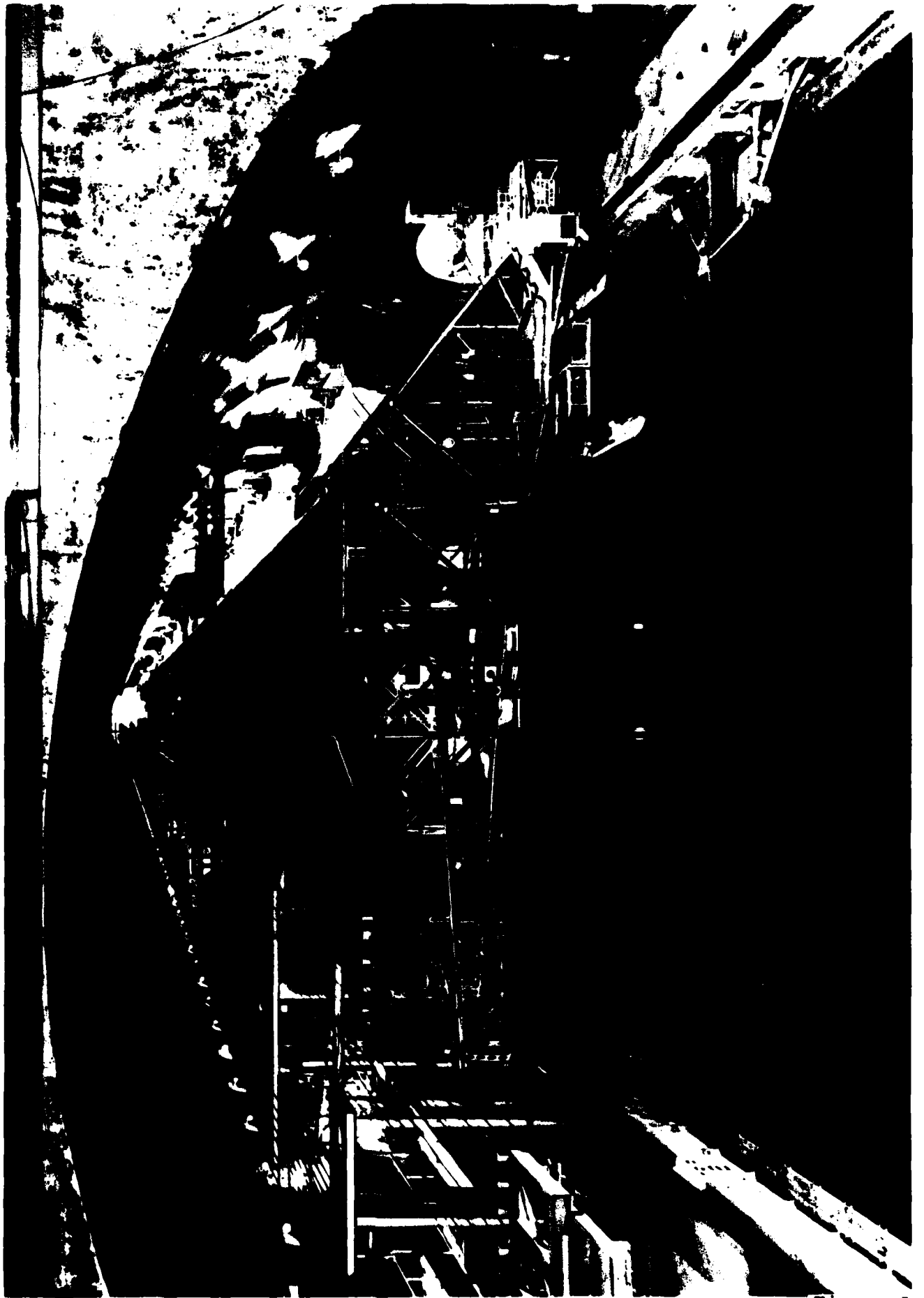
Figure A-

Figure B-1.

Response to steady tows with flume flow (top) and without flume (bottom). Variability of signals illustrates difficulty of making accurate calibrations of flowmeters with large drag area.

Figure B-1

-115-
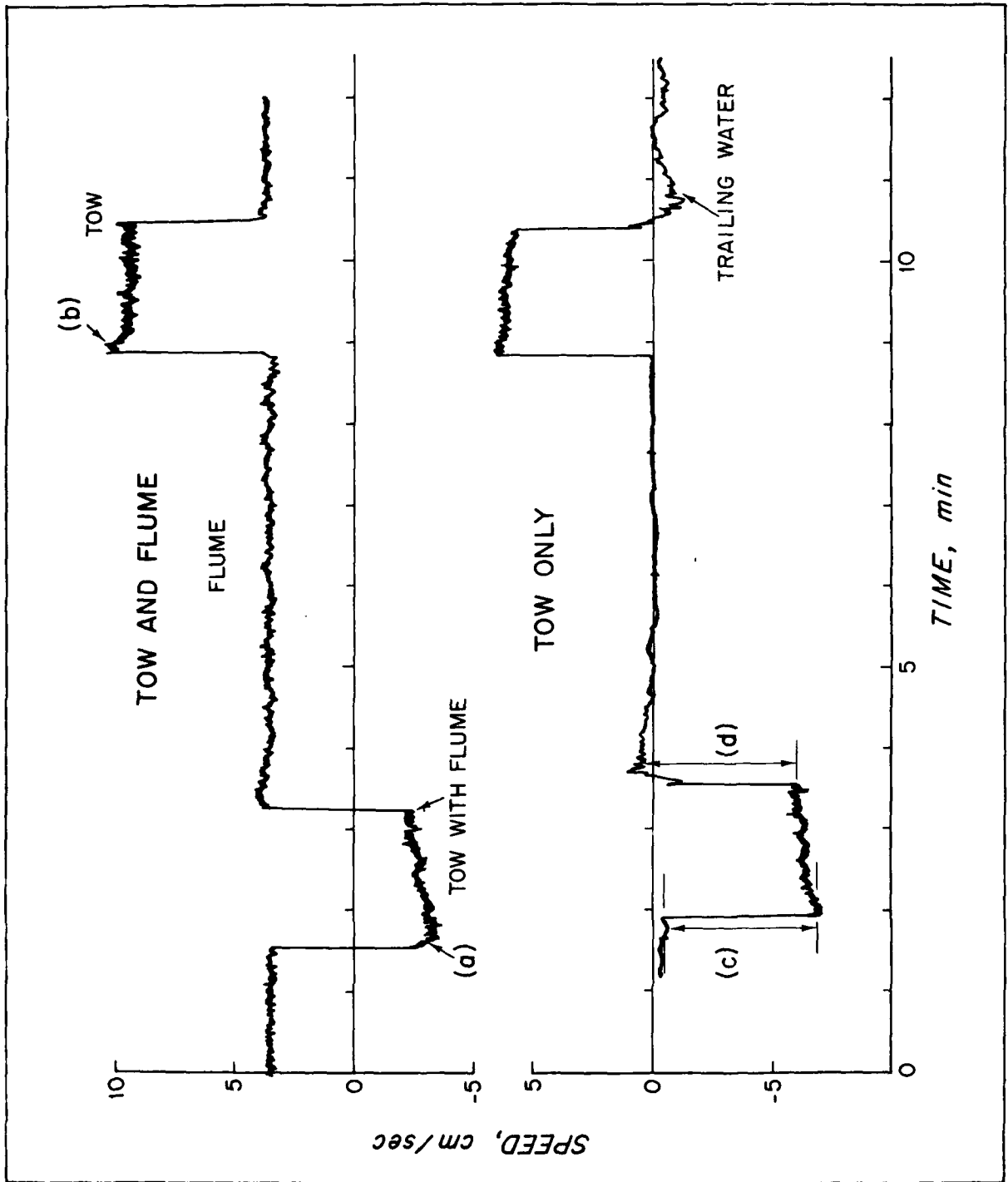
Figure B-2.

Instantaneous two-axis response. Each trace is a 30-second
sample of the x-y NBIS model 1 analog voltages. (a) Response
to 3.4 cm/sec flow from various horizontal angles. (b) Two-
axis noise level 15 min after a tow run (similar to that of
previous figure, lower trace). (c) Noise level after
overnight wait. Voltage scales are the same in all samples.
Traces in (b) and (c) have been arbitrarily offset in the
x-direction for clarity. (Nominal calibration coefficient is
3.2 mv per cm/sec.)

(a)

y

15 mv

x

15 mv

FLUME

SPEED = 3.4 cm/sec
(30 sec samples)

(b)   15 min

(c)   OVERNIGHT
                                             (30 sec samples)

SPEED = "O"
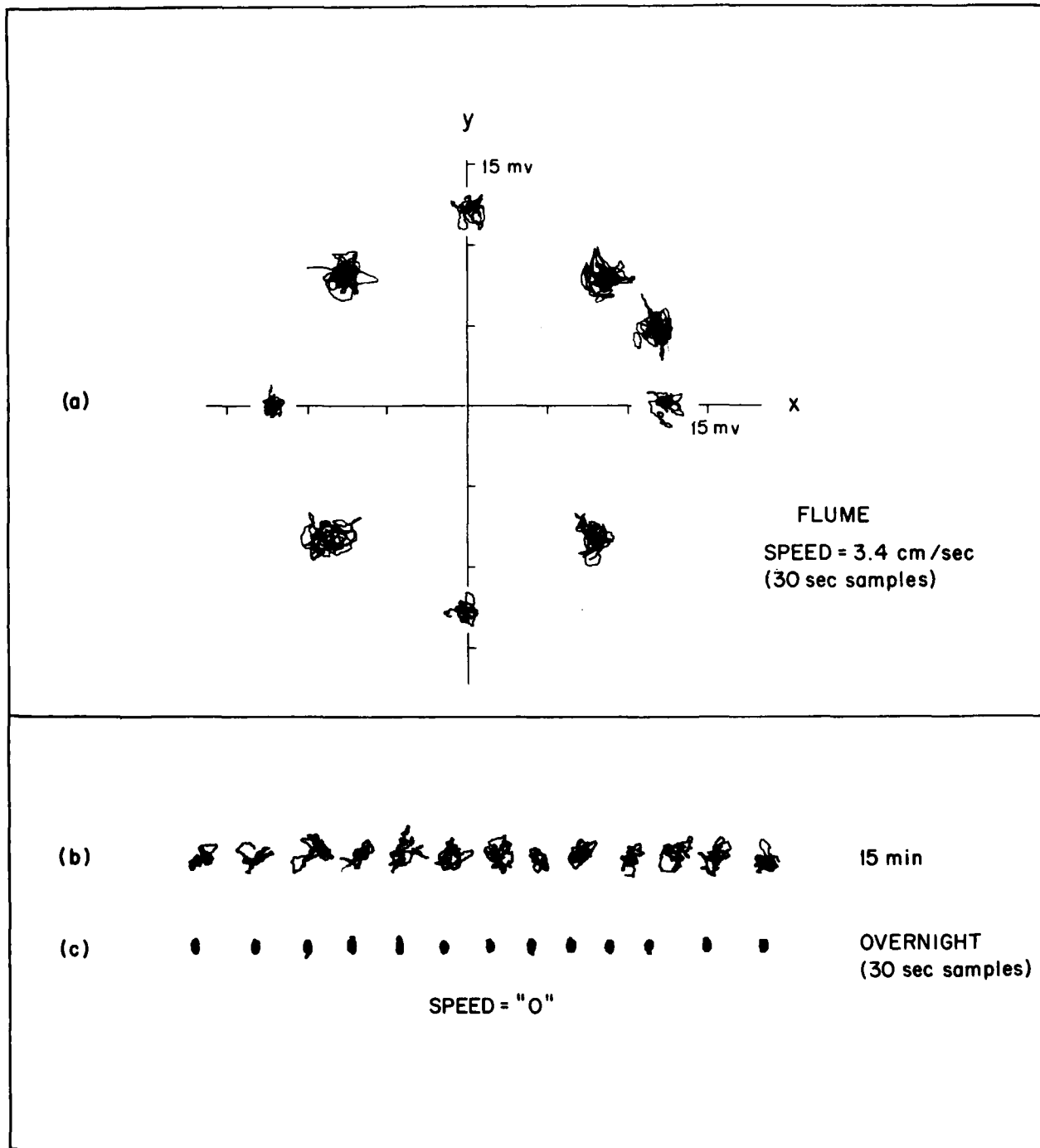
Figure B-2

MANDATORY DISTRIBUTION LIST

FOR UNCLASSIFIED TECHNICAL REPORTS, REPRINTS, AND FINAL REPORTS
PUBLISHED BY OCEANOGRAPHIC CONTRACTORS
OF THE OCEAN SCIENCE AND TECHNOLOGY DIVISION
OF THE OFFICE OF NAVAL RESEARCH

(REVISED NOVEMBER 1978)

1   Deputy Under Secretary of Defense
     (Research and Advanced Technology)
     Military Assistant for Environmental Science
     Room 3D129
     Washington, D.C.   20301

     Office of Naval Research
     800 North Quincy Street
     Arlington, VA   22217
3   ATTN: Code 483
1   ATTN: Code 460
2   ATTN: 102B

1   CDR J. C. Harlett, (USN)
     ONR Representative
     Woods Hole Oceanographic Inst.
     Woods Hole, MA   02543

     Commanding Officer
     Naval Research Laboratory
     Washington, D.C.   20375
6   ATTN: Library, Code 2627

12   Defense Documentation Center
     Cameron Station
     Alexandria, VA   22314
     ATTN: DCA

     Commander
     Naval Oceanographic Office
     NSTL Station
     Bay St. Louis, MS   39522
1   ATTN: Code 8100
1   ATTN: Code 6000
1   ATTN: Code 3300

1   NODC/NOAA
     Code D781
     Wisconsin Avenue, N.W.
     Washington, D.C.   20235

Woods Hole Oceanographic Institution
WHOI-79-92

MOORED ACOUSTIC TRAVEL TIME (ATT) CURRENT METERS: EVOLUTION, PERFORMANCE AND FUTURE DESIGNS by James R. McCullough and Wilhelm Graeper. 117 pages. December 1979. Prepared for the Office of Naval Research under Contract N00014-76-C-0197; NR 083-400.

New laboratory measurements and numeric model studies show the present folded-path ATT current meters are stable and sensitive, but are not well suited for mean flow observation in surface gravity waves. Alternate designs which reduce unwanted wake effects are proposed. ATT flowmeter history, principles of acoustic flow sensors, mean flow near cylinders, and the need for linear flow sensors are reviewed.

1. Flowmeter
2. Acoustic travel time
3. Response
I. McCullough, James R.
II. Graeper, Wilhelm
III. N00014-76-C-0197; NR 083-400

This card is UNCLASSIFIED